ISTANBUL TECHNICAL UNIVERSITY ★ GRADUATE SCHOOL OF SCIENCE ENGINEERING AND TECHNOLOGY

PRELIMINARY DESIGN TOOL FOR HYBRID ROCKET ENGINE POWERED LEO NANOSAT LAUNCH VEHICLE AND ITS APPLICATION

M.Sc. THESIS

Nazmi Erdi COŞKUNPINAR

Department of Aeronautical and Astronautical Engineering

Aeronautical and Astronautical Engineering Programme

NOVEMBER 2019

ISTANBUL TECHNICAL UNIVERSITY ★ GRADUATE SCHOOL OF SCIENCE
ENGINEERING AND TECHNOLOGY

PRELIMINARY DESIGN TOOL FOR HYBRID ROCKET ENGINE POWERED LEO NANOSAT LAUNCH VEHICLE AND ITS APPLICATION

M.Sc. THESIS

Nazmi Erdi COŞKUNPINAR
(511151152)

Department of Aeronautical and Astronautical Engineering

Aeronautical and Astronautical Engineering Programme

Thesis Advisor: Prof. Dr. Alim Rüstem ASLAN

NOVEMBER 2019

İSTANBUL TEKNİK ÜNİVERSİTESİ★ FEN BİLİMLERİ ENSTİTÜSÜ

HİBRİT ROKET MOTOR İTKİLİ İLEO NANO-UYDU FIRLATMA ARACI ÖNCÜL TASARIM PROGRAMI VE UYGULAMASI

YÜKSEK LİSANS TEZİ

Nazmi Erdi COŞKUNPINAR
(511151152)

Uçak ve Uzay Mühendisliği Anabilim Dalı

Uçak ve Uzay Mühendisliği Programı

Tez Danışmanı: Prof. Dr. Alim Rüstem ASLAN

KASIM 2019

Nazmi Erdi COȘKUNPINAR, a M.Sc. student of ITU Graduate School of Science Engineering and Technology student ID 511151152, successfully defended the thesis entitled "PRE- LIMINARY DESIGN TOOL FOR HYBRID ROCKET ENGINE POWERED LEO NANOSAT LAUNCH VEHICLE AND ITS APPLICATION", which he/she prepared after fulfilling the requirements specified in the associated legislations, before the jury whose signatures are below.

Thesis Advisor : **Prof. Dr. Alim Rüstem ASLAN** ....
Istanbul Technical University

Jury Members : **Assist. Prof. Dr. Bülent YÜCEİL** ....
Istanbul Technical University

Prof. Dr. Emrah KALEMCİ ....
Sabancı University

Date of Submission : 20 September 2019
Date of Defense : 28 November 2019

To my family,

FOREWORD

First and foremost, I would like to express my deepest appreciation for my supervisor Prof. Dr. A. Rüstem ASLAN for his inestimable support, encouragement, guidance and patience. Without her guidance and support, this project would not be completed. I would like to express my deepest gratitude firstly to my all friends but especially for Begüm OKTAY, Bute Naz ERBAŞ and Mert Bilal BIÇAKÇI for their all supports during my one of the most important life period and and my teammates from PARS Rocketry Group for helping me to improve project. I owe them a debt of gratitude for their precious friendship. Thanks to my family for their consistent love, support and efforts they have put into raising me.

November 2019 Nazmi Erdi COŞKUNPINAR

Astronautical Engineer

TABLE OF CONTENTS

Page

ABBREVIATIONS

GEO	**:** Geosynchronous Equatorial Orbit
LV	**:** Launch Vehicle
GLOW	**:** Gross Lift-Off Weight
GLOM	**:** Gross Lift-Off Mass
LEO	**:** Low Earth Orbit
LEO	**:** Sun-Synchronous Orbit
HRM	**:** Hybrid Rocket Motor
HRP	**:** Hybrid Rocket Propulsion
USA	**:** United States of America
LOX	**:** Liquid Oxygen
LRM	**:** Liquid Rocket Motor
GOX	**:** Gaseous Oxygen
NSLV	**:** Nanosatellite Launch Vehicle
WW2	**:** World War 2
ONERA	**:** Office National d'Etudes et de Recherches Aérospatiales
PE	**:** Polyethylene
NASA	**:** National Aeronautics and Space Administration
AMROC	**:** American Rocket Company
HTPB	**:** Hydroxyl-terminated polybutadiene
PB	**:** Poly Butadiene
HRPE	**:** Hybrid Rocket Power Engine
SRM	**:** Solid Rocket Motor
PMMA	**:** Poly (methyl methacrylate)
PBAN	**:** Poly Butadiene acrylonitrile
PBAA	**:** Poly Butadiene acrylic acid
CEA	**:** Chemical Equilibrium Application
CTPB	**:** Carbon-terminated polybutadiene
HEM	**:** Homogeneous Equilibrium Model
HNE	**:** Homogeneous Non Equilibrium
NHNE	**:** Non Homogeneous Non Equilibrium
NHNM	**:** Non Homogeneous Non Equilibrium Model
NIST	**:** National Institute of Standards and Technology
JANAF	**:** Joint Army-Navy-NASA-Air Force
NS	**:** Nassi – Schneiderman Diagram
He	**:** Helium
HLV	**:** Hybrid Launch Vehicle
PANUFA	**:** PARS Nanosatellite Launch Vehicle

SYMBOLS

ΔP	: Pressure Difference
t,Δt	: Time, Time Step Interval
O/F	: Oxidizer to Fuel Ratio
L/D	: Aspect Ratio of Combustion Chamber or Aspect Ratio of Injector
T/W	: Thrust to Weight Ratio
α, n	: Ballistic Coefficients of Regression Rate Formula
ρ	: Density of Fluid
$\dot{m}$	: Mass Flow Rate
h	: Specific Enthalpy
H	: Enthalpy
m	: Mass
κ	: Nonhomogeneous Nonequilibrium Model-Weighting Parameter
χ	: Quality of Fluid Mixture (vapor mass fraction)
s	: Specific Entropy
S	: Entropy
R	: Universal Gas Constant
P	: Pressure
C_d	: Discharge Coefficient of Injector
A_0	: Injector Orifice Area
N	: Number of Orifices
A_c	: Injector Total Orifice cross-sectional Area
T	: Thrust
T	: Temperature
W	: Weight
M	: Molecular Mass
ε	: Structural Mass Ratio
Λ	: Mass Ratio
ζ	: Payload Ratio
R_E	: Radius of Earth
I_{sp}	: Specific Impulse
D	: Drag
C_d	: Drag Coefficient
t_b	: Burning Time
ΔV	: Velocity Change
X	: Ground Range
H	: Altitude
γ	: Flight Path Angle
θ	: Pitch Angle
σ	: Yield Stress
g	: Gravitational Acceleration

LIST OF TABLES

Page

LIST OF FIGURES

Page

PRELIMINARY DESIGN TOOL FOR HYBRID ROCKET ENGINE POWERED LEO NANOSAT LAUNCH VEHICLE DENSITY OVER FOR AND ITS APPLICATION

SUMMARY

Launch Vehicle technology is a critical technology for many of nations to reach space freely. Space is new "racing" and "defense" area for the most of the countries on the earth. Launch Vehicles were used to transport the military and observational satellites from the beginning of the cold war. They were used mainly for governmental purposes and limitedly for science. Rocket and satellite technologies were extremely expensive to develop in that era, hence these technologies were under the control of governments. However nowadays, decreasing on the development cost on satellite and rocket technologies and ability to scale them to smaller size with the same mission requirements lead many universities and their students to develop rocket and satellites on their own.

These small satellites are called as nano and micro satellites, moreover they create a wide range of experimental researches for universities. When the space history is analyzed, a variety of launch vehicles systems are developed according to mission requirements. Today, according to trend of the nano – micro satellites, there should be new launch vehicle systems to meet with the nano- micro satellite developers demands. This technological area is new for the world. "Nano – Micro Satellite Launch Vehicle Technology area". This is great opportunity to catch world's technological trend on this area for Turkey. As a result of this situation, a conceptual design tool is developed and verified for hybrid rocket engine powered nanosatellite launch vehicles according to purpose of this study. At the end of this study, a hybrid rocket launch vehicle system (PANUFA) is designed for preliminary mission analysis with this tool.

A conceptual layout of nanosatellite launch vehicle and its hybrid rocket engine are the main outputs of this tool. There are some user defined limitations such as diameter, length and maximum available instantaneous thrust. According to these limitations and the mission requirements, tool is firstly checking the whether a feasible design is possible. If a feasible design is possible, tool starts to design the launch vehicle and its required hybrid motor. In this frame, a code has been written in MATLAB. This code consists of 6 modules which are feeding each other to find the preliminary design of the launch vehicle which is meeting with the user limitations. These modules are listed from last module to first one: Trajectory Module, Material Selection, LV Geometry - Mass Model, Propulsion System Module, Staging Module, ΔV Module. These modules are mainly for creating a conceptual design of nanosatellite launch vehicles.

In literature, these type of simulation codes are based on the optimization of the trajectories. In these studies, the main objective is optimizing the trajectory to achieve mission targets using a certain motor specifications. Unlike to these studies, the current

study is focusing on designing and optimizing the propulsion system to achieve the mission targets. The trajectory module is just used for checking whether the vehicle design is reaching to targets and additionally a propulsion system design tool is integrated to this conceptual design tool. Thus, if the designed vehicle is not capable to reach the targeted mission orbit, the conceptual design tool is calling the propulsion system design tool to improve the motor specifications which are burn time, instantaneous thrust ,propellant amounts and if required complete system. Then conceptual design tool redesign the launch vehicle. This iteration process is ending with the proper launch vehicle and motor design.

The algorithm of the tool start with firstly the propulsion system design tool which is creating the performance parameters of the propellant combination and these parameters are feeding the conceptual design tool modules. Secondly, according to the mission requirements, the required velocity change is calculated with ΔV Module via employing the Tsiolkovsky's Rocket Equation then the staging optimization module runs to find the optimum mass distribution along the stages according to initial structural mass ratios. In this module, the performance parameters of the propulsion system design tool is used. The next step is defining the propulsion system requirements of the launch vehicle then sizing the motor according to these requirements. This step is realizing by the propulsion system module. The fourth step is mass determination of each system according to material selection of the user then the recalculating the structural mass ratios for each stages. If the initial and final structural mass ratios are not close enough to each other, tool iterates this procedure till these initial and final ratios converge to each other. Finalization of these fourth and fifth steps mean that the launch vehicle conceptual design is created. All these design information is transferred to trajectory module to simulate the design trajectory of the vehicle. The whole algorithm of the tool can summarized as above.

The validation of the mass and trajectory modules are realized via comparing with the VEGA Rocket information. Finally a hybrid rocket nanosatellite launch vehicle is designed to carry a 60 kg payload to 300 km altitude.

HİBRİT ROKET MOTOR İTKİLİ LEO NANO-UYDU FIRLATMA ARACI ÖNCÜL TASARIM PROGRAMI VE UYGULAMASI

ÖZET

Fırlatma Aracı teknolojisi birçok ulus için uzaya özgürce ulaşabilmek adına kritik teknolojilerdir. Uzay, dünya üzerinde birçok ülke için yeni yarış ve savunma alanıdır. Soğuk savaşın başlangıcından itibaren fırlatma araçları daha çok askeri ve gözlem amaçlı uyduların fırlatılması için kullanılmıştır. Ayrıca daha çok devlet amaçlı kullanılmış ve bilim için limitli sayıda kullanılmışlardır. Bahsi geçen dönemde Roket ve uydu teknolojileri geliştirme maliyetleri çok yüksek düzeydedir ve bu durum bu teknolojilerin geliştirilmelerinin kontrolünün daha çok devlette olmasına sebebiyet vermiştir. Fakat günümüzde bu alanlardaki geliştirme maliyetlerindeki azalma ve bu sistemleri daha küçük yapabilme yetilerinin oluşması ile birlikte birçok üniversite ve bu üniversitilerin öğrencileri kendi roket ve uydu sistemlerini geliştirmeye yönelmiştir.

Bahsi geçen küçük uydular nano ve mikro uydular olarak adlandırılmaktadır hatta bu uydular sayesinde üniversieteler için geniş bir araştırma alanı oluşmuştur. Uzay teknolojilerine bakıldığı zaman, fırlatma araçları dönemin ihtiyaçlarına bağlı olarak tasarlanmış ve inşa edilmiştir. Günümüzde, nano ve mikro uydularının sahip olduğu artış trendi göstermektedir ki bu uyduların da fırlatma taleplerini karşılayabilmek için yeni sistemlerin tasarlanması gerekmektedir. Bu teknolojik alan şu an tüm dünya için yenidir "Nano-Mikro Uydu Fırlatma Araçları Teknolojileri". Bu Türkiye için dünyadaki teknoloji trendini yakalamak adına büyük bir fırsattır. Tüm bunlar göz önünde bulundurularak, bu çalışma kapsamında hibrit roket motorlu nano- mikro uydu fırlatma araçlarının kavramsal tasarımını gerçekleyen bir programın kodlanmasına karar verilmiştir. Bu programın doğrulama çalışmaları da yine bu tez kapsamında gerçekleştirilmiştir. Çalışma sonunda bu program ile öncül görev gereksinimlerini analiz etmek amacıyla, hibrit roket motorlu bir fırlatma aracı sistemi tasarlanmıştır.

Nano-Uydu Fırlatma aracının kavramsal gösterimi ve bu gösterime uygun hibrit roket motorunun tasarımı, bu programın ana çıktılarıdır. Program kapsamında bazı kullanıcı tanımlı parametereler girilmektedir. Bunlar, fırlatma aracı çapı, boyu ve mümkün olabilen en yüksek anlık itki değeridir. Program önce bu kısıtlara ve görev tanımına göre uygulanabilir bir tasarımın mümkün olup olmadığını tayin etmektedir. Eğer uygulanabilir bir tasarım mümkünse, program fırlatma aracını ve onun motorunu tasarlamaya başlar. Bu çerçevede, kodlar MATLAB ortamında yazılmıştır. Kod uygun fırlatma aracının öncül tasarımını bulmak için birbirini besleyen 6 modülden oluşmaktadır. Bu modüller, sondan başa olacak şekilde sıralanmıştır; Yörünge Modülü, Malzeme Seçimi Modülü, Fırlatma Aracı Geometri ve Kütle Modülü, İtki Ssistemleri Modülü, Kademelendirme Modülü ve Hız Değişimi modülü. Bu

modüllerin ana amacı belirtildiği gibi bir fırlatma aracının kavramsal tasarımını oluşturmaktır.

Literatürde, bu tarz simülasyon kodları yörünge optimizasyonu üzerine kurgulanmıştır. Bu çalışmalarda, ana amaç istenilen görev kısıtlarını gerçekleyebilmek için belli bir motor tasarımı kullanarak yörüngenin optimizasyonunun gerçekleştirilmesidir. Bu çalışmalardan farklı olarak, şu an anlatılan çalışmada istenilen görev kısıtlarını gerçekleyebilmek için odak alan motorun tasarımı ve optimizasyonudur. Bu çalışma kapsamında yörünge modülü sadece istenilen görev kısıtlarının gerçeklenebilip gerçeklenemediğini kontrol etmek için kullanılmıştır. Ayrıca bir itki sistemi tasarımı kodu kavramsal tasarım koduna entegre edilmiştir. Böylece, eğer tasarlanan araç hedeflenen irtifa ve yörüngeye ulaşamazsa, kavramsal tasarım aracı motorun belli özelliklerini geliştirmek amacıyla itki sistemi tasarım aracını çağırır. Bu özellikler; yanma süresi, anlık itki değeri, yakıt miktarları ve eğer gerekirse tüm sistemdir. Sonrasında kavramsal tasarım aracı tüm sistemi tekrar tasarlar. Bu iteratif süreç uygun fırlatma aracının tasarımının bulunmasıyla beraber sonlanır.

Kavramsal tasarım programının algoritması öncelikle itki sistemi tasarım programını çalıştırmakla başlar. İtki sistemi tasarım programında yakıcı-yanıcı yakıt çiftinin performans parameterelerinin hesaplanması gerçekleştirilir ve bu performans parametreleri yukarıda belirtilmiş olan kavramsal tasarım programının alt modüllerini besler. Bu kapsamda itki sistemi tasarım programı belirlenmiş olan yakıcı – yanıcı çifti için en yüksek özgül itki değerinin elde edildiği karışım oranını bulur. Bu değeri bulurken yanma odası sıcaklığı gibi motorun belli başlı özelliklerini hesaplar. Bu hesaplamalar kapsamında yanma odasında gerçekleşen tepkimeleri tepkime kinematiği kapsamında analiz edrek yanma sonucu oluşan ürünleri ve mol sayılarını belirler. Sonrasında yanma odası sıcaklığı ve buna bağlı tüm motor performans parametreleri hesaplanır. Burada çözüm için Gibbs Enerji Enazaltması yöntemi kullanılmaktadır.

Sonrasında program ilk modülü olan hız değişim modülünü çalıştırır. Bu modül gerekli hız değişimini bulabilmek için öncelikle hedeflenen irtifadaki dairesel bir yörüngede gerekli olan hızı hesaplar sonrasında bütün sürüklenme, yerçekimi ve itki kayıplarını dahil ederek bir marjin içerisinde toplam gerekli hız değişimini bulur. Bu hesaplamayı yaparken Tsiolkovsky'nin roket denklemini baz alır. Gerekli olan hız değişimi belirlendikten sonar bu değer ve itki sistemi tasarımı programından elde edilen motor performans verileri kullanılarak kademelendirme modülü aracılığı ile kademeler arası en optimum kütle dağılımı hesaplanır. Bu hesaplama yapılırken yapısal kütle oranı için ilksel bir değer atanır. Kademeler arası kütle dağılımı belirlendikten sonra uygun itki değerleri belirlenerek itki sisteminin boyutlandırılması ve tasarımı gerçekleştirilir. Bu aşamada itki sistemi modülü kullanılır. Ardından 4. ve 5. adımlar olarak, belli komponentler için malzeme tercihleri gerçekleştirilerek bütün fırlatma aracının kütlelendirilmesi yapılır. Bu aşamadan sonra final yapısal kütle oranları her kademe için hesaplanır ve ilksel olarak atanan değerler ile karşılaştırılır. Eğer bu karşılaştırmada değerler birbrine yeteri kadar yakın değilse, değerler birbirine yakınsayana kadar program iteratif bir süreç başlatır. Bu iteratif sürecin tamamlanması ile birlikte bütün fırlatma aracının tasarımı tamamlanmış olur. Bütün tasarım verileri yörünge modülüne simülasyon için aktarılır. Yörünge modülü 2 boyutlu bir analiz gerçekleştimektedir. Bu analizleri gerçekleştirebilmek için 3 serbestlik derecesinde harelet denklemleri kullanmaktadır.

Bütün kod yazıldıktan sonra çalışırlığının kontrolü için benzer sistemlerin dataları ile karşılaştırılması gerekmektedir. Bu doğrulama çalışması öncelikli olarak itki sistemi tasarım programı için gerçekleştirilmiştir. Bu kapsamda öncelikli olarak NASA tarafından geliştirilmiş olan CEA programının sonuçları ile programın sonuçları karşılaştırılmıştır. Bu karşılaştırma farklı yanıcı – yakıcı çifti karışım oranları için hesaplanan özgül itki değerleri için yapılmıştır. Elde edilen veriler grafik haline getirilerek üst üste getirilmiş ve birbirine olan yakınsamaları değerlendirilmiştir. Aradaki farklılıkların sebepleri yorumlanmıştır. Sonrasında aynı program aracılığı ile elde edilen itki zaman grafiği PARS Roket Grubu tarafından çalışmanın yazarı ile birlikte geliştirilen labaratuvar skalasındaki bir hibrit roket motorunun sıcak akış denemesi sonucu ile karşılaştırılmıştır. Bu sıcak akış denemesindeki kütle debisi gibi real datalar programa aktarılarak bir itki zaman grafiği oluşturulmuş ve grafik test sonucu elde edilen grafikle karşılaştırılarak sonuçları değerlendirilmiştir.

Bu çalışmanın akabinde kavramsal tasarım programının kütlelendirme ve yörünge modüllerinin validasyonu gerçekleştirilmiştir. Kütlelendirme modülünün doğrulama çalışması için literatürden bir hibrit roket motorlu nano-uydu fırlatma aracı çalışmasındaki değerler baz alınarak program kapsamında benzer tasarım elde edilip edilmediği ve değerlerin elde edildiği çalışmadaki tasarlanmış olan fırlatma aracının kütle değerlerine ne kadar yakınsandığı değerlendirilmiştir. Aynı zamanda bir katı yakıtlı fırlatma aracı olarak Minotaur da bu doğrulama çalışması kapsamında değerlendirilmiş ve elde edilen sonuçlar Minotaur'un Kullanıcı Manual'indeki verilerle karşılaştırılmıştır. İki doğrulama çalışmasının sonuçları arasındaki farklar değerlendirilerek nedenleri açıklanmıştır.

Yörünge modülü doğrulama çalışmaları kapsamında VEGA LV baz alınmıştır. Bu fırlatma araçları kontrollü yörünge tasarımlarına sahip oldukları için belli başlı bazı farklıklıklar gözlemlenmiştir.Ancak yapılan doğrulama çalışması kapsamında bu farklılıklar gözardı edilerek değerlendirmeler gerçekleştirilmiş ve böylece modülün kendi şartları kapsamında ne kadar yakınsayabildiği değerlendirilmiştir. Yörünge Modülünün de doğrulaması gerçekleştirildikten sonra son olarak program ile 60 kg faydalı yükü 300 km irtifaya taşıyabilecek olan bir fırlatma aracının tasarımı yapılmıştır.

1. INTRODUCTION

1.1 Hybrid Rocket Propulsion, Launch Vehicles & Proposed NANOSAT Launch Vehicle

Rocket technology is not a new technology for the world. The first “current known shaped” rockets were used by Chinese army by 1232 A.D. Certain writings of the era indicate that the Chinese used small explosive charges to send other explosive charges into the air for entertainment. It is believed that the Chinese had adapted the use of gunpowder from firecrackers to fireworks according to historic scientists [1]. These rockets are named as “Fire–Arrow”. An illustration for “fire-arrow” is showed in Figure 1.1[1].

Figure 1.1 : Chinese Fire-Arrow rocket.

After this usage of rocket technology, in 1663 first rocket powered man flight had achieved by Lagari Hasan Çelebi who is Ottoman rocketeer [2]. Lagari had invented his rocket vehicle with 8 propelled rods which are surrounding a capsule. In Sarayburnu, he attempted to launch himself directed to the sea. He has approximate 230 meters altitude from sea level. He landed safely with himself designed and built wings [2]. An illustration regarding to this epic event is showed in Figure 1.2 [2].

Figure 1.2 : Illustration of Lagari’s Launch Attempt.

These two key milestones from the history shows that humankind always had an interest about rocket technology. Until early 20th century, all of the rocket technology studies were made with solid propellants which are based mostly black powder. In 1926, Dr. Robert H. Goddard had tested first liquid rocket engine in the world. In the meantime, Wernher von Braun who is a German Engineer started to work on liquid rocket engines and missiles. He was also a member of Nazi Party and technical chief of rocket-development facility at Peenemünde on the Baltic Coast. The first long–range missile V-2 were developed by a team which is leaded by Von Braun as shown in Figure 1.3 [3].

Figure 1.3 : Chinese Fire-Arrow rocket.

At the end of World War 2 many of German scientists and engineers were moved to United States of America. Wernher von Braun also had moved to USA with all of his knowledge about the rocket science. With the end of the WW2, rocket studies in Germany has ended. A new era started which is called as “Cold War” [3]. Since the beginning of the space race between the Soviet Union and the United States, many of launch vehicles in variety options have been developed to achieve mission requirements such as placing first artificial satellite into orbit, reaching to moon etc. The space race officially has begun in 1957 via launching Sputnik 1 which the first artificial satellite is built by the Soviets. In 1950’s, the only two countries which have launch vehicle technology, are the Soviet Union and the United States after the World War II, thanks to technology improvement until today, nowadays a large number of countries have enough technology to perform their own missions. In Figure 1.4 [4], current operational US Governmental and commercial launch vehicles are showed.

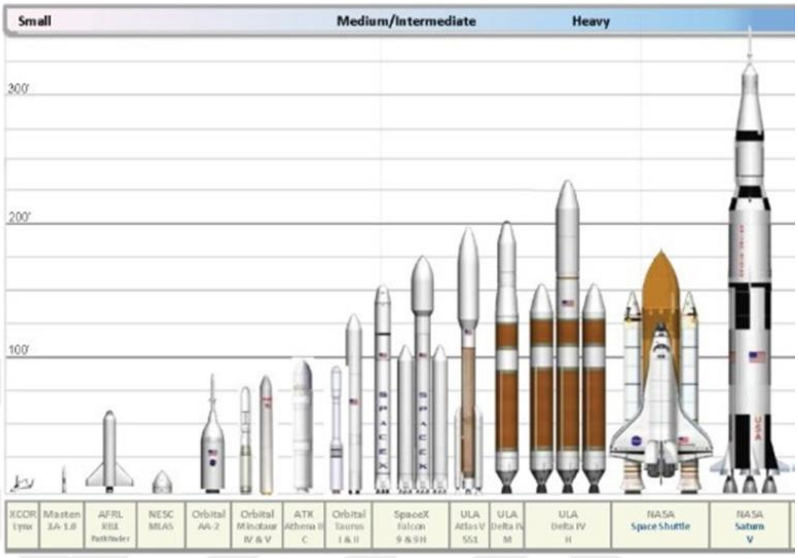

Figure 1.4 : Operational US Governmental and commercial launch vehicles.

The main mission of space launch vehicles is delivering the payloads into desired orbits which have specific orbital parameters and altitudes. Space Launch Vehicles must move as faster as possible to overcome Earth’s gravity and after they can reach to the desired orbits to release and place the payloads at very high speeds. Many of launch vehicle systems are launched vertically from the ground and they are subjected to atmospheric drag during their ascent phase. Because of this atmospheric drag, launch vehicles moving as faster as possible to minimize drag losses. The other factor of losses is launch site which is affecting the launch conditions. To instance, launch from a site near equator requires fewer propellants in addition to the optimum advantage of Earth’s rotational speed. On the other hand there are two more options to launch the rocket to overcome earth gravitational force and atmospheric drags.

One of them is air launch and the other one sea launch. Sea based launch systems were used for sounding rocket launches during past years; however, because of their advantages on the propellant amount and safety; they were started to be used for space launch vehicles to deliver the payloads into orbits. The other important advantage of sea launch is its movable platform allows to launch the rockets into desired missions such as launching closer to the equator and extinguishes plane change for GEO orbit. Air Launch systems can be classified new systems for present time. Because the first air launched rocket is Pegasus developed by Orbital ATK which started operation in 1990. Main purpose of air launch systems is minimizing the atmospheric ascent phase of launch to decrease the amount of the propellant and as a result of this increasing the launch efficiency. Air Launch systems had popularity during last years with the increment on the private launch vehicle developer entrepreneurs. Land, sea and air-based samples are given in Figure 1.5 [5–7].

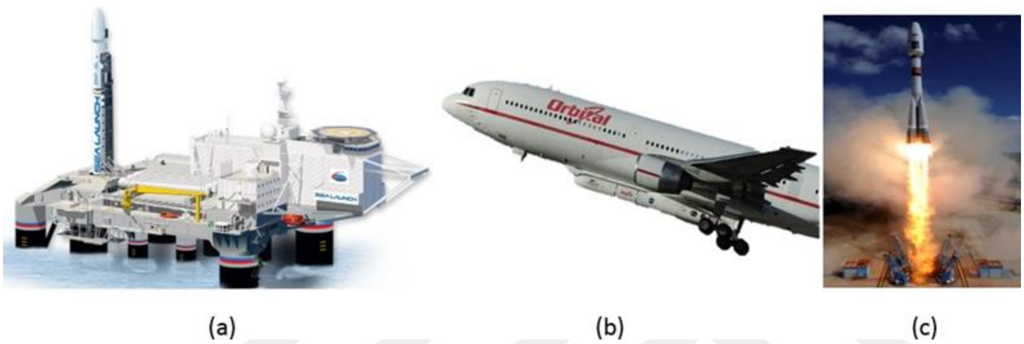

Figure 1.5 : Land, sea and air-based samples of launch platform.

Staging is one of the performance developer strategy for the launch vehicles. Different staging operations are showed in Figure 1.6 [8]. The purpose of staging is improving the performance of launch vehicle via reducing its gross mass. There is sequential process during ascent phase of launch. For instance regarding to two stage launch vehicle which is launching from ground and vertically, once the all propellant of first stage is consumed, there is no need to keep this stage which is empty and useless. As a result of this, first stage can be separated then second stage will be ignited to power rest of the launch vehicle which has reduced gross mass compare to initial conditions. As a result, rest of the vehicle can be accelerated much faster and less propellant is required to reach the desired orbit. This design method is affecting mainly the size of the rocket to minimize the losses.

On the one hand increasing the stage number of launch vehicle offers reduction on mass specializing the rocket motors according to required thrust of operating altitudes thrust but on the other hand, reliability of launch vehicle is decreasing with higher number of stages [9]. This situation is one of the optimization in the launch vehicle design process.

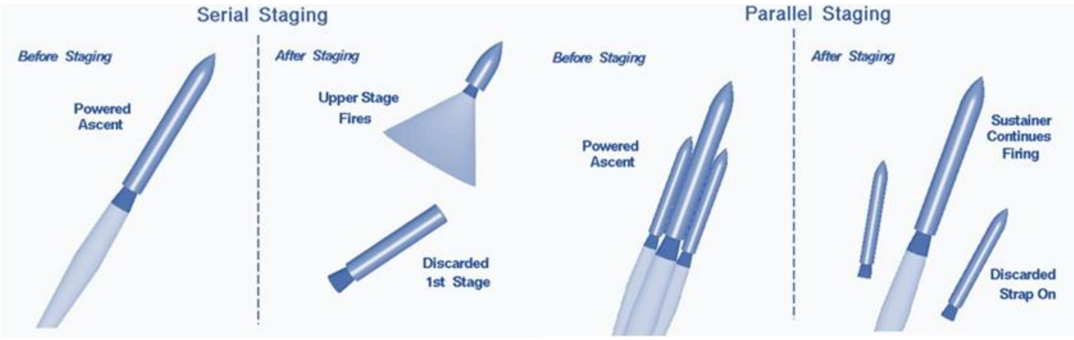

Figure 1.6: Staging Operations.

Size is one of the classification form of launch vehicles. In actual, launch vehicles are classified with their launch platform selections, sizes or target orbits.Platforms and target orbits are explained above. The last classification is “size” which is affecting by payload size and mass trends, mission trends and also platforms. Size is an output of all these factors during the design phase. If launch vehicles are analyzed according to their mission requirements we should consider following statements. Sounding rockets, which are used to carry out unmanned space and microgravity experiments, are not able to carry a payload to LEO because they cannot provide required velocity change which is used for inserting a satellite into orbit. According to their mission purpose, they follow a suborbital trajectory for turning back to the earth.

After all, when the launch vehicles are classified with their sizes, all of these factors should be considered. To sum up launch vehicles can be classified as small, medium and heavy from traditional mission requirements point of view. This classification is valid for launch vehicles which are built between 1950 and 2000. Small launch vehicles can deliver payloads up to 2,000 kg, medium launch vehicles can deliver between 2,000 kg and 20,000 kg, heavy launch vehicles can lift between 20,000 kg and 50,000 kg into LEO orbit. As mentioned above, these vehicles are built to meet that period’s mission requirements. New mission requirements are coming sight with new technological improvements on reducing the size of the satellites and interplanetary researches at the present time. This situation is resulting with new classes which are super heavy launch vehicles and nano-micro launch vehicles. Nano

–Micro launch vehicles are mostly developing by new space startups from all around the world. Main idea behind this new class is delivering the micro-nanosatellites and their constellations to their own specific orbits. These launch vehicles are designed to deliver payloads which are between 20 – 200 kg in general. There is only one super heavy launch vehicle ever built “Saturn V”. This launch vehicle was built to perform a lunar manned missions. Mars missions gaining impotency for humankind.

This situation is resulting with new super heavy launch vehicles to perform manned interplanetary missions. Super Heavy Launch Vehicles can lift more than 50000 kg to LEO orbit. To summary, new era’s for space technology leads to develop new nano-micro launch vehicles from all point of views and super heavy launch vehicles. This is the main idea behind the motivation of this thesis.

1.2 Motivation

During last two decades, placing smaller satellites (nano and microsatellites) in space has been gaining more and more attention. Small satellite constellations are one of the important concept for future space projects. This means that satellites under 50 kg are now becoming to be leader in the market. On the other hand, launch vehicle industry is not capable to answer this competing demand. This has been exacerbated with the standardization of the buses, especially the CubeSat phenomenon [10]. Current launch vehicles are designed to deliver the big satellites to space as mentioned previously. Because of this gap in the industry, small satellites are not meeting with their original mission orbital parameters. The other restrictive factor is launch costs per kilogram. Satellite launches have an exorbitant cost that still makes it challenging for small ventures to place their satellites into orbits. This situation has a trend to change in positive way in recent years with a many of solutions such as reusability and reduction on development costs. Before coming to today, launch vehicles are developed by governmental programs. There were no private company which develops launch vehicles until this century, however; with the beginning of 21th century launch vehicle industry has begun to commercialize by US Entrepreneur Elon Musk. The big success of Space X Company motivates many of entrepreneurs all around the world [11].

All these statements show that, development of new launch vehicles special to small satellites is critical to answer market demand. There is a rule in commerce “First Come Firs Served”. There are limited private companies which are not governmental, working on small launch vehicles all around the world. Hence to make Turkey as an international competitor for this new space race, placing “Made in Turkey” satellites (firstly nano – micro satellites) into orbit via “Made in Turkey” Launch Vehicles to gain Turkish Space freedom. As a result, design optimization of small launch vehicles and propulsion systems are gaining priority in defense industry of Turkey. Design of a launch vehicle is a challenging process which requires multi-disciplinary studies in which propulsion, aerodynamics, mass and sizing, trajectory and even and cost must be considered [12]. Because of its complex and interdependent nature, optimization techniques are important to define initial vehicle configuration which satisfies the requirements and limitations. Therefore, optimization tools in which vehicle design and the trajectory simulations are running simultaneously; are needed to determine the performance parameters and capability of the proposed launch vehicle configurations from the level of system engineering.

Propulsion systems occupy most of the volume of launch vehicles. As a consequence of this fact, launch vehicle design process mostly influenced by propulsion systems, therefore; inclusion of an independent code for propulsion system design into such an optimization tool of launch vehicle design is advantageous to achieve more precise and reliable output. Main idea behind the propulsion system design is defining the optimized system parameters regarding to design limitations for the following requirements, specific impulse of the propellants, volume & mass of the system, safety and design feasibility. Hybrid Rocket Motor technology was chosen as propulsion system for this study to design a nano-satellite launch vehicle A hybrid rocket motor (HRM) is an intermediate type between solid and liquid rocket motors.

The engine design process firstly focuses on maximizing the performance and reliability of the system in the meantime keeping mass, volume and cost as minimum as possible. This is affecting the overall design of launch vehicles. Sizing of the propulsion system mainly dependent on propellants thermochemical performance. On the other hand, manufacturing capabilities are also affecting the design constraints to keep dimensions in minimum. All of these parameters are collecting in one space to create optimum design conditions in the tool. Resulting outputs of search process in the tool can be too populated with continuous and discrete variables for multistage launch vehicles. This situation may create a convergence problem in major system design parameters such as mass distribution along the stages or engine sizing. Launch Vehicle Design has been being topic to many of books and book chapters for a long time [13–16]. Details about how to establish the models for analysis of the each different disciplines are given separately in these books. However, the only author which explains the logic flow between different disciplines in an integrated workspace for system level of optimization of launch vehicle conceptual design; is Hammond [17, 18]. There are different propulsion system analysis tools, trajectory optimization tools and vehicle design optimization tools in the software market, however; there is no such a tool which integrating propulsion and system design optimization.

In actual, there is no such a tool which offers a propulsion system based launch vehicle design optimization tool. On the other hand, there are many projects and software's which offer trajectory analysis based optimization on fixed launch vehicle systems. Moreover, all of these software packages have been developed by governmental agencies or universities for their national space projects and there is a restriction on exporting of these software's to other countries. Therefore, there is still a need for an integrated and reliable system optimization tool for launch vehicle performance analysis and simulations to obtain an efficient design.

There are different academic studies to develop these type of tools but not commercial. In this thesis, according to all of these facts it had seen that an individual optimization tool development regarding to selected propulsion system and design constraints is important at the preliminary stage of the design process to minimize the development time. For thermochemical performance parameters determination of propulsion systems, there are some software which are running simultaneous optimization codes to make analysis for different type of propellants and rocket engines; however they are not specific to hybrid rocket engines. Because of the some unknowns behind the hybrid rocket propellants, development of individual propulsion tool is being a mandatory for this project.

1.3 Previous Studies

First studies about this research subject made by author in 2015 for Graduation Project. That study involves just a basic thermochemical performance analysis and 2D altitude calculations for sounding rockets. In that project, thermochemical performance analysis were realized with decreased water – gas shift reactions. An excel format was developed to find adiabatic combustion chamber temperature for a given propellant set and their fixed oxidizer to fuel ratio. In the meantime PARS Rocketry Group developed Turkish first hybrid rocket engine to verify this tool. Then this tool is written in MATLAB to make it more reliable and faster. The first improvement was realized with extension on thermochemical performance analysis code. Firstly, detailed chemical equations set is established for paraffin – liquid nitrous oxide combustion. This increased the reliability and precision of the code.

To find the optimum oxidizer to fuel ratio and specific impulse match, an ability was gained to code to run itself for different oxidizer to fuel ratios. Hence thermochemical performance analysis code is became to be able to find adiabatic flame temperature, performance properties of propellants and optimum point of oxidizer to fuel ratio and specific impulse match. This study is also integrated with 2D altitude calculations to optimize the propulsion system size (especially solid fuel grain) according to rocket design constraints such as diameter of body. This study is represented on AJCPP [19]. After previous works in this study, the new main tools are staging of launch vehicle, extended 2D trajectory calculations and feed system calculations extension on propulsion code. Aerodynamic and gravitational loss calculations and statistical data are also included in 2D trajectory calculations.

1.4 Scope & Objectives

The main goal of this thesis is developing a design optimization tool which is including a propulsion performance code to design a hybrid rocket engine more quickly; to evaluate an optimal launch vehicle within the limit of the given constraints. Main objective of this design tool is meeting an expectation of following main tasks:

I) Preliminary mission design of a launch vehicle (propulsion and trajectory optimization of a variable system) to produce the optimum Hybrid Launch Vehicle.

II) Multistage Launch Vehicle optimization with integration of propulsion system design code.

The preliminary design and optimization of launch vehicles has been the focus of several research studies. In the conceptual design of a launch vehicle, minimization of gross lift-off mass for a specific mission is primary objective. The minimum GLOW can be obtained by staging and propulsion optimization with integration of commercial trajectory analysis tools. This type of interdependent optimization is an alternative design algorithm, whose characteristics are more reliable for a launch vehicle design process [20] In the scope of this thesis, first step is staging (determining the mass distribution along the launch vehicle, number of stages and the propulsion and propellant masses) which is for minimizing the gross lift-off mass of the launch vehicle just after determination of propulsion system parameters.

The staging code is structured and solved based on the required velocity change for orbit insertion of the LEO satellites. A general formulization of statement is created to solve staging problem to handle different launch vehicle configurations with arbitrary number of stages which can be serial, parallel or clustered. Moreover various propulsion system designs (with changeable thrust profiles) can be integrated directly to this problem for finding optimum stage configuration. Aerodynamic (atmospheric) and gravitational losses which are directly related to propulsion system and dimension of the launch vehicle considered with approximate assumption of the conditions during staging optimization. After determination of possible stage configurations regarding to mission requirements; propulsion system design, actual mass and geometry determination of the vehicle and development costs are engaging to whole program algorithm to finalize the required launch vehicle preliminary design as an iterative process.

The following actions are taken to improve the tool precision and to achieve the target goals.

1. Improving of the Propulsion Tool (discussed in Chapter 3):

i. Providing one fuel – oxidizer combination performance data by detailed thermochemical performance code
ii. Providing a proper regression rate model (which is special to solid fuel nature) which is validated with PARS Rocketry Group hybrid rocket motor hot fire tests.
iii. Creating a thrust profile to use it in trajectory simulations.
iv. Sizing of the grain according to design limitations
v. Feed System modeling to simulate tank pressure changes during self-pressurized discharging of oxidizer

2. Launch Vehicle Dimensioning and Mass Module (Chapter 3 and 4):

i. Pressurized feed system (both self-pressurized and pressurant-requiring) historical data, and overall propulsion system dimensioning and developing a generalized statement for the masses of solid fuel Case and a Liquid Oxidizer tanks
ii. Providing Aerodynamic Shelf, Structure and Overall Stage Mass Models
iii. To dimension the nozzle and fairing components [21].
iv. To estimate the mass of individual components

The final step of the algorithm is trajectory simulation. The importance of trajectory simulations and optimization is minimizing the atmospheric flight time to decrease aerodynamic drag losses and gravitational losses. As a result of these advantages, increasing on the precision of trajectory calculations will increase the launchers efficiency also. Trajectory optimization is not the main goal of this thesis. Hence, a 2D trajectory calculation (with approximate assumptions) is enhanced to involve in the main tool, moreover; a commercial software is used to compare the results. On the other hand, a historic and statistical analysis have to be performed in the perspective of minimization of drag and gravity losses [22, 23].

These optimization efforts for both overall design and trajectory of the vehicle prior to critical design phase is important to increase the reliability and decrease the cost of launching (per kilogram) resulting with saving on both money and time. This is the main idea behind the targeted goals and scope.

1.5 Thesis Outline

Chapter 1 is the introduction to the thesis. This chapter includes a view from wide perspective of the rocket technology and discusses the motivation of this study and explains the scope, objectives and organization of the thesis.

Chapter 2 presents a general literature review for nanosatellites and their launch opportunities, hybrid rocket motors. The existing study concerned with the design optimization of nanosatellite launch vehicles. Some historical and statistical data about launchers is also given to pursue researchers that although small satellite technology have got big milestones in the past years, nonetheless the development of nano-launchers were not parallel to these improvements.

Chapter 3 describes firstly the idea behind the hybrid rocket motors their description from both chemical and physical perspectives. This chapter shows the all subsystem elements of hybrid rocket motors and their designing criteria's and technics. These subsystems are mainly feed system, injectors, oxidizer tanks, solid fuel grains and nozzle. The main part of this study which is a propulsion performance code, also introduced within this chapter. Because of the volume of propulsion systems, they are main element of launch vehicles, as a result this chapter firstly focused on the motor design. This part of the chapter is existing to show the idea behind the sizing model of hybrid rocket motors.

Chapter 4 focuses on the conceptual design code in order to determine the launch vehicle layout regarding to selected user defined limits. Such as diameter, length and maximum available instant thrust. One of the main purpose during the design is maximizing the payload mass while satisfying the mission constraints. Chapter 4 gives firstly information about the problem behind the code development and overview of resulted algorithm which is the skeleton of the main design tool. The modules of main tool also investigated in this part of the thesis detail. The first module is velocity change module and the second one is staging module. Moreover, propulsion system sizing algorithm, material selection, mass models and the trajectory model were involved within this chapter. This chapter is ended with trajectory simulation of launch vehicle. An author developed basic 2-D trajectory code and a commercial software are presented to finalize the design process. This chapter presents the mathematical framework and illustrative examples of the algorithm as Nassi – Schneiderman flow diagrams to find optimal vehicle configuration in the early design phases by simultaneous change on the propulsion system and thrust profile.

Chapter 5 includes the validation process of the tool. Firstly, the propulsion performance code is verified and validated. The resulted plots and test results comparisons are showed within this chapter. Then the mass module and the trajectory module of this conceptual design tool is validated via running the designed and operational launch vehicle information. At the end of this Chapter a nanosatellite launch vehicle is designed via developed tool according to initial given constraints. Hence this chapter deals with firstly the validation of the tool then the initial sizing of the nanosatellite launch vehicle, stage analysis, required propulsion system design and trajectory calculations are included. The proposed launch vehicle is illustrated within this chapter. Required thrust profile for each stages is showed in graphs as one of the main output of tool.

Chapter 6 shows the present hybrid rocket motor and sounding rocket studies by PARS Rocketry Group. These studies are the validation activities for the current study.

Chapter 7 draws the whole picture of the study in summary. This chapter also includes a brief information about future steps of the research.

2. LITERATURE REVIEW

The purpose of this chapter is to present history behind the current existing study. Launch vehicles and nanosatellite market trends are presented within this chapter. Because of the main structure of this study depends on the practice of the optimization theory, a brief overview of several optimization methods and their advantages and limitations are given to show general history of knowledge.

This chapter is organized in four sections. Section 2.1 presents available literature on the hybrid rocket motors, Section 2.2 shows trajectory optimization methods history, Section 2.3 gives an introductory summary of available software packages and academic studies for design optimization of launch vehicles. Finally, the existing research on nanosatellites and their launch opportunities are given in Section 2.4 including their relevance to the subject of this thesis.

2.1 Brief Survey about Hybrid Rocket Propulsion

2.1.1 History

The concept of HRP is not new, as can be seen from the Figure 2.1.

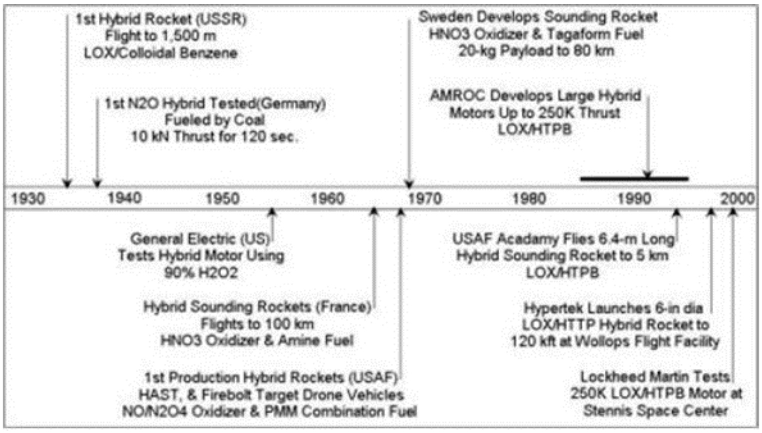

Figure 2.1: Hybrid Rocket motors between 1960 and 2000.

During the last two decades, hybrid rocket propulsion has been gaining more and more attention. One of the propellants is stored as a solid grain in the combustion chamber whereas the other, which is usually the oxidizer, is stored in liquid form in a separate tank. The combustion starts with ignition and injection of oxidizer into the solid fuel grain. This concept features some advantages and disadvantages compared to both solid and liquid rocket motors. The main advantage over the solid motors is throttling possibility and re-start capability. Moreover, the concept of separate oxidizer tank and combustion chamber provides safety and reliability [24]. The main advantage over the liquid motors is the much lower development cost and simplicity.

Because of their safe and reliable nature, there is an increment on the hybrid rocket motor projects in last years. Moreover, this technology has small cost of development and comparatively cleaner environmental characteristics. The main theatrical disadvantages of HRM’s are creating the main research areas which are low specific impulse compared to LRMs and low regression rates compared to composite solid propellants. These are the main subjects of researches during last decade with combustion efficiency.

The earliest work on hybrid rockets was realized in 1933 by Tikhonravov and Korolev. This first hybrid rocket was powered by a propellant combination of LOX and jellified gasoline. This hybrid rocket is used to launch GIRD-9 sounding rocket which reached an altitude of 1.5 km. In the late 1930s, both Germany and the USA started also developing hybrid engines and a rocket was taken to an altitude of about 9 km in June 1951 [25].

Some of the first hybrid rocketry studies with hybrid rocket propulsion made by Pacific Rocketry Society is documented on mid-1940s. These studies based on wood, solid wax with carbon-black additive, and rubber-based fuels with oxygen as an oxidizer. Many experiments were done by several researchers. According to their experimental study results a program is developed to build a hybrid rocket motor “XDF-23” which is consisted of liquid oxygen and rubber-based fuel. The XDF-23 hybrid rocket motor successfully powered the rocket to an altitude of approximately 9 km in June 1951.

Flight tests of the earliest hybrid sounding rockets were accomplished by the French Aerospace research center ONERA (Office National d'Études et de Recherches Aérospatiales) and Volvo-Flygmotor in Sweden. The propellants used in ONERA's sounding rockets were a combination of liquid nitric acid and solid amine fuel consisting of metatoluene diamine/nylon. Over the testing period, from April 1964 to November 1967, ONERA launched eight sounding rocket vehicles with recorded apogees of more than 100 km. Like the former program, Volvo-Flygmotor experimented on a hypergolic propellant configuration of nitric acid as liquid oxidizer and Tagaform (polybutadiene with aromatic amine additive) as solid fuel. This 20 kg payload capability hybrid vehicle was flown in 1969 to an altitude of 80 km [25].

There are many experiments by General Electric Company for hybrid rocket propulsion. Hypergolic propellants were investigated by this company and solidated them from the late 1940s to mid-1950s. The research, spearheaded by G. Moore and K. Berman [26], involved the burning of 90% hydrogen peroxide and polyethylene as oxidizer and fuel, respectively. A unique rod and tube grain design configuration, more than 300 motor static tests were performed to analyses and characterize the combustion process. According to static test experiment; uniform surface burning, combustion insensitivity caused by grain cracks, high combustion efficiency and stable combustion are observed. According to Korting study research results and experiments showed that the regression rate is affected by the following factors: the mass flux, the geometry and the fuel- oxidizer composition. Polymethylmethacrylate (PMMA) and polyethylene (PE) was used as solid fuel and gaseous oxygen (GOX) was used as oxidizer. The pressure interval in study was from 0.3 to 2.0 MPa. The regression rates varied from 0.2 to 1.0 mm/s [27].

Lockheed Martin Corporation developed and launched a large scale hybrid sounding rocket which is composed with liquid oxygen and hydroxyl-terminated polybutadiene [28].This was a part hybrid sounding rocket program which is initiated in 1999 to demonstrate a single-stage hybrid propulsion system power. A multiport grain configuration was involved with dimensions of 61 cm diameter and 174 cm long. The motor had a thrust value which it powered a rocket is approximately 267 kN and the motor was specifically designed to reach an apogee of 100km. Launch event is realized from NASA Wallops Flight Facility in December 2002, the sounding rocket accomplished its flight with an apogee of 71 km. Similar projects, previously carried out by Starstruck and American Rocket Company (AMROC) in the 1980s, were unsuccessful due to oxidizer valve malfunctions; they were frozen by the low temperature liquid oxygen.

These projects were developed with Hydroxyl-terminated polybutadiene (HTPB) which is a synthetic rubber, as a fuel and the nitrous oxide as oxidizer, better known as laughing gas. According to AMROC studies which are performed in test facility of NASA Stennis Space Center. These engines were ranging from 4.4kN to 1.1MN thrust and they were tested successfully tested. In the meantime, SpaceDev Company tested engines using PMMA as a solid fuel with the combination of different oxidizers which are liquid oxygen, nitrous oxide and hydrogen peroxide. The regression rate study of the propellant combination of HTPB (solid fuel) and the oxygen (oxidizer) was realized by Chiaverini [28]. The designed hybrid rocket motor geometry was laboratory scale, allowing a radiography system to obtain on real time data of the instantaneous solid fuel regression rate in any axial position. Additives effects on regression rate of solid fuel, such as aluminum powder, were also investigated within Chiaverini's study.

Another research about the additives for HTPB solid fuel and ammonium perchlorate was studied by [29]. According to these studies, the regression rate was improved while reducing the port diameter. In 2002 Arif Karabeyoğlu identified a class of paraffin fuel that burns at high regression rate and he proposed a regression rate model whose name is liquefying layer model [30]. In the meantime, a higher scale test series with GOX hybrid engines were conducted in the Hybrid Combustion Facility of NASA Ames Research Center. These tests showed nice agreement with the small scale, lower pressure and small mass fluxes conducted by the Stanford University laboratories. Therefore, it was confirmed a higher regression rate to solid fuels based on paraffin with chamber pressures and mass fluxes conditions representative of commercial applications. Moreover in the same year Lockheed Martin Space Systems Company, with the Stanford University, and following the Karabeyoglu et al researches, launched two sounding rockets of 4 in external diameter, based on hybrid technology and paraffin-nitrous oxide propellant pair [30].

Waxman et.al has studies about the characterization of nitrous oxide to show all details of this oxidizer nature. Because of its two phase nature, nitrous oxide injection process is not as easy as compare to liquid oxygen and the other liquid propellants. According Waxman's studies, feed system coupled instabilities of hybrid rocket motor is investigated. These studies suggest some solution regarding to instability problems.

The other research was on mixing of the gaseous oxygen and nitrous oxide to improve the efficiency of the propellant combination. These studies carries out by the Karabeyoglu team under the auspices of this space propulsion group company [31]. It has seen from the history that the first applications of HRPE were as sounding rockets, launch vehicles, micro satellites and tactical missiles. On the other hand a decade ago, this technology is also applied in sub-orbital manned vehicles, like Space Ship One and more recently the Space Ship Two. These vehicles powered with hybrid rocket engines which have HTPB and nitrous oxide propellant combination inside. These engines were based on AMROC Studies which are explained above in this chapter. The illustrations regarding to Spacehip One showed below, Figure 2.2 [32].

Figure 2.2 : Virgin Galactic Spaceship One.

These attempts were epic for hybrid rocket engine history. Because usage of hybrid rocket motors in a manned sub-orbital vehicle shows that their safety and reliability at the same time. That's why these attempts were milestones of this technology.

All of these studies and launch attempts provided a strong basis for today's studies and attempts. Just after first years of 21^{th} century, there are many of studies about hybrid rocket motors which are worked by universities, private companies and rocketeers. These studies investigated every subpart of hybrid rocket motor technology in detail. A summary about these companies and university studies will be mentioned in 2.1.4. The historical improvement of the HRM's are listed below according to their date of the improvement and based on the country in Table 2.1.

2.1.2 Hybrid rocket motor fundamentals and functionality

A classical HRM separates the liquid or gaseous oxidizer from the solid-fuel grain in the storage compartments prior to the feed valve opening. This concept reduces the ignition failures. A typical schematic of classical HRMs is given in Figure 2.3 [25].

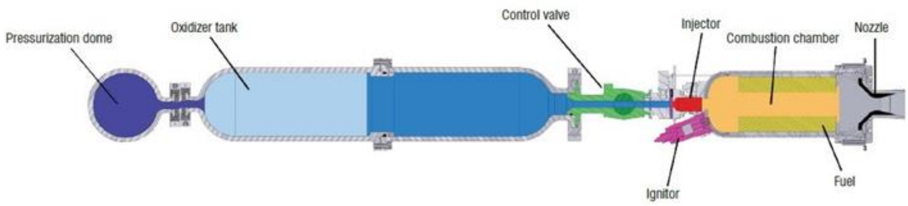

Figure 2.3 : HRM General Overview.

In general the main components of the HRMs are; 1) Pressurizing Tank, 2) Oxidizer Tank and 3) Combustion chamber. For some liquid oxidizers a pump is necessary to force injection of the liquid propellant into the combustion chamber. These types of pressurization systems include a turbine driven pump. Some of the propellants (like nitrous oxide) can pressurize itself with its thermophysical properties which brings this self-pressurizing specification. A pump system is complicated and non-cost effective compare to these type of self-pressurant system. On the other hand an external pressurant tank can be employed for self-pressurized and non-self-pressurized oxidizers. This type of system choices depend on the engineering, mission and design requirements. All of these pressurization properties and systems are used to maintain the oxidizer pressure as constant as possible throughout the injector to combustion chamber. The oxidizer flow is controlled by a valve in the feed system which also has the capability of throttling the mass flow rate to the combustion chamber.

Table 2.1 : Historical Improvement of HRMs

Date	Country	Name/Company	Fuel Type	Thrust (kN)	Result
1932-33	Soviet	GIRD-9	LOX/Jellified Gasoline	0.266	Unsuccessful
1937	Germany	-	Coal/Gas N_2O	10	Unsuccessful
1938-39	Germany	-	LOX/Graphite		Unsuccessful
1938-41	USA	California Rocket Society	Coal/GOX	-	Unsuccessful
1947	USA	Pacific Rocket Society	Douglas Fir Wood/LOX	-	Unsuccessful
1951	USA	XDF 23	LOX/HTPB (Rubber)	-	Successful
1951	USA	Rocket Miss	Mix Acids/KCLO3-Asphalt	-	-
1956	USA	General Electric	H2O2/PE	-	Successful
1956	France	**ONERA HRM start to research.**			
1960	USA	Rocketrdyne	Plexy/Oxygen	-	-
1961-62	**Marxman and Gilbert explained the first regression rated formula.**				
1960's	USA	US Army	F2/O2-(PB+AN)wLithium		Successful
1961	USA	**UTC has started their hybrid rocket researches.**			
1964-67	France	ONERA	-	10kN-100km	Successful
1965-80	**There is no exact developments because of the scientific researches.**				
1971	Sweden	Volvo Flygmotor	-	80km	-
1984	USA	STARTRUCK/Dolphin	LOX/HTP B	155.7	Prt. Successful
1974-87	Germany	-	-	-	-
1985	USA	AMROC	LOX/HTP B	324	Prt. Successful
1989	USA	AMROC/SET-1	LOX/HTP B	Launch	Unsuccessful
1995	USA	**NASA-DARPA created HPDP program.**			
1996-97	USA	eAc-Hyperion 1A	N20/HTP B	-	Successful
1999	USA	NASA-DARPA	-	250	Successful
2001	USA	Cesaroni Hyperion 1C	-	112.5	Successful
-	USA	Cesaroni Hyperion 2	-	225	Planned

Spray of the oxidizer realized throughout the injector. Injector is important to provide designed mass flow rate, required atomization of the oxidizer and stability of combustion. Hence injector production requires a carefully manufacturing process in order to well atomize to very fine droplets the oxidizer. In particular, an injector design is based on liquid rocket motors with the commonly used: 1) axial showerhead, 2) impinging, and 3) swirl flow configurations. A pre-combustion chamber is required at the fore end of the motor to achieve proper vaporization of the atomized oxidizer flow which supplies the combustion mechanism. The length to diameter ratio of the pre – combustion chamber is 0.5 to account for efficient residence time of the propellant [33]. Moreover, a post-combustion chamber, which is between the end of grain and the nozzle in general, is required in order to provide additional volume for well mixing of combustion products just prior to flow through the For the post – combustion, a length-to-diameter ratio of 0.5 to 1.0 is commonly adopted for the post combustion chambers for best mixing of the gaseous products [33]. These additional combustion chambers can improve HRM's poor volumetric fuel efficiency (volume of fuel / volume of chamber) [34]. HRM working sequences can be listed in summary as below:

1) Igniting the igniters.
2) Opening the oxidizer tank valve to start the mass flow of the oxidizer.
3) Injection of the oxidizer into the combustion chamber via injector.
4) The motor provides an internal pressure as a result of the combustion and then thrust will start.
5) After burning time the oxidizer tank valve is closed and stop the motor.

Combustion Model of Hybrid Rocket Motor can be explained with following expressions. Liquid oxidizer is injected to burning surface. Reactions are occurred on the burning surface and the combustion process gives its products as gases into combustion chamber. This is general statement of the combustion for HRM type rocket motors. Polymer based solid fuel HRM systems combustion process occurs in boundary layer. As a result of this situation, combustion cannot be occurred between boundary layer and burning surface instead of the directly burning surface. As a result of the high Reynolds Number of the injection process, the boundary layer have to be turbulent.

The diffusion flame region is occurred after ignition. The heat is transferred to burning surface via convection and radiation. This energy flux provides the splitting the fuel particle from the burning surface for vaporization. This vaporized particles are transferred to flame region via diffusion effect. These transferred vapor particles create a reaction with oxidizer. The heat of this reaction provides sustainability to split the fuel particles from the surface. This mass flux (as a result of the splitting) affects the heat transfer between the burning surface and flame region. This effect calls “Block Effect”. This situation reduces the regression rate of the fuel [30]. To solve this problem; many different techniques are experienced, nonetheless; the required efficiency was not achieved. Then some interesting experiments are performed with solidified cryogenic fuels. These experiments were resulted with increased regression rates compare to traditional polymer based fuels. These fuels called as “Liquefying Fuels”.

Classical models were not enough to explain the combustion process of these liquefying fuels. After many of different experiments, Karabeyoglu develops a model that calls “Liquid Layer Theory”. Validation of this theory with lab-scale hybrid rocket motor static fire tests shows that the theory outputs and test results were coincidence with each other .This liquefying property of the cryogenic fuels shows that the availability of the fuels that may have same property. Because of their storage conditions which required well cooled storage buildings, cryogenic solid fuels are difficult to store and transfer. This situation leads to research new fuels that may have same liquefying property. Hence paraffin was found as a result these researches.

According to liquid layer theory, increasing the mass transfer from the burning surface to flame zone is most important mechanism to increase the regression rate. HRM solid fuel had to design to provide an additional mass transfer mechanism to increase the regression rate. This additional mechanic mass transfer can be supplied by droplets from a thin low viscosity liquid layer on the fuel surface [30]. This model shown in Figure 2.4 [30].

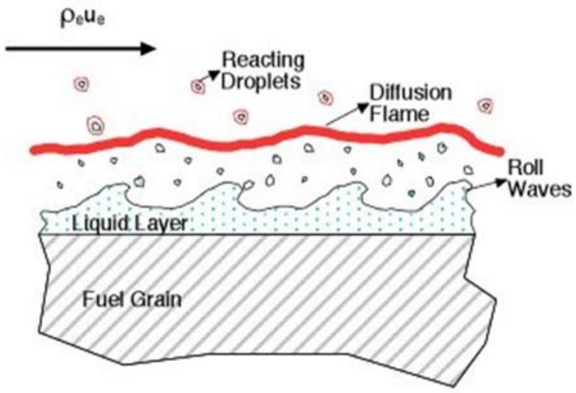

Figure 2.4 : Liquid Layer Theory.

Actually this situation is required a detailed investigation on the combustion. Because there will be fluctuation on the liquid layer along the burning surface. From the good way of the point, this fluctuations provides the droplets. But on the other hand, these fluctuation have to be optimized and model numerically very well to avoid combustion instabilities. This method also called as “Droplet Entertainment Method” in literature. The heat transfer values are changeable locally along the surface because of the high flow rates of the combustion products. As a result of this the regression rate is changeable along the surface.

2.1.3 Advantages and disadvantages with respect to the SRMs and LRMs

Advantages compare to LRMs

1) Hybrid Rocket Motors require only one liquid propellant to control.
2) HRMs are mechanically easier than LRMs.
3) Higher fuel density compare to LRMs.
4) Specific impulse increment availability with some metal and other additives.
5) Fire hazards are lower than LRMs. Safer.
6) Manufacturing process tolerance is higher than LRMs.

Advantages compare to SRMs

1) Explosion risk is much less then SRMs and explosion is controllable.
2) Higher specific impulse.
3) Fuel grain deformation sensibility is lower than SRMs.
4) Chemically easier and manufacturing process tolerance is higher.

5) Green propellants, there is no toxic combustion gas products.

General Disadvantages

1) Mixture ratio shifting during combustion.
2) Mechanically more complicated compare to SRMs.
3) Low regression rates.
4) Combustion instabilities.

2.1.4 Current studies

In Europe; there are many university students and companies are focused on hybrid rocket propulsion. However a small portion of these studies are breaking through for scale-up hybrid rocket motors. Most of the studies are standing on laboratory scale tests. These broke through studies are mostly populated in Holland, Italy, Germany and Norway. In Holland, TU Delft DARE works on hybrid rocket propulsion based on sorbitol and nitrous oxide. Their STRATOS II+ sounding rocket was designed to reach an altitude of 50 km. In October 2015, they launched their rocket and reached to 21.5km which is European student rocketry altitude record. They still work to improve their engines and rockets.

2.1.5 Typical hybrid rocket motor propellants

Different propellant combinations of the hybrid rocket motor due to its unique characteristics make it essential to undertake a comprehensive research. Reveres hybrid rockets its dimension limits is to high compare to classical hybrid rockets compare to oxidizer solid grains. Because of this situation reverse hybrid rocket motors less accessible. A brief of typical oxidizers and fuels of hybrid rocket propulsion systems is given below according to reference [28] and [33].

The major fuels are the polymer based materials such as polyethylene. The rubber and plastics are carbon based materials. That's why their usage. Typical polymers are; Polybutadiene (PB), Polyethylene (PE) and Plexiglas (polymethylmethacrylate or PMMA). The polybutadiene monomer (PB with the formula C4H6) can be further sub classified as PB-acrylonitrile (PBAN), PB-acrylic acid (PBAA), hydroxyl-terminated polybutadiene (HTPB), and carbon-terminated PB (CTPB). The PMM fuel is most studied fuel in the past due to its cost effective and availability properties. The HTPB is most used fuel nowadays because of its inherent safety, low cost and availability. Addition to these polymer based fuels there are hydrocarbon based fuels. The typical hydrocarbon based fuels are; paraffin waxes, metatoluene diamine/nylon, and, in the early history of hybrid technology, coal and wood. Additives can be uniformly mixed with PB polymers and paraffin waxes to enhance the fuel density and consequently reduce vehicle mass fraction. Table 2.2, which has been reproduced from [28], shows a list of common hybrid propellant combinations.

Table 2.2 : Common HRP combinations

Fuel	Oxidizer	Optimum O/F	Specific Impulse Sea Level	c*(m/s)
HTPB	LOX	1.9	280	1820.3
PMMA	LOX	1.5	259	1660.9
HTPB	N2O	7.1	247	1604.5
HTPB	RFNA	4.3	247	1590.7
HTPB	FLOX	3.3	314	2042.5
PE	LOX	2.5	279	1791.3
PE	N2O	8	247	1599.6
Paraffin	LOX	2.5	281	1804.4
Paraffin	N2O	8	248	1605.7
HTPB/Al(%40)	LOX	1.1	274	1757.5
HTPB/Al(%40)	N2O	3.5	252	1636.8
Cellulose	GOX	1	247	1572.5
Carbon	Air	11.3	184	1224.4
Carbon	LOX	1.9	249	1598.7
Carbon	N2O	6.3	236	1521.6
JP-4	NP	3.6	259	1669.1

2.2 Brief Survey about Micro-Nano Satellites & Launch Vehicles

Micro and Nano satellites are coming into glance more than more compare to previous years because of their low development cost and technology availability. Moreover, they can provide a big range of missions such as earth observation, and telecommunication. Generally, these scale of payloads are mainly secondary payloads for many of launch vehicles, because with current technology, there is no launch vehicle to transport a 10 kg nanosatellite to its desired orbit.

This situation creates a gap in the launch vehicle industry as mentioned above. There are many companies which are pretender to meet with this demand. According to Spaceworks Enterprise market study [35] for number of developed under 50 kg satellites yearly, this market has a potential for near future. The growth forecast for these satellites is showed in Figure 2.5 [35]

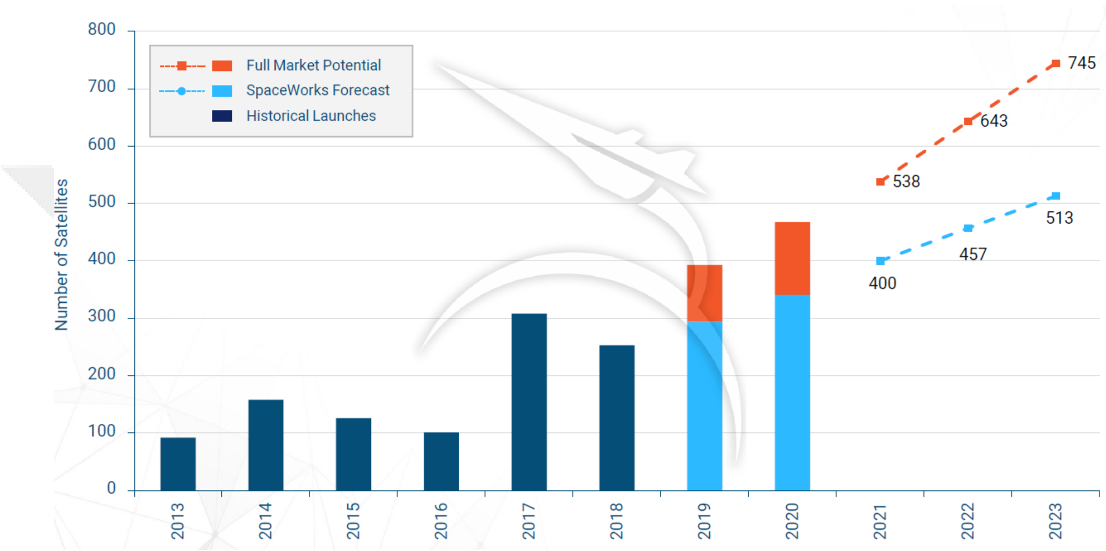

Figure 2.5 : Forecast of Nano-Micro Satellites.

As a result of these statements, small/micro satellite launch vehicle market is growing rapidly with the new entrants from all around the world. This market gap on these area and the feasible costs to develop this technology without big amount of money are exciting many of space sector investors. Moreover, there are many of student teams or companies also to develop launch vehicles for approximately under 150 kg payload LEO missions. These student teams/companies are coming together with these space sector investors to enter the market as soon as possible. When the latest status of market is analyzed there are approximately 38 companies which are actively working to develop their small/micro launch vehicles. [36]. It can be also interesting to mention that 5 of these companies are working hybrid rocket launch vehicles.

Firstly mention about the world's first operational commercial small launch vehicle Electron. This launch vehicle is developed by RocketLab Company to transport a 150 kg payload for 550 km SSO orbit. [37] One of the student team which became a launch vehicle company is PLD Space based on Spain. For now, they are developing a suborbital sounding rocket which will carry 100 kg payload to 120 km altitude. The other student based company is Vector. VECTOR H is their micro satellite launch vehicle which will carry 120 kg payload to LEO. [38] The comparison table for some of the micro launchers is showed in Figure 2.6. This table is gathered from PwC market study. [39]

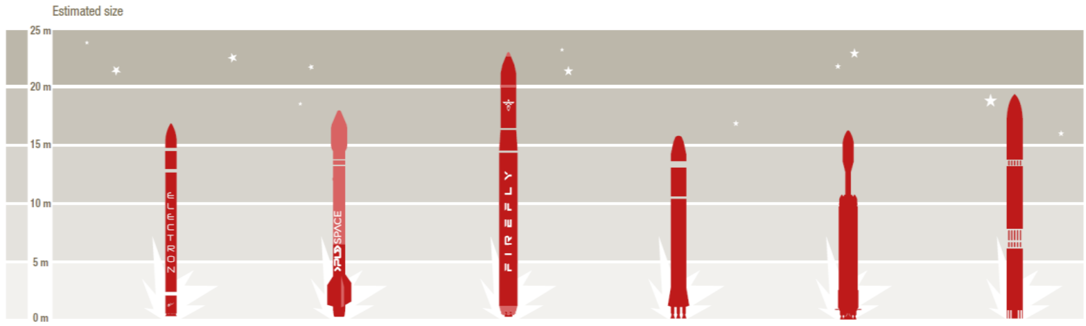

System	Electron	Arion 2	Alpha	Vector H	Taymyr 7	VLM 1
Manufacturer	Rocket Lab	PLD Space	Firefly Space Systems	Vector Space Systems	Lin Industrial	CTA
Country of Origin	USA / New Zealand	Spain	USA	USA	Russia	Brazil
Max payload	225 kg LEO	150 kg LEO	200 kg LEO	120 kg LEO	180 kg LEO	200 kg LEO
First launch	2017 (expected)	2021 (expected)	Unknown	Unknown	Unknown	2018
Status	In development	In development	Most likely cancelled	In development	In development	In development

Figure 2.6: Operational and In-Development NSL.

Table 2.3 : Non-Operational Hybrid Rocket Motor Powered LV Companies

	RocketCrafter	**Gilmour Space**	**HyImpulse**	**Nammo**
Vehicle Name	Intrepid	ERIS - S	-	North Star
Propellant Combination	LOX/3D-Print	H_2O_2/ 3D Print	LOX/Paraffin	H_2O_2/HTPB
Payload	150	200	500	20
Altitude	LEO	LEO	LEO	LEO

2.3 Propulsion Modules

There are many different modules developed by different studies such as NASA's Chemical Equilibrium Application (CEA). There is an additional propulsion analysis module which name is Rocket Propusion Analysis (RPA). ESA has itheir own propulsion module which name is ESPSS. Moreover, many of the universities are developing their own propulsion modules.

3. HYBRID LAUNCH VEHICLE DESIGN AND MODELING

The first purpose of this chapter is to present the physical and chemical background of designing a hybrid rocket engine. Second purpose of this chapter is defining the subparts of the hybrid rocket motors and giving details about their modeling process. The third and final goal is explaining the dimensioning of the launch vehicle via geometry models of each individual part of the vehicle.

The thermochemical performance code details and description is given also in this chapter. Algorithm behind the thermochemical performance code, its inputs and also desired outputs are detailed within this chapter.

3.1 Description of the Hybrid Rocket Motor Physical & Chemical Models

A HRM can be separated into three control volumes to analyze its performance during the combustion. In this study, these three control volumes were independently modeled and also coupled between each other to execute the overall motor performance parameters. The first control volume is discharging process of oxidizer. These control volumes are shown in Figure 3.1.

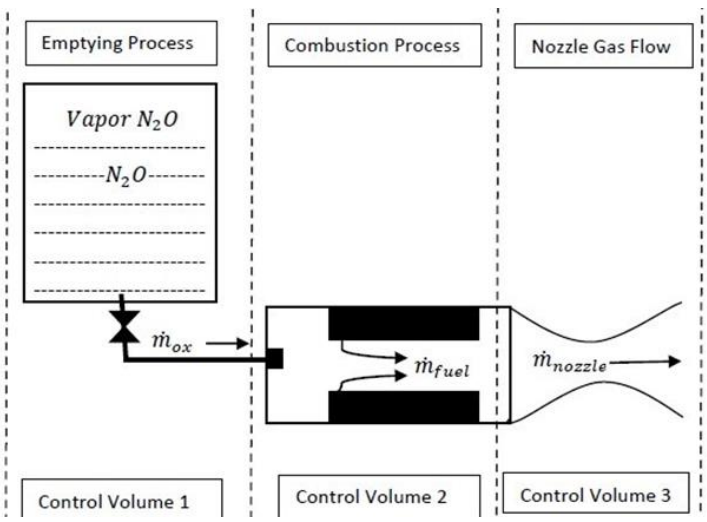

Figure 3.1: Control Volumes of HRM.

The oxidizer mass flow rate is modeled by the discharging process of the tank, and the discharging model is available for blow-down of self-pressurizing oxidizer. The combustion chamber is the second control volume where thermochemical performance analysis and ballistic modeling of the solid fuel grain are performed. The sizing of the solid fuel grain is analyzed according to the regression rate and the specific impulse values. Thirdly, the rocket nozzle function is used to accelerate the gas flow to supersonic velocity at the nozzle outlet, where it produces thrust. In addition, the mass flow rate of the combustion products within control volume three is the main factor in determining the flow velocity at the nozzle outlet.

3.2 Oxidizer Feed System Design

3.2.1 Oxidizer tank pressurization

G Feed system is one of the most important subjects in HRM propulsion systems since it provides the oxidizer mass flow at required level. The tank pressure must be constant to maintain the oxidizer flow steady. For this reason, different pressurization systems are developed. One of these systems contains additional pressurant gas tank to pressurize the oxidizer tank. This pressurant gas is generally inert gas such as helium which is transferred into the oxidizer tank via regulators and vanes. The high pressure of the inert gas can be reduced by a regulator to the oxidizer tank level through a controllable process.

The blow-down model of the self- pressurized oxidizer has been selected in this study. The oxidizer fluid properties change with time due to discharging during the combustion. Understanding these changes on thermodynamic properties is essential to determine the mass flow rate into the combustion chamber through the injector4. The vapor pressure of the nitrous oxide during the blow-down process can be calculated by using vapor temperature and liquid-vapor mass within the tank. The thermodynamic properties of liquid nitrous oxide depend on the oxidizer tank ambient temperature. Different type of feed systems are shown in Figure 3.2 [15].From left to right, pressurant gas regulated system, supercharged blow-down and self-pressurized blow-down process.

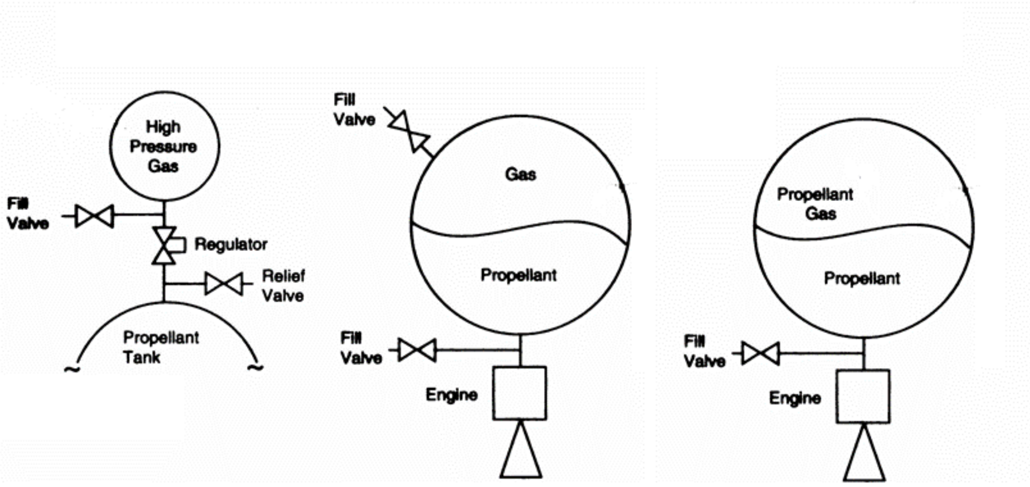

Figure 3.2: Feed Systems.

According to this thesis choices, first and final selections will be considered in the rest of the work. A pressure regulated system, which requires an external pressurant gas tank, provides continues constant pressure to the combustion chamber. These systems coming with an additional mass and complexity over their advantages. These systems are generally used for LOX type propellants to pressurize them to required oxidizer pressure to maintain the mass flow rate from oxidizer tank to combustion chamber.

On the other hand, self-pressurized systems are not capable to provide a constant oxidizer pressure for a constant mass flow rate from oxidizer tank to combustion chamber. These systems always have a pressure drop between the beginning and final moment of the process. As a result, the mass flow rate is decreasing and O/F ratio is increasing. This created O/F shift is resulted with uncontrolled modulated thrust.

Hence, in this work although a self-pressurized propellant is used as an oxidizer, an external regulated high pressure gas system is integrated to whole system to maintain the oxidizer mass flow rate as constant. At the same time because of the required additional gas amount is lower than LOX type system, as a result the final dimensions and masses of additional are lower compare to traditional systems.

3.2.2 Liquid nitrous oxide flow models & injector design

In control volume 1, the properties of the self-pressurizing propellant vary as the oxidizer tank is discharged over time. Modeling this change in the fluid thermodynamic property is critical for determining the oxidizer mass flow rate through the feed line. The thermodynamic state variation of nitrous oxide is dependent on the oxidizer tank environmental temperature and on the liquid flowing out of CV1. During the blow-down process, there is a loss of internal energy due to the draining of the liquid nitrous oxide. As the tank empties some of the liquid oxidizer evaporates to equilibrate the system resulting in a decrease in thermal energy. The loss in thermal energy of the system, as the change in oxidizer temperature, reduces the tank pressure accordingly. This causes a noticeable decay in motor thrust which correlates to the decrease in vapor pressure of nitrous oxide, that is, tank pressure. Injector design is influenced by the mass flow rate which depends on the conditions inside tank. That’s why selection of tank discharging model is important to model system well close to real conditions.

When a typical constant pressure injector design, the propellants are assumed as quasi-incompressible liquids the incompressible discharge coefficient can be written as below equation 3.1 [42].

$$\dot{m}_{ox} = C_d \cdot A_0 \cdot N \cdot \sqrt{\rho_{ox} 2\Delta P} \tag{3.1}$$

Discharge coefficient should be determined accurately to get better design outputs for injector. The mass flow rate is constant, area is total injector hole area, ΔP is the pressure difference across the injector. This model assumes that the flow through the orifice is single phase and that variations in density are negligible.

Existing Two-Phase Injector Models are investigated in below sections.

3.2.2.1 Homogeneous equilibrium model

Self-Pressurizing propellants are generally operating at the saturation pressure and when flowing across the injector port, flow losses cause drop on the exit pressure well below the saturation pressure. This is a local static pressure drop. This drop can be resulted with vapor cavitation and make flow choke through injector port. This situation will limit the designed condition of oxidizer mass flow. Assumption of phase equilibrium between liquid and vapor phases of the propellant shows there will be no velocity difference (no-slip) between both phases. This flow condition is referred to as homogeneous equilibrium. Leung [42] shows that the fluid enthalpy drop across the orifice can be used to express the injector mass flux, when the no-slip fluid equilibrium assumption is applied, and if the expansion process is assumed isentropic.

This mass-flux model is homogeneous equilibrium model (HEM) [47].

$$\frac{\dot{m}_{\mathrm{HEM}}}{A_c} = C_d \cdot \rho_2 \sqrt{2\left(h_1 - h_2\right)} \tag{3.2}$$

In equation (3.2), $\dot{m}_{HEM}$ is the homogeneous equilibrium mass-flow rate, ρ_2 is the total two-phase fluid density, h_1 is the upstream specific enthalpy, and h_2 is the downstream specific enthalpy. If there is big pressure difference across the injector orifices (downstream pressure is gradually lowered for a fixed upstream pressure to increase the mass flow rate) the HEM predicts a critical pressure ratio across the injector, where the mass flux (also its mass flow rate in actual) reaches a maximum value. The traditional incompressible expression does not limit the mass flow rate to a maximum value for higher pressure drop across the injector orifices. HEM-predicted mass flow rates are significantly lower than actually occur according to experimental results for low-aspect-ratio (ratio of length to diameter) orifices which tend to favor the incompressible model of equation (3.1) [43]. On the other hand, the other reason for this effect can be flow slip between vapor and liquid phase according to some explanations of researchers [44]. This nonequilibrium effect does not allow for the flow to reach thermodynamic equilibrium for a short-run length [43].

3.2.2.2 Homogeneous non-equilibrium (HNE) model

When L/D (aspect ratio) increases, the measured mass flux value approaches to predicted mass flux value of HEM, [45]. This nonequilibrium effect is more pronounced as the incoming pressure rises. The homogeneous nonequilibrium model (HNE) was developed to calculate and include to model this mass transfer rate by assuming that vaporization is not finished till the oxidizer has got over a minimum distance along the flow path. [45] These nonequilibrium effects can be accounted in The HNE model by creating a nonequilibrium multiplier to scale the predicted rate of vapor–liquid mass transfer. When the orifice length increases, the HNE model converges on the HEM model predicted rates. When compared with the HEM, the

HNE model results in a higher overall mass flux. From general point of view, this model is sensible for most fluids through longer tube like orifices; but it is not ready to apply for simple orifices with low aspect ratios. Also, the developed correlation multiplier for the scale factor does not perform a good role in the model when compared with nitrous-oxide injector data. Typically, the HNE model over predicts the mass flux by a significant amount for nitrous oxide [43].

3.2.2.3 Nonhomogeneous nonequilibrium model (NHNM)

To overcome these modeling gaps, Dyer et al. [43] have proposed a model which gathers the incompressible equation (3.1) models and HEM. When the fluid remains longer across the injector orifices, fluid has time to vaporize and reach to homogeneity according to this nonhomogeneous nonequilibrium model (NHNM). The degree of vaporization that occurs depends on the rate of bubble growth when compared with the dwell time within the port. [46]. Fyer et al proposed a modified form of the cavitation number which is proportional to the ratio of the vapor-bubble-formation time to the port-dwell time. The NHNE weighting parameter is given as a function of the orifice inletP_1, the outlet pressure P_2, and the vapor pressure P_V of the fluid at the outlet temperature, the equation 3.3;

$$k = \sqrt{\frac{P_1 - P_2}{P_v - P_2}} \tag{3.3}$$

According to NHNE obtaining equations, the mass flux should vary between the HEM results and incompressible predictions in a smooth way. Hence The NHNE formulation can be created va weighting these two models. [47], equation 3.4 ;

$$\frac{\dot{m}_{\mathrm{NHNM}}}{A_c} = \frac{\left(\dot{m}_{\mathrm{inc}} / A_c\right) + \kappa\left(\dot{m}_{\mathrm{HEM}} / A_c\right)}{1+\kappa} \tag{3.4}$$

The experimental data, which is collected by Dyer et.al from over 100 hot fires of nitrous-oxide hybrid motors with mass flows up to 0.6 kg/s, shows that this model works well to predict the injector mass flow rate when upstream fluid properties are well characterized. This model predicts mass flows to with approximately 85% accuracy share in all cases; moreover with an overall experimental standard deviation of 98.5%.

3.2.2.4 Adiabatic two-phase entropy model development

This model is involved by Whitmore et.al. [47]. In this section, development of the complete engineering model which is built on NHNE model via taking the entropy as basis, for the N_2O tank evacuation is presented. It's expected that developing an entropy based model will overcome the mass-flow inaccuracies for both the HEM and HNE models. According to rules of thermodynamics, the total entropy of CV1 (sum of the entropy of discharged nitrous oxide and the entropy of nitrous oxide in the tank) is equal to initial total fluid entropy of the system before evacuation starts. On the other hand, the total entropy in the tank decreases (as mass leaves the tank) during the evacuation process of nitrous oxide. Thus, it can be said that the flow is isentropic regarding to entire process which is represented as CV1 in this study. However the process is nonisentropic only for propellant tank which is one part of the CV1.

This isentropic assumption for the expansion process is quite similar to isentropic flow assumption which is used to develop De Laval flow equations for modelling performance of rocket nozzles [48] For working fluid of this study as liquid nitrous oxide, the isentropic assumption provides a model which offers accurate prediction for the critical parameters of tank pressure, tank temperature and exit mass flow value.

The other assumptions for this flow are listed below:

1) The pressure inside the tank can be equalized instantly during the evacuation process with the advantage of small enough tank volume.
2) There is no external heat transfer.
3) Hydrostatic pressure of the fluid is negligible compared with the vapor pressure at saturation point.
4) The oxidizer tank wall is assumed to be adiabatic and in thermal equilibrium with the propellant.
5) The liquid phase consists of pure nitrous oxide whereas the gas phase is a mixture of nitrous oxide vapor and helium gas.
6) Potential and kinetic energy of the propellant is neglected.
7) The gravitational head in the tank is negligible for both static and flight tests.

Vapor only phase is allowed to be calculated when all liquid has been discharged from the tank. To improve the model condition, a vapor vent at the top of the tank will be included despite of there is no such a vent in this study. Figure depicts this tank model. As the liquid escapes through the outlet, fluid boils off to create additional vapor that occupies the volume at the top of the tank. Some of the vapor simultaneously condenses near the liquid interface.

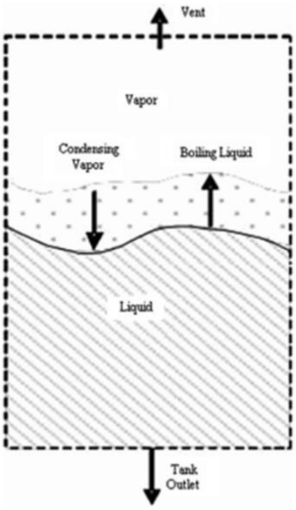

Figure 3.3: Blowdown Process.

Consider the blowdown process of an oxidizer tank partially filled with liquid nitrous oxide as shown in Figure 3.3. [47] The tank ullage contains a mixture of nitrous oxide and helium vapor which expels the liquid nitrous oxide out of control volume 1 due to the differential pressure between the tank and combustion chamber. Following the laws of mass and energy conservation, with general assumptions to simplify the model, the pressure history of the system can be solved for the initial known parameters of nitrous oxide mass and tank temperature.

Firstly the initial conditions have to be defined:

To define the initial conditions of saturated propellant, NIST saturation property charts are used calculate initial densities of the saturated liquid and vapor phases for given initial temperature and pressure of the saturated propellant in the tank. Firstly, the fluid quality is calculated because the initial propellant mass and the volume of the tank are known. The fluid quality can be calculated as:

$$\chi = \frac{\rho_V \cdot \rho_L - \rho_V \cdot \rho_0}{\rho_0\left(\rho_L - \rho_V\right)} = \frac{\left(\rho_V \cdot \rho_L\right) - \rho_V \cdot \left(m_0 / V_{\text{tank}}\right)}{\left(m_0 / V_{\text{tank}}\right)\left(\rho_L - \rho_V\right)}$$
$$= \frac{\left(\rho_V \cdot \rho_L\right) V_{\text{tank}} - \rho_V \cdot m_0}{m_0\left(\rho_L - \rho_V\right)} \tag{3.5}$$

The specific entropy s_0 can be calculated via equation 3.6 using the calculated value of chi, the specific entropies of vapor and liquid phases (they are looked and found from NIST Tables).

$$s = \frac{s_L \cdot m_L + s_V \cdot m_V}{m_L + m_V} = s_L \frac{m_L}{m_L + m_V} + s_V \frac{m_V}{m_L + m_V}$$
$$= s_L \cdot (1 - \chi) + s_V \cdot \chi \tag{3.6}$$

The total entropyS_0, which is stored in the tank at the beginning of the discharging, is calculated via multiplying the initial oxidizer mass in the tank by the initial effective specific entropy, the equation 3.7:

$$S_0 = m_0 \, s_0 \tag{3.7}$$

Let's define the two phase propagation algorithm; after completion of the first step, which is the specification of initial conditions, with the initial conditions now specified, propellant properties in the tank can be calculated during entire evacuation process. As mentioned before there is a vent, which vents the vapor continuously, on the top of the tank in order to avoid over pressurization during the motor firing. However, as mentioned before, in this study there is vent hole on the oxidizer tank. Thus, the vent mass flow rate is neglected during this study ran. Both the liquid propellant escaping from the tank outlet and the vapor propellant escaping from the vent are modeled to provide to users more choices. The liquid mass flow rate from the outlet of the tank (or through an orifice):

$$\dot{m}_{L,\,\text{out}} = A_{\text{out}} \cdot \frac{\left(\dot{m}_{\text{inc}} / A_c\right) + \kappa\left(\dot{m}_{\text{HEM}} / A_c\right)}{1+\kappa} = \left(A_{\text{out}} \cdot C_{\text{dout}}\right)$$
$$\cdot \frac{\left[\sqrt{2\rho_L\left(P_{\text{tank}} - P_{\text{out}}\right)\left(P_v - P_{\text{out}}\right)} + \rho_2\sqrt{2\left(P_{\text{tank}} - P_{\text{out}}\right)\left(h_{\text{tank}} - h_{\text{out}}\right)}\right.}{\sqrt{P_v - P_{\text{out}}} + \sqrt{P_{\text{tunk}} - P_{\text{out}}}} \tag{3.8}$$

The mass flow from the top vent can be expressed by equation 3.9:

$$\dot{m}_{\text{vent}} = \left(A_{\text{vent}} \cdot C_{d_{\text{veat}}}\right) \cdot \sqrt{\gamma P_{\text{tank}} \cdot \rho_V \left(\frac{2}{\gamma+1}\right)^{(\gamma+1)/(\gamma-1)}} \quad (3.9)$$

In equations. 3.8 and 3.9, $C_{d,out}$ and $C_{d,vent}$ are the discharge coefficients for the tank-outlet orifice and the vapor vent, A_{out} and A_{vent} are the exit areas of the tank outlet orifice and vapor vent, P_{tank} is the vapor pressure in the tank, γ is the ratio of specific heats for the vapor thermodynamic state, and P_{out} is the downstream pressure. P_v is the vapor pressure at the tank-outlet temperature. equation 3.8 assumes that the vapor pressure in the tank is sufficient to insure that the outlet fluid is liquid and only flashes to vapor after entering the injector port. During the discharging process, the sum of mass of liquid that is expelled from the orifice and the mass of vapor vented off the top of the tank, is the total change of mass in the tank for a unit time. The new total tank entropy is can be expressed as below in equation 3.10:

$$S_{i+1} = S_i - \left(m_{L,\text{out}} \times s_L\right)_i - \left(m_{\text{vent}} \times s_V\right)_i \quad (3.10)$$

In equation 3.10, the subscript i is the discrete time index, and the time interval between indices is Δt In equation 3.9, $\dot{m}_{L,out}$ is the liquid mass that escapes through the tank-outlet valve, and is $\dot{m}_{vent}$ the vapor mass that escapes through the top vent. These mass values are calculated by numerically integrating Eqs. 3.8 and 3.9:

$$\begin{aligned} m_{i+1} &= m_0 - \int_0^t \dot{m}_{L,\text{out}}\,\mathrm{d}t - \int_0^t m_{\text{vent}}\,\mathrm{d}t \\ &\approx m_i - \left(\dot{m}_{L,\text{out}} + \dot{m}_{\text{vent}}\right) \cdot \Delta t \end{aligned} \quad (3.11)$$

The updated effective tank-specific entropy is calculated via using the mass and total entropy from the current step;

$$s_{i+1} = \frac{S_{i+1}}{m_{i+1}} \quad (3.12)$$

And the new effective density can be calculated by;

$$\rho_{i+1} = \frac{m_{i+1}}{V_{\text{tank}}} \quad (3.13)$$

The new temperature, pressure, and fluid quality in the tank can be calculated with the new specific entropy and density values by using a table lookup on the data in the NIST property tables described earlier in this section. The remaining fluid masses in the tank can be calculated with:

$$\begin{bmatrix} m_V = c \times m_{i+1} \\ m_L = (1 - c) \times m_{i+1} \end{bmatrix} \tag{3.14}$$

Equations 3.8–3.13, along with the saturation properties of Figures 3.2 and 3.3, collectively make up the engineering model that describes the tank-evacuation tank-evacuation process. These equations are numerically integrated over time (and the database is parsed) to continuously calculate the tank-fluid state properties as a function of time. This model intrinsically takes into account the masses of liquid and vapor that change phase due to boiling and condensation. The model also allows for some fraction of two-phase flow through the lower-tank outlet port.

$$\dot{m}_{V,\,\mathrm{out}} = A_{\mathrm{out}} C_{d_{\mathrm{out}}} \cdot \sqrt{\gamma P_{\mathrm{tank}} \cdot \rho_V \left(\frac{2}{\gamma+1}\right)^{(\gamma+1)/(\gamma-1)}} \tag{3.15}$$

$$\dot{m}_{v,\,\mathrm{out}} = A \cdot C_d \sqrt{\frac{2\gamma}{\gamma-1}\rho_v P_{\mathrm{tank}} \left[\left(\frac{P_2}{P_{\mathrm{tank}}}\right)^{2/\gamma} - \left(\frac{P_2}{P_{\mathrm{tank}}}\right)^{(\gamma+1)/\gamma}\right]} \tag{3.16}$$

3.3 Thermochemical performance code

This section describes the combustion process occurring in a hybrid rocket motor while utilizing various oxidizers and fuels. General state of all reactants and products from the reactions are defined and used to calculate adiabatic flame temperature. In the absence of any work interactions and any changes in kinetic or potential energies, the chemical energy released during a combustion process either is lost as heat to the surroundings or it is used internally to raise the temperature of the combustion products. The smaller the heat loss, the larger the temperature rise. In the limiting case of no heat loss to the surroundings (Q = 0), the temperature of the products reaches a maximum, which is called the adiabatic flame or adiabatic combustion temperature of the reaction [49].

The process is refined to account for dissociation of minor species after an adiabatic flame temperature is found by assuming a stoichiometric and fuel rich reaction. Therefore, element balances must be performed in order to achieve it. Mole numbers are calculated for each exhaust gas constituent, and the combustion reaction can be modeled for varying oxidizer to propellant ratios. Several reactions are used to determine the mole numbers of the combustion products according to the chemical kinetic mechanism. Gibbs minimization method has been used to determine equilibrium constants, which are used in calculation of the mole numbers. Afterwards, they are used in enthalpy equilibrium calculations. Hence, the adiabatic flame temperature, other variables of combustion process and the performance parameters of propellant combination can be evaluated as the results of this code.

3.3.1 Simplified reaction mechanism for N_2O/Paraffin propellant combination

Reaction mechanisms can contain only few steps (elementary reactions) or several hundred in general. Reduced kinetic mechanism can be obtained from the detailed one by two main assumptions. First, quasi-steady state approximation which can be described as some (fast) intermediate species or radicals reach an equilibrium state. Also, their mass fractions are nearly constant, and their overall reaction rates are negligible. Second, partial equilibrium assumption can be described as some elementary reactions in the chemical reaction mechanism reach equilibrium [50]. The number of reactions and their species decrease as a result of these assumptions.

The amount of reactions and their species reduces as a result of these assumptions, and this is very important for developing more compact code with a narrower range of validity. The next step is fluid analysis for interaction between each species via reacting flow transfer and momentum. Reduced mechanisms, which are useful for multidimensional simulations, are more difficult when heavy hydrocarbons fuels are considered. The formulation of global chemical kinetic mechanism is convenient, but it leads to various difficulties. Even though the number of species and reactions are decreased considerably, the reaction constants still have complex expressions. The system of algebraic equations combined with the standard reaction constants become mathematically complex, and these reaction rates can also feature molar fractions with negative exponents leading to practical difficulties, especially in the initiation of the simulation [41].

Table 3.1 : Simplified reaction mechanism of the current study

$C_{28}H_{58} \rightarrow 14C_2H_4 + H_2$	$O + H_2 \leftrightarrow OH + H$
$C_{10}H_8 + 5O_2 \rightarrow 10CO_2 + 4H_2$	$OH + OH \leftrightarrow H_2O + O$
$C_2H_4 + O_2 \rightarrow 2CO + 4H_2$	$H + OH \leftrightarrow H_2O + M$
$2CO + 1/2O_2 \rightarrow 2CO_2$	$O_2 \leftrightarrow 2O$
$2H_2 + 1/2O_2 \rightarrow 2H_2O$	$H_2 \leftrightarrow 2H$
$CO + O \leftrightarrow CO_2 + M$	$O + N_2 \leftrightarrow NO + N$
$CO + OH \leftrightarrow CO_2 + H$	$O_2 + N \leftrightarrow NO + O$
$H_2 + O_2 \leftrightarrow OH + OH$	$N + OH \leftrightarrow NO + H$
$H + O_2 \leftrightarrow OH + O$	$2H + O \leftrightarrow H_2O$
$OH + H_2 \leftrightarrow H_2O + H$	$H + O \leftrightarrow OH$
$N_2 + O_2 \leftrightarrow 2NO$	$N + O \leftrightarrow NO$
$N_2 + 3H_2 \leftrightarrow 2NH_3$	$N_2 \leftrightarrow 2N$
$C_2H_4 + 2N_2 \leftrightarrow 2HCN + 2NH$	$CO + H_2O \leftrightarrow CO_2 + H_2$

In Table 3.1 the presented combustion system involves 13 species and 26 reaction steps and this system mainly consists of N_2O and $C_{28}H_{58}$ as propellants. With a pyro solid fuel grain on the chamber head to serve as an ignition heat source and some catalytic effects for the nitrous oxide, a diffusion flame is established upon the injection of nitrous oxide into a combustion chamber with a single port $C_{28}H_{58}$ grain. The generated heat from the diffusion flame continues to decompose the nitrous oxide and $C_{28}H_{58}$ through convective and radiative heat transfer. Then, the decomposed gas species are mixed and combusted in the diffusion flame to produce mainly water vapor and carbon dioxide [10].

If the solution is made by only one global reaction, the combustion temperature will be much higher than actual value due to the absence of dissociation reactions of major species with minor species and radicals. The dissociation reactions are generally highly endothermic; therefore, the combustion temperature decreases.

3.3.2 Thermochemical performance algorithm

The equilibrium constants have to be determined for each reaction of simplified reaction mechanism. The equilibrium constant is given below:

$$K_p = e^{\frac{-\Delta G}{R \cdot T_c}} \tag{3.17}$$

K_p is equilibrium constant of the reaction, and ΔG is the Gibbs free energy of the reaction. In addition, the standard state Gibbs function change can be defined as:

$$\Delta G_T = \sum_{P}^{n} (n_i \times g_{f,i}) - \sum_{R}^{n} (n_i \times g_{f,i}) \tag{3.18}$$

At start, the Gibbs free energy values of the all species have to be determined. The final step of this thermochemical code is iterative, and it uses the results of this process. In addition, this step is also iterative because of the change of the Gibbs free energy values with the combustion temperature.

The code has five general interval 0 – 1000 K, 1000 – 2000 K, 2000 – 3000 K, 3000 – 4000 K, and 4000 – 5000 K to find the combustion temperature. All iterative processes are calculated step by step in these intervals until they converge. In addition, the mole number of species must be formulized or solved numerically. The second and third step depend on each other. As a result of the third step the final mole numbers of species will be determined. In addition, the mole numbers are defined according to the first temperature assumption.

Heat of formation values for reactants and products have to be determined for this process. Nitrous Oxide heat of formation can be found from literature, and the paraffin wax heat of formation can be found similar to nitrous oxide. According to third step requirements the enthalpy change of the combustion products have to be determined via empirical formulations, which are published at NASA JANAF Table [52].

$$\frac{H^{\circ}T}{RT} = a_1 + a_2\, {}^{T}\!/_{2} + a_3\, {}^{T^2}\!/_{3} + a_4\, {}^{T^3}\!/_{4} + a_5\, {}^{T^4}\!/_{5} + {}^{b_1}\!/_{T} \tag{3.18}$$

Enthalpy change of the products during reaction can be given as:

$$\Delta h = H^{\circ}T + h_f \tag{3.19}$$

$$\sum_{R}^{n}\left(\bar{h}_f^{\circ} + \bar{h} - \bar{h}^{\circ}\right) = \sum_{P}^{n}\left(\bar{h}_f^{\circ} + \bar{h} - \bar{h}^{\circ}\right) \tag{3.20}$$

Once the reactants and their states are specified, the enthalpy of the reactants H_{react} can be easily determined. The calculation of the enthalpy of the products $H_{product}$ is not so straightforward since the temperature of the products is not known prior to the calculations. Therefore, the determination of the adiabatic flame temperature requires the use of an iterative technique unless equations for the rational enthalpy changes of the combustion products are available. According to this study case the equation 3.20 becomes:

$$\left(n_r \times h_{f,r}\right) - \left(n_p \times h_{f,p}\right) = \Delta H_P \tag{3.21}$$

Enthalpy changes of products are calculated according to equation 3.19 with an assumption as the combustion temperature value and the formation enthalpies of both reactants and products are known. Also, the mole numbers of the products are calculated according to assumed combustion temperature value. The combustion temperature value must be iterated till the both sides of the equation 3.19 converged and are equal to each other.

Finally, the propellant performance values can be calculated after determination of the combustion temperature according to thermochemical results. These parameters are listed below:

- Specific heat ratio,
- Specific impulse,
- Characteristic exhaust velocity,
- Thrust coefficient,
- Nozzle dimensions.

First, the specific heat with constant pressure of the products must be determined to calculate the specific heat ratio of the products.

$$C_{p,mix} = \frac{\sum_P n_p \times C_{p,procuxts}}{\sum_P n_P} \tag{3.21}$$

$$k_{mix} = \frac{C_{p,mix}}{C_{p,mix} - R_u} \tag{3.22}$$

Second, the characteristic exhaust velocity can be calculated according to specific heat ratio value.

$$c^* = \frac{\sqrt{k_{mix} \times R_{mix} \times T_c}}{k_{mix} \times \sqrt{\left(\frac{2}{k_{mix}}\right)^{\frac{k_{mix}+1}{k_{mix}-1}}}} \tag{3.23}$$

To calculate this value the specific gas constant of the products have to be determined from:

$$R_{mix} = \frac{R_u}{M_{products}} \tag{3.24}$$

Also, the thrust coefficient can be calculated with the value of specific heat ratio.

$$C_f = \sqrt{k^2 + \frac{2}{k+1} + \left(\frac{2}{k+1}\right)^{\frac{k+1}{k-1}} - \frac{P_0}{P_c}} \tag{3.25}$$

Now the specific impulse of the hybrid propellant can be calculated from:

$$I_{sp} = \frac{c^* \times C_F}{g_0} \tag{3.26}$$

As a result of this code an O/F ratio- I_{sp} graphic is obtained. This graphic is used to select optimum O/F ratio for maximum thrust performance.

3.4 Solid Fuel Regression Rate Model & Combustion Chamber Pressure

The combustion mechanism of an HRM essentially relies on the propellant regression rate characteristics. The regression rate of a solid fuel, also referred as the burning rate or pyrolysis process, determines the degree of oxidizer-to-fuel mixture composition throughout the local grain port during the combustion process. The classical regression rate [53] equation can be written as:

$$\dot{r} = \alpha \dot{G}_{ox}^{n} \tag{3.27}$$

α, n are the ballistic coefficients of propellant combination, and $\dot{G}_{ox}$ is total oxidizer flux in the fuel grain which can be described as the oxidizer mass flow per unit area. The increment on the speed and density of the reactants from the solid fuel surface means increment on the transferred reactant value from the boundary layer. This increases the oxidizer mass flux and the regression rate.

$$\dot{G}_{ox} = \frac{\dot{m}_{ox}}{A_p} \tag{3.28}$$

There are four main effects to determine the ballistic performance of the rocket such as:

Liquid nitrous oxide phase change.

Tank pressure changes

Oxidizer to fuel ratio shift during the combustion process.

Thermodynamic properties changing during the rocket operation.

The laws of the conservation of mass and energy are applied to the combustion chamber to obtain the change in the chamber pressure, oxidizer-to-fuel ratio and combustion gas properties.

$$\frac{dP_c}{dt} = \frac{k_c - 1}{V_c}\left[\dot{m}_{ox} - \dot{m}_f - \left(\dot{m}_{out} \cdot c_p \cdot T_c\right)\right] - \frac{k_c \cdot P_c}{V_c} \cdot \frac{dV_c}{dt} + \frac{P_c}{V_c - 1} \cdot \frac{dk_c}{dt} \tag{3.29}$$

The fuel mass flow rate is a function of regression rate and the port geometry.

$$\dot{m}_f = \rho_f \dot{r} A_p L \tag{3.30}$$

Where the ρ_f, A_p , L represent the fuel density, burning area and the length of the grain.

$$\dot{m}_{out} = P_c A_t k_c \sqrt{\frac{\left[\frac{2}{k_c+1}\right]^{\frac{k_c+1}{k_c-1}}}{k_c R T_c}} \tag{3.31}$$

Where A_t is the cross sectional area of the throat. R is the gas constant. T_c is the combustion temperature, and k_c is the specific heat ratio of gas combustion gas.

3.5 Nozzle Design

The first criteria of the nozzle design is that the speed of the combustion gases has to be 1 Mach at the throat. First, the combustion products and their thermochemical properties have to be determined. The combustion products are assumed as unique gases, and all calculation can be made by using the combustion pressure and temperature.

$$C = \sqrt{k_{mix} R_{mix} T_c} \tag{3.32}$$

C is the speed of sound. This parameter will be used for determining the Mach number of the combustion products.

$$M_e = \sqrt{\frac{2 \times \left(\left(\frac{1}{P_c} \right)^{\frac{k-1}{k}} - 1 \right)}{k-1}} \tag{3.33}$$

The Mach number at the exit and the nozzle expansion ratio have a relation as given below:

$$\frac{A_e}{A_t} = \frac{1}{M_e} \times \sqrt{\left(\frac{1 + \frac{k-1}{2} \cdot M_e^2}{1 + \frac{k-1}{2}} \right)^{\frac{k+1}{k-1}}} \tag{3.34}$$

Critical throat area and diameter can be determined as:

$$A_t = \frac{\dot{m}_{nozzle}}{\rho_c \times \sqrt{k_{mix} \times \left(\frac{R_u \times T_c}{M_e}\right) \times \left(\frac{2}{k_{mix}} + 1\right)^{\frac{k_{mix}+1}{k_{mix}-1}}}} \tag{3.34}$$

The exit diameter can be found by using the equation 3.34. The propulsion system design code have the capability of developing two nozzle configurations: bell- or conical-shaped nozzles. The code determines the critical design parameters of contour shaped nozzle and shapes the internal converging-diverging geometry. The output file, which is an excel file, contains the coordinates required to form the nozzle's inner geometry. A bell-shaped nozzle differs from a conical-shaped one in the diverging section. It decreases the losses as the flow is gradually turned and trended to an ideal axial direction at the nozzle exit where the divergence angle is smaller compared to conical-shaped nozzles [54]. Two performance correction factors account for combustion efficiency of the gaseous species and the divergence cone angle loss of the De-Laval nozzle.

$$c^*_{actual} = \eta_c c^*_{theo} \tag{3.35}$$

$$\lambda = \frac{1}{2}(1 + \cos\alpha) \tag{3.36}$$

$\boldsymbol{\lambda}$ is cone angle loss coefficient used to calculate thrust reduction across the nozzle, and η_c is the combustion efficiency. Nozzle throat diameter is calculated according to total propellant mass flow rate at $t_b = 1$. The nozzle mass flow rate changes during the combustion process because of both oxidizer mass flow rate changes and combustion pressure changes.

$$\dot{m}_{nozzle} = \frac{P_c A_t}{c^*} \tag{3.37}$$

4. CONCEPTUAL DESIGN TOOL

As mentioned previously the first section, the goal of this thesis is to produce a tool capable of rapid sizing a nanosatellite launch vehicle and its propulsion system (hybrid rocket motor) for LEO missions as a preliminary design. The tool must be malleable hence it can give a design variables outputs for a variety of vehicles based on the provided mission objectives and desired launch vehicle properties. The tool is developed in MATLAB.

This section describes the main tool algorithm with starting definition of the problem statement. After defining the introductions of each module of the tool, primary references which are used to develop modules and verify them, are introduced. The introduced modules during this chapter are mainly staging module, sizing module, mass module and trajectory module. The main equations and algorithms of each module is given in detail. As a result of this, this chapter contains most of the equations which are necessary to develop the code of the tool.

4.1 Problem Definition

As mentioned previously the first section, the goal of this thesis is to produce a tool capable of sizing a nanosatellite launch vehicles and its propulsion system (hybrid rocket motor) for LEO missions. The tool must be malleable hence it can give a design variables outputs for a variety of vehicles based on the provided mission objectives and desired launch vehicle properties. The tool is developed in MATLAB.

The capabilities are this tool are given below;

- Sizing of launch vehicle and its propulsion system,
- Determining the basic geometry of the launch vehicle (lengths and diameters for each stage and the total vehicle)
- Mass estimations of each subsystems.

The main limitations of the tool:

- **Only serial staging is allowed for launch vehicle design.**

  Parallel staging is excluded from this fist version of the tool because of its significant difficulties into the sizing process.

- **The calculated ΔV required for the mission orbit is for a circular orbit.**

  Other types of orbits, including transfer orbits to other celestial bodies, are currently not included for first version of the tool.

- **Only hybrid rocket engines are permitted.**

  Hybrid Rocket Engine development is one of the main idea behind this thesis. One of the main goal is development of green and cost-friendly hybrid launch vehicle for Nanosatellite's LEO missions. As a result of this situation, currently liquid rocket engines and solid rocket engines are not included for this version of tool.

- **The propellant tank diameters are equivalent to the stage diameter.**

  The thickness values of tank insulation, structure and any other item which's surrounding the propellant tank and solid grain case, are neglected for the launch vehicle diameter calculation.

This tool has been divided into different modules in order to develop an easily modifiable code. Each module includes one portion of the sizing, for instance, propulsion module which calculates the thrust requirements and then the number of engines required based on provided engine by user.

To provide an easy readable tool flow, Nassi–Shneiderman (NS) diagrams were created before beginning of the study for each module and they were updated continuously during the coding process. An NS diagram is a visual depiction of the program that details its flow and the logic used [55]. The NS diagram for the system may be seen in Figure 4.1.

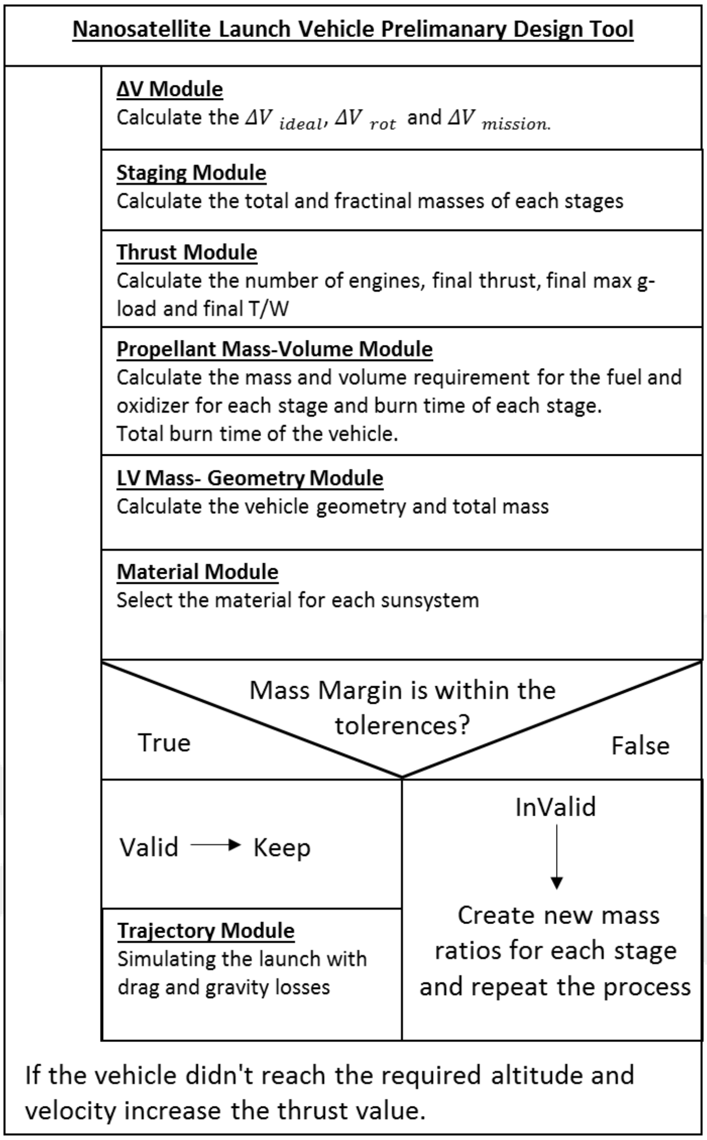

Figure 4.1 : Launch Vehicle Sizing Program NS Diagram

The general steps of the algorithm to size the vehicle are listed below:

1) Request inputs from the user.
2) Determine the specific impulse values for each stage.
3) ΔV calculation which is needed to reach the final orbit.
4) Staging optimization for minimum GLOW.

5) Generating the mass of each stage for the launch vehicle and each stages subsystem masses.
6) Determine the required minimum thrust and burn time according to T/W for all stages. If needed determine the engine numbers according to user input maximum available thrust value.
7) Find the masses and volumes for the fuel and oxidizer for each stage.
8) Size each stage for their geometry determination
9) According to sizing step outputs generate a second estimate for the structure and equipment masses of each stage If there is an out of tolerance difference (which is defined previously) between the original estimate and second estimate, then correcting mass ratios by a factor of ratio between the first and second estimate mass ratios. If the difference between original and second estimate is within defined tolerance, it means that this design is a potential design to consider evaluating.
10) Calculate the atmospheric drags for trajectory simulation. Define applicable the maximum pressure (g force) on the vehicle for determining the maximum thrust.
11) Trajectory Simulation to check. If this thrust and burn time values are not providing required velocity change at the parking orbit, thrust values should be increased with defined range. This step will be repeated till reaching to required velocity change.
12) Perform

All of modules, which are used in above system, are allocated in a main function. When they are needed, they called by main function to evaluate its program purpose to size the vehicle.

Details of modules will be discussed rest of this chapter.

4.2 Modules for Design of Launch Vehicle

4.2.1 ΔV module

This module evaluates the required velocity change of an N-stage launch vehicle ($\Delta V_{vehicle}$) which must be able to insert its payload into desired orbit via overcoming the loss effects from variety sources which are gravity, aerodynamic drag and propulsive changes during the flight. The other losses which are named generally steering losses (also called as yaw losses), although they are negligible during the conceptual design phase of the launch vehicle. Launch Vehicle just do not overcome these effects but also accelerate the payload to orbital velocity (V_{orbit}). This module is created with the information from Curtis and Walker. [56-57]

According to above statements, for evaluation of velocity change to get into orbit ($\Delta V_{mission}$), all of the losses/gains due to various effects should be considered during the calculation phase. The formulation can be expressed as,

$$\Delta V_{\text{mission}} = V_{\text{orbit}} + \Delta V_g + \Delta V_d + \Delta V_p - \Delta V_{gain} + \Delta V_m \tag{4.1}$$

- V_{orbit} is the orbital velocity (Please see Appendix A)
- ΔV_d is the aerodynamic drag loss
- ΔV_p is the propulsive loss due to ambient pressure change,
- ΔV_g is the gravitational loss,
- ΔV_{gain} is the velocity gain due to Earth's rotation ,
- ΔV_m is the performance margin for unexpected disturbances and inaccuracies.

4.2.1.1 Tsiolkovsky's rocket equation

This equation is a famous fundamental equation for the rocketry. It's derived from Newton's second law of motion via governing the relationship between the mass change during the fuel consumption and the rocket velocity. This equation allows to estimate propellant mass of the launch vehicle necessary to accelerate it to desired velocity and can be expressed as;

$$\Delta V_{\text{vehicle}} = C \cdot \ln \Lambda \tag{4.2}$$

$\Delta V_{vehicle}$ is the velocity change of the vehicle,

Λ is the burn-out mass ratio of the vehicle,

C is the effective exhaust velocity of the engine.

This equation shows that there are mainly two parameters which are effecting the overall performance of the vehicle: the burn out mass ratio and exhaust velocity. Λ is a measure of structural efficiency of the rocket. While C is a common performance figure for the propulsion system and depends mainly on the chemical composition of the propellants. The ratio of the initial mass to the final mass is the *burn-out mass ratio* (Λ), can be defined as;

$$\Lambda = \frac{m_0}{m_f} = \frac{m_0}{m_0 - m_p} = \frac{m_s + m_p + m_{pl}}{m_s + m_{pl}} \tag{4.3}$$

In equation 4.3, m_{pl} represents the payload mass. m_0 represents the initial mass, m_p represents the propellant mass, mf represents the final mass, $m_s$represents the structural mass, Λ is in the range from 4 to 14 depending on today's technology according to [58] for a typical multistage rocket. Because of the limitations on I_{sp} and Λ, maximum allowable velocity for the vehicle ($\Delta V_{vehicle}$) is also limited. The effective exhaust velocity (C) can be defined as;

$$C = I_{sp} \times g_0 \tag{4.4}$$

In equation 4.3,

I_{sp} is the specific impulse (vacuum),

g_0 is the gravitational acceleration at sea level (g_0 = 9.80665 m/s2),

I_{sp} value of different type of rocket propellant combinations varies between 180 s - 475 s. Current study employs hybrid rocket propulsion system which generally has 320 s specific impulse (vacuum) for paraffin – nitrous oxide propellant combination.

4.2.1.2 Orbital velocity equation

A launch vehicle should be accelerated to provide the required energy to insert a satellite into its desired orbit by means of velocity and altitude. Calculation of orbit velocity. (V_{orbit}), which is the required velocity to keep the satellites in a specified altitude, is easy to evaluate by using equation (A.1) given in Appendix A. As mentioned previously, this study only employs the circular orbit requirements.

4.2.1.3 Velocity losses and gains

Properly determination of $\Delta V_{mission}$, firstly a trajectory simulation must be run which is taking in consideration the gravity and aerodynamic drag losses. Since a simulation can't be run without a design of launch vehicle, an estimation for the losses should be used during initial design sizing. Most of the texts, [59,60,61,62], recommend a generic assumption for these losses between 1.5 km/s and 1.7 km/s. low Earth orbit and 2 km/s as applied for a rocket launched to a geosynchronous orbit, for instance, [63] proposed 1.5 km/s value for the possible velocity losses [62].

Compare to other loss effects, it is seen that the ΔV loss for the gravity losses (ΔV_g) and the drag losses (ΔV_d) are the most significant ones. According to [54] there is relation between these losses and the lift-off thrust-to-weight ratio (*T/W*). To evaluate the drag and gravity losses in this study, the variations of ΔV_g and ΔV_dversus *T/W* are used as illustrated in Figure 4.x from to [54]. These data sets are gathered and composed from real data samples can be used for rough estimations of drag and gravity losses.

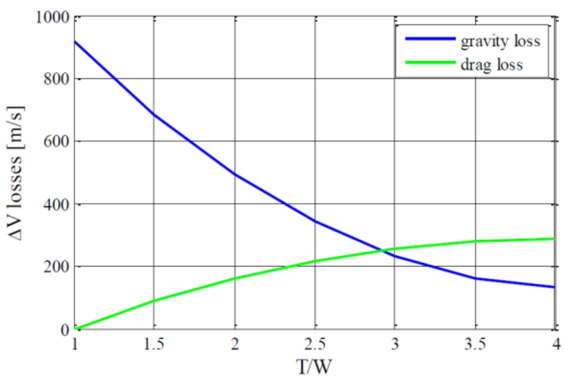

Figure 4.2 : Gravity and Drag Velocity Change Loss vs. T/W [64]

The T/W ratio relates to the thrust, T, and the weight, W, of a rocket. This ratio generally expressed with g. Thrust to weight ratio is limited with a safe range. To avoid any damages on equipment or not harm any manned mission crew, it cannot be high to make the vehicle as faster as possible. Obviously *T/W* should not be smaller than unity for the launch vehicle to leave the launch site in stable way and according to [56], however should be as small as possible to optimize the entire vehicle performance. So, the typical range for lift-off *T/W* values are in the between 1.3 and 2 [56]. This value can be affected by stage configuration and propellant type. Especially in the first stage, which has to overcome a significant air drag; the increment on the *T/W* means, launch vehicle can fly faster the in the dense atmosphere and then drag losses increase, while gravity losses decrease.

On the other hand, the decrement on the *T/W* means that the atmospheric flight will be longer for the launch vehicle hence the gravity losses increase. Approximated values which are showed in obtained from real data samples can be used for rough estimations of gravity and drag losses.

As mentioned at the beginning of this section, the launch vehicles also face with propulsive losses due to the static pressure difference at the nozzle exit during their atmospheric flight. They are much smaller compare to other losses and it’s difficult to estimate them without trajectory simulation. These losses are around 20-50 m/s for reaching a low Earth orbit applications According to [65]. Moreover they also consider a margin of 1-2% to be included in the ΔV budget for unexpected inefficiencies.

The last item to be considered for ΔV budget is rotation of the Earth. This item has positive effect on the ΔV budget, if the payload’s orbit and rotation of earths are in same direction. This situation (also called prograde orbit) decreases the required velocity change. On the other hand, if the payload’s orbit and the earth’s rotation are on the opposite direction, there will be an increment for the ΔV budget. This situation is called as retrograde orbit. In this study, just prograde orbit is considered. The benefit provided by the Earth's rotation may be calculated with equation which is showed below. This is a rough estimation for this study gathered from [56].

$$\Delta V_{rotation} = \pm 4.64 * \cos(\omega) \tag{4.5}$$

In this equation, the latitude of the launch location in radians "ω" and the resulting value of $\Delta V_{rotation}$ is in meters per second. It can be seen that the largest benefit from the Earth's rotation can be gathered by launching at the equator, but the minimum benefit can be included when the latitude approaches either pole because of the reducing on the velocity of earth rotation in radian form.

ΔV Module
Inputs Launch location information, estimated velocity losses
Calculate the ΔV_{ideal}
Calculate the ΔV_{rot}
Calculate the $\Delta V_{mission.}$
Output Calculate the $\Delta V_{required}$

Figure 4.3 : NS Diagram of the ΔV Module.

4.2.2 Staging module

The main aim of staging is determining the mass distribution among the stages with the given estimation of structural mass ratios for this study. The first assumption of structural mass ratios are possible maximum value then it's correcting with mass correction process via mass model of this study after detailed subsystem mass determinations. Staging starts with the definition of parameters such as payload mass, desired orbit and etc. it can be said that in general mission requirements. Using these parameters, staging properties (propellant mass, stages overall masses etc.) are defined to minimize the launch vehicle's gross lift-off mass which is considered as a key parameter for this study. Staging shows a rapid perspective about the vehicle performance capability without a trajectory simulation with the minimum available vehicle data such as structural ratios and specific impulses of engines propellants.

4.2.2.1 Staged rocket design

As mentioned before, just serial staging is included for the tool code. Hence, in this section serial staging will be examined to provide a better knowledge for readers as a summary.

At the beginning, remind the Tsiolkovsky's Rocket Equation for the ideal velocity increment for an *N*-stage rocket expressed as a sum of the velocity increments of the each individual stages via neglecting drag and gravitational attraction in field free space, Tsiolkovsky's Rocket Equation becomes,

$$\Delta V_{\text{vehicle}} = \sum_{k=1}^{N} C_k \cdot \ln \Lambda_k \tag{4.6}$$

In the further analysis of this section, payload of any particular stage (*k*) of N – Stage rocket can be considered as the mass of the remained stages (*k*+1… *N*) as illustrated in Figure 4.4.

$$m_{pl,k} = m_{0,k+1} \tag{4.7}$$

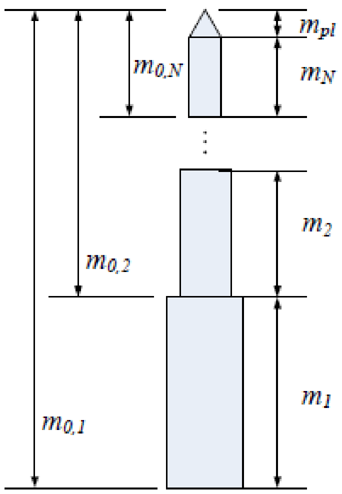

Figure 4.4 : Stage Explanation.

The above picture is show that, for last stage payload is vehicle payload for N –Stage launch vehicle. The expression is below.

$$m_{pl,N} = m_{pl} \tag{4.8}$$

For LEO Launches, in generally the payload is about 2-4% of the total vehicle mass, and for GEO Launches it is around 1% of the total vehicle mass [66]. The *total payload ratio* (λ_t) can be expressed as;

$$\lambda_t = \frac{m_{pl}}{m_0} = \frac{m_{pl}}{m_{0,1}} \tag{4.9}$$

In equation, $m_{0,1}$ is the *gross lift-off mass* (GLOM/GLOW) of the launch vehicle.

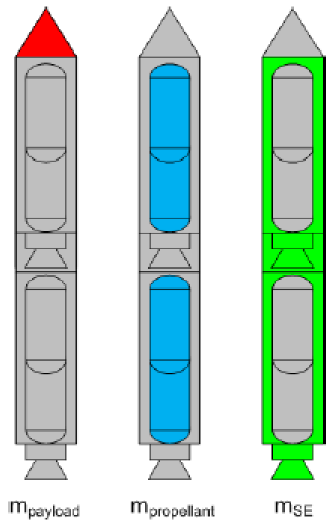

Figure 4.5 : Launch Vehicle's Mass Components (for 2 stage rocket).

The mass of the k^{th} stage can be expressed as according to figure 4.5;

$$m_k = m_{s,k} + m_{p,k} \tag{4.10}$$

The remained mass of the vehicle after k^{th} stage operation finishes can be expressed as according to Figure 4.5;

$$m_{0,k} = m_k + m_{0,k+1} \tag{4.11}$$

The final mass of each stage after its burnout can be expressed as according to Figure 4.5;

$$m_{f,k} = m_{s,k} + m_{0,k+1} \tag{4.12}$$

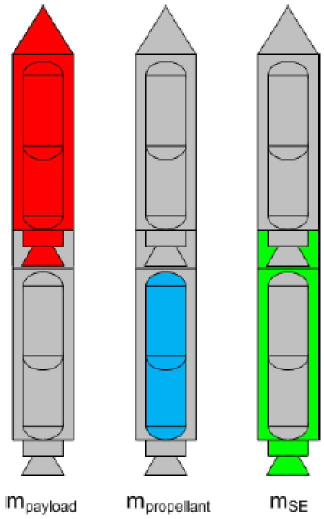

Figure 4.6 : Launch Vehicle’s First Stage Mass Components (for 2 stage rocket).

For serial staging, the overall mass ratio, structural mass ratio, propellant mass ratio and payload mass ratio for individual *k*th stage are defined with the following expressions. All of these ratios are relevant dimensionless ratios.

The overall *mass ratio* of the k^{th} stage (Λ_k) is;

$$\Lambda_k = \frac{m_{0,k}}{m_{f,k}} = \frac{m_{0,k}}{m_{s,k} + m_{0,k+1}} \tag{4.13}$$

The structural ratio is defining the how much of the vehicle is structure. Definition of structure for this study includes the mass of propellant tanks and cases, aero structures, all mechanisms, propulsion systems, control and navigation systems, etc. every system excluding the propellant and the payload. The *structural ratio* of thek^{th} stage (ε_k) can be defined as:

$$e_k = \frac{m_{s,k}}{m_{s,k} + m_{p,k}} = \frac{m_{s,k}}{m_k} \quad (4.14)$$

The propellant ratio is defining the how much of the vehicle is propellant. The *propellant ratio* of the *each individual* stage (ζ_k) can be expressed as;

$$z_k = \frac{m_{p,k}}{m_{s,k} + m_{p,k}} = \frac{m_{p,k}}{m_k} \quad (4.15)$$

According to above equations, the below relation can be written between structural and propellant ratios.

$$e_k + z_k = 1 \quad (4.16)$$

Table 4.1 : Literature of Mass Ratios for Solid Rocket Motors [67]

Engine	Propellant	Insulation	Case	Nozzle	Ignition	Others	Inert	ζ_k	ε_k
Castor IVA	10101	234	749	225	10	276	1494	0.871	0.129
GEM	11767	312	372	242	7.9	291	1225	0.906	0.094
ORBUS 21	9707	145	354	143	16	7	665	0.936	0.064
OBUS 6E	2721	64.1	90.9	105.2	9.5	5.3	275	0.908	0.092
Star 48B	2010	27.1	58.3	43.8	0	2.2	131.4	0.939	0.061
Star 37XFP	884	12.7	26.3	31.7	0	1.3	72	0.915	0.085
Star 63D	3250	71.4	106	60.8	1	11.6	251.1	0.928	0.072
Orion 50S AL	1216	265.2	548	235.4	9.1	21	1079	0.918	0.082
Orion 50	3024	75.6	133	118.7	5.3	9.9	342.9	0.898	0.102
Orion 38	770.7	21.9	39.4	52.8	1.3	10.6	126	0.859	0.141

Many of textbooks state that the structural mass varies typically between 5% and 15% of the stage mass depending. This value is depending on which material, propellant and engine system is used to develop launch vehicle design. [65]. According to this information it can be said that typical values of ζ_k and ε_k are respectively in the range of 0.95 > ζ_k >0.85 and 0.15 >ε_k > 0.05.

The *payload ratio* of the *each individual* stage (λ_k) can be expressed as:

$$\lambda_k = \frac{m_{pl,k}}{m_{s,k} + m_{p,k}} = \frac{m_{0,k+1}}{m_k} \tag{4.17}$$

We can rewrite the overall mass ratio in terms of payload mass ratio, structural mass ratio and propellant mass ratio as described below:

$$\Lambda_k = \frac{1+\lambda_k}{\varepsilon_k + \lambda_k} \tag{4.18}$$

4.2.2.2 Problem definition and solution

The main objective of the staging is designing a launch vehicle which has possible minimum gross – lift of mass (GLOM,m_0) for specified payload mass (m_{pl}). This goal can be achieved with optimal solution for mass distributions among the stages via finding the optimal mass ratios of each individual stages (Λ_k) .The general statement regarding to this problem definition can be expressed as;

$$m_0 = m_{0,1} = \sum_{k=1}^{N} m_k + m_{pl} \tag{4.19}$$

The objective function (minimization of $m0$) can be written in terms of mass ratios of each individual stages (Λ_k) by dividing the above equation by m_{pl} [60] describes that the below relation could be obtained by using the definitions of $\Lambda_k$and ε_k The following expression for whole launch vehicle can be expressed in terms of mass and structural ratio of each individual stages:

$$\frac{m_0}{m_{pl}} = \prod_{k=1}^{N} \frac{(1-\varepsilon_k)\Lambda_k}{1-\varepsilon_k \Lambda_k} \tag{4.20}$$

Taking the natural logarithm of both sides, we get;

$$\ln\left(\frac{m_0}{m_{pl}}\right) = \sum_{k=1}^{N} \ln\frac{(1-\varepsilon_k)\Lambda_k}{1-\varepsilon_k \Lambda_k} \tag{4.21}$$

It can be said that the $\Delta V_{vehicle}$ must be equal to $\Delta V_{mission}$ for a launch vehicle which must able to provide the required velocity change to insert the satellite into the mission orbit. Thus;

$$\Delta V_{\text{vehicle}} = \sum_{k=1}^{N} C_k \cdot \ln \Lambda_k = \Delta V_{\text{mission}} \tag{4.22}$$

To sum up, the optimization problem for the minimization of the GLOM can be formulated as below:

Minimize

$$f = \sum_{k=1}^{N} \ln \frac{(1-\varepsilon_k)\Lambda_k}{1-\varepsilon_k \Lambda_k} \quad \text{(objective function)} \tag{4.23}$$

Subject to

$$g = \sum_{k=1}^{N} C_k \cdot \ln \Lambda_k - \Delta V_{\text{mission}} = 0 \quad \text{(constraint equation)} \tag{4.24}$$

4.2.2.3 Stage optimization

To optimize the required mass of each individual stage, the Lagrange multiplier method will be used, in this study specific impulse, structural ratio ε_k, mission velocity change$\Delta V_{mission}$ and number of stages N are specified to find the optimal mass ratios (Λ_k) for an N – Stage launch vehicle for a given payload mass.

p can be introduced as the Lagrange multiplier ,and combining it with objective function and constraint equation the following augmented objective function can be expressed with $f^* = f + pg$;

$$f^* = \sum_{k=1}^{N} \ln \frac{(1-\varepsilon_k)\Lambda_k}{1-\varepsilon_k \Lambda_k} + p\left(\sum_{k=1}^{N} C_k \cdot \ln \Lambda_k - \Delta V_{mission} \right) \tag{4.25}$$

Expanding the logarithms on the right side leads to;

$$f^{*}=\sum_{k=1}^{N}\left[\ln\left(1-\varepsilon_{k}\right)+\ln\Lambda_{k}-\ln\left(1-\varepsilon_{k}\Lambda_{k}\right)\right]+p\left(\sum_{k=1}^{N}C_{k}\cdot\ln\Lambda_{k}-\Delta V_{\text{mission}}\right) \tag{4.26}$$

The optimality condition can be gathered via differentiating f* *with* respect Λ_k *:*

$$\frac{\partial f^{*}}{\partial\Lambda_{k}}=\frac{1}{\Lambda_{k}}+\frac{\varepsilon_{k}}{1-\varepsilon_{k}\Lambda_{k}}+p\cdot C_{k}\frac{1}{\Lambda_{k}}=0 \tag{4.27}$$

Thus, Λ_k as;

$$\Lambda_{k}=\frac{1+p\cdot C_{k}}{p\cdot C_{k}\cdot\varepsilon_{k}} \tag{4.28}$$

At the mass ratio of above given equation 4.27 forΛ_k, thus *f* will* be minimum; the second derivatives of f* must be positive for all values of mass ratio.

$$\frac{\partial^{2}f^{*}}{\partial\Lambda_{k}^{2}}=-\frac{1+p\cdot C_{k}}{\Lambda_{k}^{2}}+\left(\frac{\varepsilon_{k}}{1-\varepsilon_{k}\Lambda_{k}}\right)^{2}>0 \tag{4.29}$$

Substituting mass ratio equation 4.28 into constraint equation, the following relation can be written:

$$\sum_{k=1}^{N}C_{k}\cdot\ln\frac{1+p\cdot C_{k}}{p\cdot C_{k}\cdot\varepsilon_{k}}=\Delta V_{\text{mission}} \tag{4.30}$$

It can be easily seen from the equation 4.30, the vehicle performance increases with the increasing on the number of stages. To increase the payload fraction of the vehicle, the allowable logical stage number is significant up to 3 or 4. However, more than 4 stages only bring complexity for the propulsion system resulting with reduction of reliability for the launch vehicle, moreover; there will not be a considerable increment on payload fraction. According to Burghes (1974) study, the optimum number of stages is between 2 and 4. [78]

Equation 4.30 can be solved by iterative methods to find the single unknown of p. In this study, Newton-Raphson method, which is a widely used method for solving transcendental equations, was used to solve equation 4.30. Once the p is evaluated for a given set of $\varepsilon_k$and $C_k$then the optimal mass ratios of each individual stages (Λ_k) can be found by substituting p into equation 4.30.

To start the iteration process by the Newton-Raphson method, firstly an initial guess of p_0 should be defined. This initial guess plays an important role in the system to eliminate any errors such as non- convergence and infinite iteration cycles. Thus, determination of the lower and upper limits of solution system will help to solve the system. The limits can be determined as explained below. Following facts are known:

- $\Lambda_k > 1$
- $1 > k > 0$
- $C_k > 0$

"1– $\varepsilon_k\Lambda_k$" in equation (4.31) *must* be greater than zero in order to satisfy Inequality expressed below:

$$\frac{(1-\varepsilon_k)\Lambda_k}{1-\varepsilon_k\Lambda_k} > 0 \tag{4.31}$$

Using equation (4.31)

$$\varepsilon_k\Lambda_k = \frac{1+p\cdot C_k}{p\cdot C_k} = \frac{1}{p\cdot C_k} + 1 < 1 \rightarrow p < 0 \quad \Lambda_k = \frac{1+p\cdot C_k}{p\cdot C_k\cdot\varepsilon_k} > 1 \tag{4.32}$$

Rearranging,

$$1 + p\cdot C_k < p\cdot C_k\cdot\varepsilon_k \quad \rightarrow \quad p < \frac{-1}{C_k(1-\varepsilon_k)} \tag{4.33}$$

Since equation 4.33 must satisfy for every k value, the upper limit for *p* is obtained as;

$$p < \frac{-1}{\min\left[C_k(1-\varepsilon_k)\right]} \tag{4.34}$$

After the calculation of mass ratios of each stage, the payload ratios can be rearranged from equation 4.33 as;

$$\lambda_k = \frac{\Lambda_k \varepsilon_k - 1}{1 - \Lambda_k} \tag{4.35}$$

The mass of each stage can be evaluated using the equation 4.34 with the known values of λ_k for each individual stages. This process will be a recursive equation system with beginning from the N^{th} stage to first stage.

$$\begin{gathered} m_N = \frac{m_{pl}}{\lambda_N} \\ m_{N-1} = \frac{m_{pl} + m_N}{\lambda_{N-1}} \\ \vdots \\ m_1 = \frac{m_{pl} + m_N + m_{N-1} + \cdots + m_2}{\lambda_1} \end{gathered} \tag{4.36}$$

Minimized GLOW Value can be calculated as:

$$m_0 = \sum_{k=1}^{N} m_k + m_{pl} \tag{4.37}$$

Each stages structural mass ratios can be calculated as:

$$m_{s,k} = \varepsilon_k \cdot m_k \tag{4.38}$$

Each stages propellant mass can be found with:

$$m_{p,k} = m_k - m_{s,k} \tag{4.39}$$

Finally, the staging optimization is finished based on the equations for serial staging. The final step for this module is evaluating ΔV's for each individual stage which can be expressed as ΔV_{stage}.

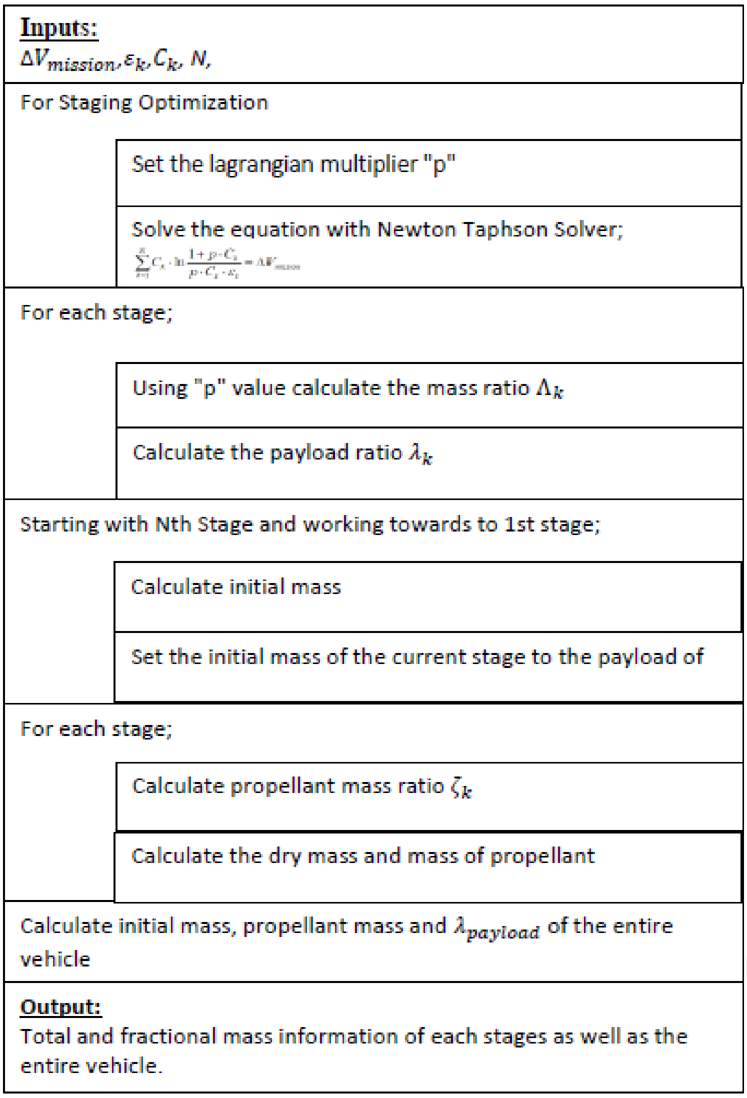

Figure 4.7 NS Diagram for Staging Module.

4.2.3 Propulsion system module

Propulsion system module defines the thrust values for each stage then the propellant mass-volumes for the next step of the study LV – Mass and Geometry model.

4.2.3.1 Thrust model

The next step in the launch vehicle design process is to determine the minimum total required thrust according to user defined minimum T/W ratio. Optimized GLOW of the vehicle calculated in the staging module, moreover; stage number is settled. If there is a limitation on the instant thrust of the engine, user should define prior to start to program.

According to maximum instant thrust, the number of engines can be determined. The algorithm for this module is shown in the NS diagram in Figure 4.8.

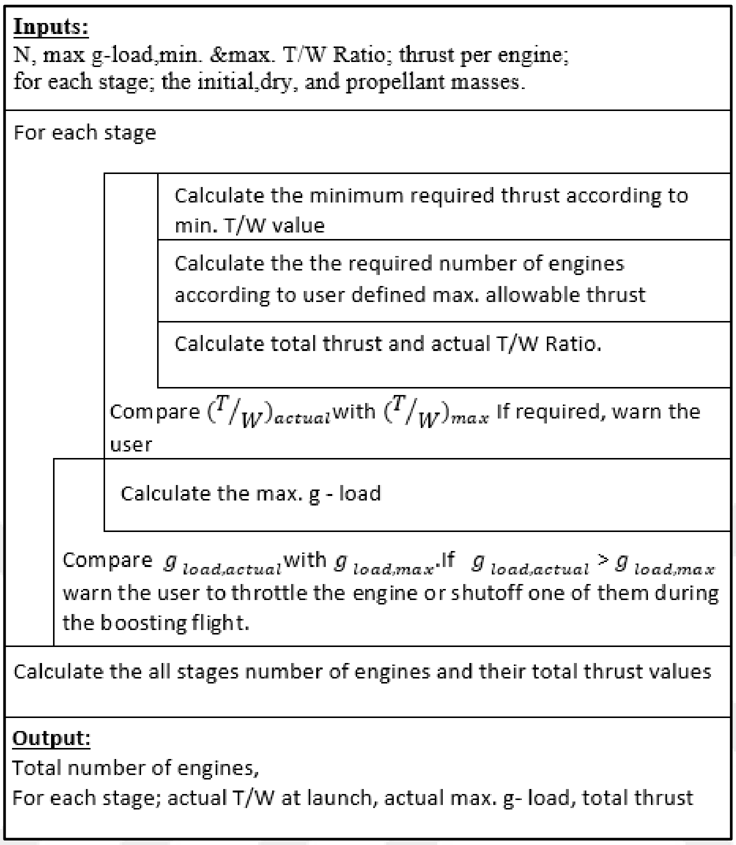

Figure 4.8 : Nassi Schneiderman Diagram for the Thrust Model.

1) Determine thrust required to meet with the minimum lift-off thrust-to-weight ratio, *T/W*.
2) The second step is finding the number of engines. Dividing the total required thrust by user defined allowable maximum thrust will be resulted with number of engines. This result should be rounded up to nearest integer
3) Final step is finding the actual thrust which can be calculated by multiplying the thrust per engine and number of engines. These 3 steps formulations are displayed in equation 4.40 through 4.42.

$$T_{\text{total required}} = (T/W)_{\min} * m_{\text{initial}} * g_o \qquad (4.40)$$

$$n_{eng} = \left(\frac{T_{\text{total,required}}}{T_{\text{eng}}} \right)_{\text{round up to nearest integer}} \tag{4.41}$$

$$T_{\text{total,}} = T_{\text{eng}} * n_{\text{eng}} \tag{4.42}$$

It should be noted that, for constant nozzle exit area, the performance of the engines vary with altitude because of the change on the atmospheric conditions such as pressure. Hence this thrust value is an average value to use. For the purposes of more detailed conceptual design, the thrust value should be tabulated regarding to change on the atmospheric pressure. This process is included in trajectory model and formulated basically in 4.2.6.1. There are two checks during the code flow.

1) Ensuring the actual T/W is whether exceeding the defined maximum T/W or not. This specified maximum value can be found by rearranging equation 4.39 and replacing $T_{total,required}$ with $T_{total,required}$ If the actual T/W is greater than the maximum value, then a warning is displayed to the user with two options:

   i. Rearrange the maximum allowable thrust value to find the engine number,

   ii. Rearrange the minimum T/W value.

2) The second check is about the maximum allowable g-load on the payload to ensure about any damage will occur or not when the stage reaches maximum velocity at the end of burn time. .If the g-load exceeds the maximum allowable value, then a warning is displayed to the user with two options:

   i. Informing the user to integrate a throttable engine,

   ii. One of the engine need to be shut downed during the one portion of the flight.

This process is repeated for all stages to define the all thrust value requirements for each individual stage of N –Stage launch vehicle.

4.2.3.2 Propellant mass – volume module

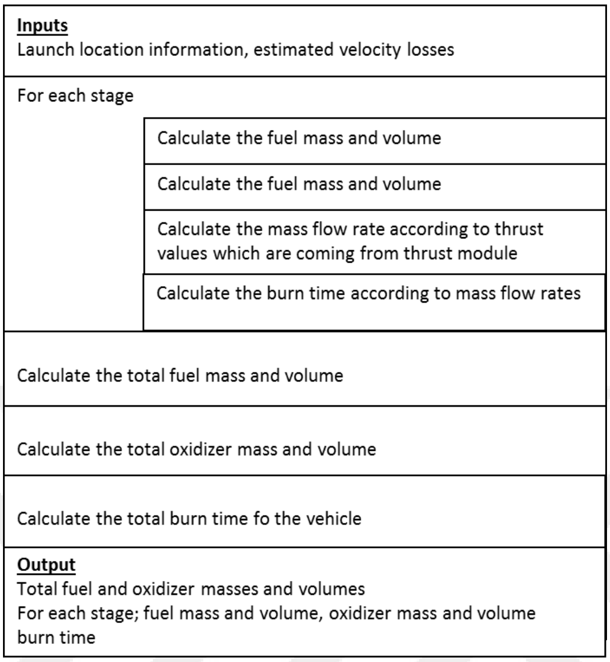

Figure 4.9 : NS Diagram of the Propellant Mass – Volume Module.

The propellant mass and volume module is one of the simplest part of this study. There is no reference to use to determine propellant mass and volume, only the fundamental relations between mass, volume and density are used. One of the output of staging module is propellant mass of each stages, moreover; one of the output of thermochemical performance analysis of the propellants is optimum oxidizer to fuel ratio. By using these known values, mass and volumes for fuel and oxidizer for each stages of N – Stage launch vehicle can be calculated with equations 4.43 through 4.51. This step is a repeated step for each individual stage of an N – Stage Launch Vehicle. After calculations for each stage, all outputs are summed together to find the total mass and volume for the fuel and oxidizer which are used for the whole vehicle.

$$\frac{O}{F} = \frac{\dot{m}_{ox}}{\dot{m}_f} \tag{4.43}$$

$$m_{fuel} = m_{propellant} / (^{O}/_{F} + 1) \tag{4.44}$$

$$V_{f,j} = m_{f,j} / \rho_{f,j} \tag{4.45}$$

$$m_{ox} = m_{fuel} \cdot (^{O}/_{F}) \tag{4.46}$$

$$V_{ox,j} = m_{o,j} / \rho_{ox,j} \tag{4.47}$$

The second step of this module is determining the burning time and the propellant mass flow rates for each stage. First, the total mass flow rate have to be determined. The oxidizer mass flow rate and fuel mass flow rate can be calculated by using oxidizer to fuel mass ratio according to this total mass flow rate. According to required thrust output of the propulsion module, total mass flow rate can be calculated with below equation.

$$\dot{m}_{prop,j} = F_j / \left(Isp_j g_0 \right) \tag{4.48}$$

The fuel mass flow rate can be calculated as:

$$\dot{m}_{f,j} = \dot{m}_{prop,j} / \left(1 + OF_j \right) \tag{4.49}$$

The oxidizer mass flow rate can be calculated as:

$$\dot{m}_{ox,j} = \dot{m}_{pop,j} OF_j / \left(1 + OF_j \right) = \dot{m}_{pop,j} - \dot{m}_{f,j} \tag{4.50}$$

The burning time can be obtained by for each individual stage of N – Stage Launch Vehicle:

$$t_{b,j} = m_{prop,j} / \dot{m}_{prop,j} \tag{4.51}$$

4.2.4 LV geometry - mass model module

This subsection deals with the estimation of the mass and geometry of all the subcomponents of each individual stage of the N –Stage Launch Vehicle. This study main idea is propulsion system based launch vehicle design and optimization. As a result of this, propulsion system optimization is a multi-discipliner process to meet a given mission requirements, because of the several variables which have dependence on trajectory and time.

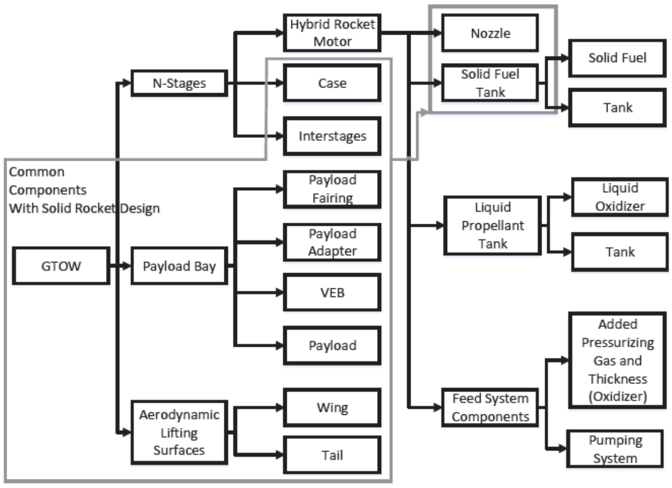

Figure 4.10 : Mass Breakdown of the Hybrid Launch Vehicle.

The mass distribution among the launch vehicle analysis require component level details (the masses of each small portion of the launch vehicle, including control-navigation system, electronics, screws, nuts, etc.) to get accurate solutions. Hence in this study, the vehicle considered, i.e., a more detailed mass distribution analysis would be considered. A mass breakdown based on fundamental systems of hybrid launch vehicle is showed in Figure 4.10 [68].

To size the launch vehicle, firstly the motor have to be sized. That’s why, this section is splitted to five subsections which are HRM Components, nozzle, fairing, stage case and the feed system. After calculation of each stage masses, the GLOW is summed with the individual components from Figure 4.10, as a result of this situation, it is necessary to explain all of them.

4.2.4.1 HRM components

The main components of the HRM are the Nozzle, the Solid Fuel Casing and the Liquid Oxidizer Tank. The outer case is treated as a component of the stage itself. In section 4.2.3.2, all masses and volumes are determined both for fuel and oxidizer. Regarding to these values the size and mass of the each components of the hybrid rocket motor are modeled in following parts of this study.

4.2.4.1.1 Fuel grain case geometry & mass

The one of the output of section 4.2.3.1 is burn time of the motor. Using the regression rate model, which is explained in section 3.4.2, the outer diameter of the fuel grain can be evaluated.

Table 4.2: Thrust Efficiencies respect to Port to Throat Area Ratio [54]

A_c/A_t	P_t (%)	Thrust Reduction (%)	I_{sp} Reduction (%)
∞	100	0	0
3.5	99	1.5	0.31
2.0	96	5	0.55
1.0	81	19.5	1.34
k=1.20 ; P_C/P_E = 1000			

Using the minimum required thrust value from section 4.2.3.1, the code starts to find motor size configuration within the given constraints. Using the outputs from 4.2.3.1 in the relations from 3.4.2, mass flux of the oxidizer can be found for the initial state via using initial port diameter. After calculation of mass flux via using the relations from the section. The initial port diameter is evaluated according to the nozzle throat diameter. Table 4.2 shows that the port to throat area ratio efficiencies.

After determination of initial port diameter, initial oxidizer mass flux can be calculated and for each time step the oxidizer mass flux is decreasing as the port diameter increases for a constant oxidizer mass flow rate. As a result of this, the regression rate decreases during the combustion. The regression rate must be calculated for each time step according to all new port diameters of each step. Therefore, the external diameter can be calculated by summing the initial port diameter and twice the regression rate for each second. This means that the port diameter is integrated over burn time using the regression rate expression which employs the relation between instant oxidizer fluxes. Assuming a single circular port, integrating equation 4.52 from t = 0 to t $=t_b$,$D_{ext,g}$:

$$D_{ext,g} = \left[(a/1000)(4n+2)\left(4\dot{m}_o/\pi\right)^n t_b + D_{int,g}^{2n+1}(0)\right]^{1/(2n+1)} \tag{4.52}$$

According to this external diameter value the length of the solid fuel grain can be calculated:

$$L_g = 4V_f / \left[\pi\left(D_{ext,g}^2 - D_{int,g}^2(0)\right)\right] \tag{4.53}$$

After determination of the fuel grain size, the chamber case dimension calculations can be initiated. Firstly, the final inner diameter have to be calculated according to external diameter of the fuel grain with insulation. So the internal diameter is $D_{int,c}$ = $D_{ext,g}$ $+2t_{ins}$, where t_{ins}= 0.003 m is assumed as the insulation thickness for this study. The fuel chamber external diameter is;

$$D_{ext,c} = D_{int,c} + 2t_{w,c} \tag{4.54}$$

Where $t_{w,c}$is the wall thickness of chamber which can be calculated with below expression?

$$t_{w,c} = \left(1 + f_s\right) P_c D_{int,c} / \sigma_c \tag{4.55}$$

Where safety factor of chamber wall stress isf_s, chamber pressure is P_c , the yielding tensile of chamber material isσ_c. The fuel chamber is consisting of the injector plate, pre combustion chamber for atomization of the oxidizer and the post combustion chamber for the well mixing of combustion products prior to nozzle. The length of injector is negligible. The pre-combustion and post-combustion lengths are assumed as;

$$L_{pre} = 0.5 D_{int,c} \tag{4.56}$$

$$L_{pos} = 0.7 D_{int,c} \tag{4.57}$$

The fuel grain case also consists the convergent part of the nozzle. Due to fact that length of the convergent section of should be calculated:

$$L_{con} = 0.5\left(D_{int,c} - D_t\right) / \tan\theta_{con} \tag{4.58}$$

Where $\theta_{con} = 45°$ is the semi-angle of convergent section. Thus, the final total length of fuel chamber can be formulated as:

$$L_{com} = L_{grain} + L_{pos} + L_{pre} + L_{con} \tag{4.59}$$

To calculate the total mass of the chamber; the insulator, chamber case, injector and the convergent section of the nozzle should be considered. The insulator mass can be neglected. And the injector plate mass is included in feed system estimations. Nozzle mass is calculated in total not special to convergent or divergent sections in the 4.2.4.4. Hence the fuel grain case mass can be calculated via directly from this study relations or mass estimations relations.

$$m_{chamber} = \pi \rho_{chamber} \left(D_{ext,c}^2 - D_{int,c}^2\right) L_c \tag{4.60}$$

The mass estimation relation from [63];

$$m_{chamber} = 0.135 m_{propellants} \tag{4.61}$$

4.2.4.1.2 Oxidizer tank geometry & mass

Nitrous oxide is a self – pressurant propellant as mentioned before. Because of this nature of nitrous oxide, the ullage volume for initial state should be calculated carefully. There are some limitations which are filling degree and filling ratio. [70]

The filling degree is percentage of the volume of liquefied gas to the water volume (at 15 C) of the tank. This percentage would fill the tank with pressure completely. The filling ratio is percentage of the mass of liquefied gas to the allowable water mass (at 15 C) of the tank. For a safe procedure the maximum filling degree should be %95. In this study, it’s taken as %90. The filling ratio is depending on the test pressure of the vessel. Please see below table. [70]

Table 4.3 : Filling Ratio [70]

Cylinder test pressure (bar)	Maximum Filling Ratio
180	0.68
225	0.74
250	0.75

All details about the filling ratio and filling degree can be found in Appendix B. After determination of the required interior volume of the tank, the design procedure can start. For this study, the tank shape is half ellipsoid shaped end cap rounded cylinder. Thus, it can be splitted to 2 sections: end caps and the cylinder as can be seen from the Figure 4.11 [71].

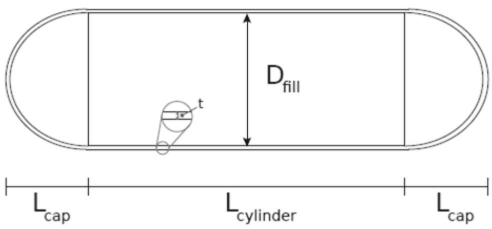

Figure 4.11 : Oxidizer Tank Shape.

Firstly the inner volume of the end caps should be calculated, and then the length of the cylinder can be calculated based on the remaining volume. The diameter is known from the fuel grain case diameter. As mentioned above, the end cap is a three-dimensional shape which is called an ellipsoid. Please see figure 4.11. For this study a hemisphere and cap is used and the all radius values are equal to radius of grain case. Hence in general, the inner volume for a single end cap can be expressed as:

$$V_{endcap} = 0.5 * \frac{4\pi * r_a * r_b * r_c}{3}$$

$$V_{endcap} = \frac{2\pi * r_a^2 * r_b}{3} \quad (4.62)$$

When the total inner volume of the end caps subtracted from the required inner volume, the remaining value is the volume of the cylinder. As the diameter is fixed at the fuel grain case diameter, the length of the cylinder can be calculated easily. These procedure is realized by equation 4.63 through 4.65.

$$V_{cylinder} = V_{totalrequired} - n_{endcap} * V_{endcap} \quad (4.63)$$

$$\pi * \frac{d_{stage}^2}{4} * l_{cylinder} = V_{total\ required} - n_{end\ cap} * V_{end\ cap} \quad (4.64)$$

$$l_{\text{cylinder}} = \frac{4\left(V_{\text{total required}} - n_{\text{end cap}} * V_{\text{end cap}}\right)}{\pi * d_{\text{stages}}^2} \quad (4.65)$$

At this time, the inner dimensions of the tank is evaluated. To finalize the final geometry of the oxidizer tank, the tank wall thickness should be determined. Tank wall thickness is determined by the stresses imposed on the tank itself. This determination for the tank is based on a simple stress model. [65] For the cylindrical part of the tank, the limiting factor is assumed to be the hoop stress and not the axial one. The required thickness for the ellipsoid part can be taken as the half of the cylindrical part thickness. [72]

$$t = P_{t,max}\, f_d\, f_s \frac{D}{2\sigma} \quad (4.66)$$

In equation 4.65 D represents the diameter which is equal to fuel grain case and t represents the tank thickness.$P_{t,max}$ is the maximum operational tank pressure,f_d is a sesign factor and f_s is the factor of safety. These factors came from the reference literatures. σ denotes the stress value depends on which material is used. The wall thickness is checked both for ultimate and yield strengths of the chosen material. The highest resulting thickness is used as the wall thickness of the tank. The thickness will be used to finalize the diameter of the tank and calculate it's mass. The external tank volume can be calculated then the mass of tank:

$$m_{tank} = \rho_{tank}\left(V_{ext,tank} - V_{int,tank}\right) \tag{4.67}$$

This calculation is repeated for each stages of the N –Stage launch vehicle. Once the lengths have been found, the total length for the fuel and oxidizer tanks is calculated by adding the cylinder length to the end cap's vertical axis radius, and the total propellant tank stack length is found by summing these two values together.

$$L_{ox} = 2 \times L_{cap} + L_{cylinder} \tag{4.68}$$

4.2.4.1.3 Pressurizing system geometry & mass

Current hybrid rocket motor is employed by a pressurant system. This pressurizing system is used to maintain the thrust as possible as constant. A small helium tank which has an internal pressure approx. 300 bar. The final pressure at the helium tank is assumed as 2 times of the pressure of the oxidizer tank, to overcome pressure losses across the valves. Initial helium mass firstly should be calculated:

$$m_{helium} = 2\,\rho_{helium}\,V_{ox,tank} \tag{4.69}$$

According to helium mass, the helium tank volume (assuming an isothermal expansion process) can be calculated as;

$$V_{helium,tank} = \frac{m_{helium} R_{helum} T}{P_{helium}} \tag{4.70}$$

P_{helium} is the stored pressure which is 300 bar for this study. So, the internal diamater of the helium tank, its wall thickness and the mass of spherical helium tank is respectively;

$$D_{int,He} = \left(6V_{tkHe} / \mathrm{p}\right)^{1/3} \tag{4.71}$$

$$t_{w,tkHe} = 0.25\left(1 + f_s\right) P_{He,i} D_{int,tkHe} / \sigma_{tkHe} \tag{4.72}$$

$$m_{tkHe} = \rho_{tkHe}\left(1 + f_{tk}\right)(\pi / 6)\left(D^3_{ext,tkHHe} - D^3_{int,tkHe}\right) \tag{4.73}$$

Once the propellant tank stack length has been calculated, the total stage length can be found by adding this length to the length of the engines used and, if the stage being calculated is not the final stage, the length required between stages. The total vehicle length is then determined by summing together all of the stage lengths and the payload length. This will be given in detail section 4.2.4.4

4.2.4.2 Feed system geometry &mass

The feed system of hybrid rocket motor consists of the opening valves, pipelines, valve opening mechanisms and any other related items for flow of the oxidizer. For all of these the related empiric formula will be used to estimate. This relation is gathered from reference. [69]

$$M_{feed} = 2.55\ x\ 10^{-4}\ T\ (N) \tag{4.74}$$

4.2.4.3 Fairing & avionics & wiring

For the fairing mass determination, the user should give the approximate payload area to define the fairing area. For this study, in the third stage it is included a fairing, assumed as cylinder with 0.8 m height and 0.6 m diameter, to carry a nanosatellite with a volume of, approximately, 0.4 × 0.4 × 0.4 m^3.After determination of the fairing area, its mass can be calculated with below expression [69]:

$$M_{fairing} = 4.95\left(A_{fairing}\right)^{1.15} \tag{4.73}$$

The payload adapter mass can be calculated with following mass relation [72]:

$$M_{adapter} = 0.004775 \times M_{payload}^{1.0132} \tag{4.74}$$

The vehicle equipment bay and the avionics can be calculated with following mass relations [69]:

$$M_{int} = 0.404 \times M_{dry}^{0.6814} \tag{4.75}$$

$$M_{avionics} = 10\ (M_0)^{0.361} \tag{4.76}$$

The final mass relation is regarding to wiring system. The wiring system mass can be calculated with:

$$M_{wiring} = 1.058\sqrt{M_0}\ (L_{vehicle})^{0.25} \tag{4.77}$$

4.2.4.4 Launch vehicle stage case geometry and mass model

As mentioned at the end of the section 4.2.4.1.3, the total length of the case can be calculated with the below relation;

$$L_{case} = 1.1(L_{chamber} + L_{tank} + L_{case} + L_{case}) \tag{4.78}$$

In which, all of these parameters are first estimations the process. A %10 margin is added to formulation to avoid any misalignments on the sizing process for the control systems, feeding lines, valves, interstage structures etc.

The internal diameter of the stage is equal to external diameter of the oxidizer tank plus oxidizer tank support rings which are used to increase the strength of the system. The external diameter of the stage case is internal diameter plus the two times the wall thickness which is depending on the material strength properties.

$$D_{ext,case} \cong \left[D_{int,case}^2 + 4 m_T g_0 (1 + F/W) / \pi\sigma_c \right]^{1/2} \tag{4.79}$$

Thus, the stage case mass can be calculated with following expression:

$$m_{case} = \rho_{case} L_{case} (\pi/4)\left(D_{ext,case}^2 - D_{intase}^2 \right) \tag{4.80}$$

4.2.4.5 Nozzle

The Nozzle for a Hybrid Rocket can be modelled identically for solid fuel grain. The nozzle dimensioning is mentioned in section 3.5. For now, the mass estimation relation for the nozzle is gathered via using simple historical data regression which is divided between a small motor range (T_{vacuum} < 200kN) and large motor range (T_{vacuum} > 200kN). Absolutely all these data are coming from the solid rocket motors. However, because of its nature, hybrid rocket motor nozzle can be conducted easilt to solid rocket motor nozzle to model its mass. [72]

Large rocket motors (T_{vacuum} > 200kN):

$$m_{\mathrm{nozzle}} = 0.0006T^2 - 0.3214T + 263.82 \tag{4.81}$$

For small rocket motors (T_{vacuum} < 200kN) with TVC:

$$m_{\mathrm{nozzle}} = -0.0018T^2 + 1.004T - 1.942 \tag{4.82}$$

For small rocket motors (T_{vacuum} < 200kN) without TVC:

$$m_{\mathrm{nozzle}} = 0.1605T^{1.2466} \tag{4.83}$$

As a result of all these calculation the total mass and length for each individual stage of N-Stage Rocket can be calculated with:

$$L_{stage} = L_{case} + L_{nozzle,div} \tag{4.84}$$

$$\begin{aligned} m_{stage} = m_{case} + m_{nozzle} + m_{fairing} + m_{wiring} + m_{avionics} \\ + m_{propellant} + m_{ox,tank} + m_{pressure,system} \end{aligned} \tag{4.85}$$

In which, $m_{pressure,system}$ contains both pressurant gas mass and it tank mass.

4.2.5 Material selection

Material selection is valid for case structure, oxidizer tank and the fuel grain case to determine masses of each component according to system requirements.

Table 4.4 : Material Properties [73]

Material	Bulk Modulus E (Gpa)	Tensile Yield Strength σ (MPa)	Density ρ (kg/ m^3)
Carbon Fiber Composite	228	3800	1810
Titanium	115	790	4460
Aluminum	71.7	503	2810
4310 Steel	200	635	7830

If these materials are not meeting with user selections, user can enter his/her materials to the system with the required specifications requested by tool.

4.2.6 Trajectory module

When the launch vehicle and its propulsion system is designed, a trajectory simulation has to be ran to verify its flight performance. As a result of this need a self-developed trajectory tool is created to simulate the trajectory of the vehicle. This tool is developed based on the ascent-to-orbit trajectory models of Curtis and Tewari [57, 63]. There are two main goals of this trajectory tool during the conceptual design phase:

- First, simulating the rocket trajectory and verifying the whether it will reach to desired orbit parameters or not.

- Second, verifying the ΔV_{losses} assumptions which are defined at the ΔV module to use them in stage mass distribution module. If the assumptions are lower than calculated ones, this means that the launch vehicle is not capable to reach desired orbit parameters; if the assumptions are higher than calculated ones, this means launch vehicle is designed overestimated for the required orbit parameters.

Because of the main idea behind this study which is propulsion system design tool integrated design tool development, a 2D trajectory simulation is considered for this study instead of a 3D simulation. A 2D Trajectory simulation will give conceptual design level of information and these level of outputs are sufficient for this study. On the other hand, a 2D simulation will be relatively faster and simple code compare to 3D trajectory tool. Non-rotating spherical Earth assumption is used for the flight and the launch vehicle is assumed to be in a fixed plane during the modelling of its trajectory. [75].

4.2.6.1 Equations of motion

Following assumptions used throughout the setting the equation of motions;

- Non – rotating & spherical earth,
- US Standard Atmosphere 1976,
- No atmospheric affect is included,
- There is no thrust vectoring and control during the launch vehicle flight.

Firstly the reference frame of the flight and the main equations of the motion should be defined. All the trajectory performance calculations are realized by solving the equations of motion. A body-fixed coordinate system is assumed as the reference frame of the launch vehicle. Mainly, there are 3 forces acting on the launch vehicle; thrust, aerodynamic forces and gravitational forces.

There are two more forces which are effecting when the launch vehicle flies in exo-atmosphere, solar wind and solar radiation pressure [69, 70]. These two forces are negligible. The longitudinal axis of the launch vehicle is x-axis, in the lateral plane the y-axis is perpendicular to the x-axis. Figure 4.12 [57] shows the reference frame of the vehicle. In this figure D is the drag force and T is the thrust.

To explain the flight path angle γ, firstly the angle of attack and the pitch angle should be defined. The angle of attack is α which is angle between the thrust direction and direction of the flight.

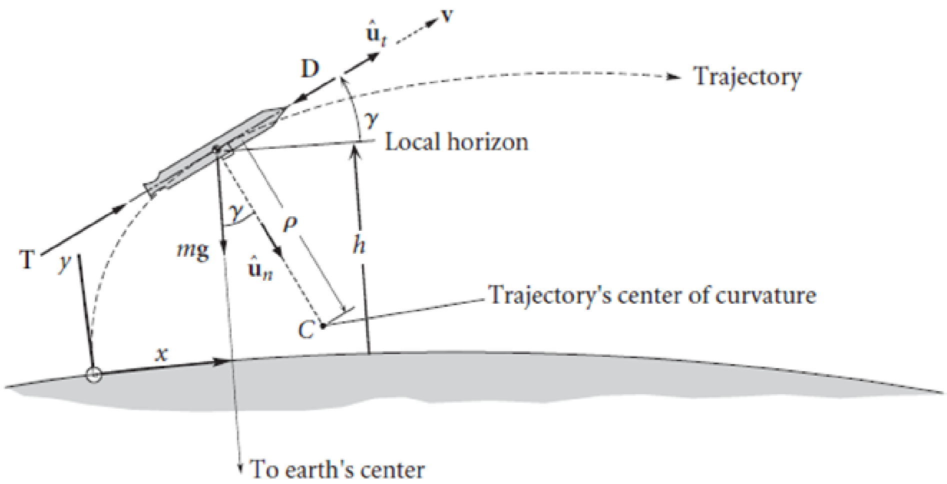

Figure 4.12 : Launch Vehicle Trajectory.

The pitch angle is θ which is angle between the thrust direction and the horizontal plane of the reference frame. The flight path angle is the sum of these two angles. It can be expressed as;

$$g = q + a \tag{4.86}$$

Four differential equations are required to simulate its motion and 2 functions are required to integrate and get the results for the velocity losses due to gravity and drag. The equations from 4.86 through 4.89 are derived for downrange distance, vertical distance, acceleration and flight path angle changes during the flight of the launch vehicle, respectively.

$$\frac{\mathrm{d}x}{\mathrm{d}t} = \frac{R_E}{R_E + h} v \cos g \tag{4.87}$$

$$\frac{\mathrm{d}h}{\mathrm{d}t} = v \sin g \tag{4.88}$$

$$\frac{\mathrm{d}v}{\mathrm{d}t} = \frac{T}{m} - \frac{D}{m} - g \sin g \tag{4.89}$$

$$v\frac{\mathrm{d}\gamma}{\mathrm{d}t} = -\left(g - \frac{v^2}{R_E + h}\right)\cos\gamma \tag{4.90}$$

Where; D is drag in [N], T is thrust in [N], g is local gravitational acceleration in $[m/s^2]$, x is downrange distance in [m], h is altitude in [m], υ is the velocity of the launch vehicle in $[m/s]$, γ is the flight path angle in [rad] and R_E is the Earth Radius in [m].

The gravity and drag losses can be expressed as below:

$$\Delta v_D = \int_{t_0}^{t_f} \frac{D}{m} \mathrm{d}t \tag{4.91}$$

$$\Delta v_G = \int_{t_o}^{t_f} g \sin\gamma \, \mathrm{d}t \tag{4.92}$$

The local gravity “g” can be calculated with following equation:

$$g = g_0 \left(\frac{R_E}{R_E + h}\right)^2 \tag{4.93}$$

Where g_0 is se level gravitational acceleration in $[m/s^2]$.

In this study, gravity turn trajectory is used for trajectory simulation. Gravity turn is a natural maneuver it’s occurring when a launch vehicle has to turn to direct itself to horizontal position at the burnout.

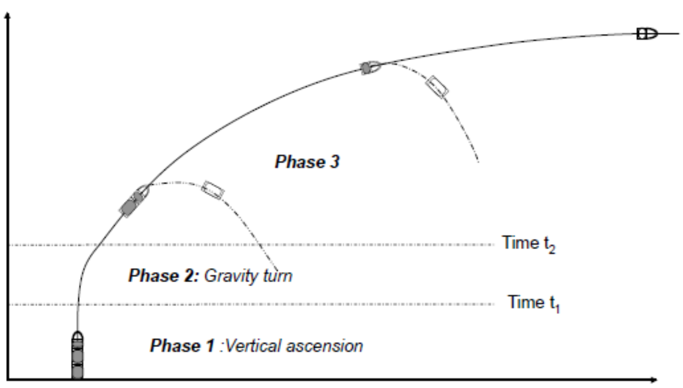

Figure 4.13 : Gravity Turn [74].

Typically, a launch vehicle starts to follow its flight path with a vertical ascent profile then this gravity phase is occurring. This trajectory is also called as pitch over maneuver. A gravity turn trajectory is represented in Figure 4.13.

According to Figure 4.13, from equation 4.87 through 4.93 can be used as equations of motion for the phase 1 and 3. But for phase 2, first flight path angle has to be added to equation 4.89 and it becomes:

$$v\dot{\gamma} = -g\cos\gamma + \frac{v^2}{R_E + H}\cos\gamma - \gamma_0 \tag{4.94}$$

The gravity turn maneuver also reduces the gravity losses during ascent phase of the launch vehicle. Because when the launch vehicle ascents vertically, the gravity acts directly against to thrust and this situation is resulting with the velocity losses.

Moreover gravity has to be realized at the vertical velocity which is as small as possible to avoid big amount of aerodynamic losses. [56]

Drag is the function of altitude. The drag can be expresses as below:

$$D(h) = {}^{1}/_{2}\ \rho(h)\ A\ C_d v^2 \tag{4.95}$$

Where C_d is the drag coefficient, ρ is air density in $[kg/m^3]$, and A is launch vehicle reference area in $[m^2]$. In this study, drag coefficient is taken as constant during the atmospheric flight of the trajectory. Normally, drag coefficient depends on local Mach number of the launch vehicle and local Mach number strongly depends on the geometric shape of the vehicle. Because of its negligible effect on the results of the trajectory simulation, this constant drag coefficient assumption is made.

Typically, at the subsonic and hypersonic region for a constant drag coefficient it can be taken approximately 0.3 for regular shape of nosecone of the launch vehicle. On the other hand, at the transonic region for a constant drag coefficient it can be taken as 0.5. Let's analyze the other terms in the drag force equation. The local density can be expressed as:

$$\rho(h) = \rho_0 e^{h/h_0} \tag{4.96}$$

Where h_0 the scale height is;

$$h_0 = \frac{R\,T(h)}{G\,M} \tag{4.97}$$

Where $T(h)$ localtemperature can be expressed as:

$$T(h) = T_0 + a\,h \tag{4.98}$$

Where a is lapse rate constant in $[K/m]$, h_0 is scale height in [m], G is gravitational constant in $[m^3/kg\ s^2]$, M is molecular mass of air in [kg/mol], R is gas constant in [J/mole K], T_0 is temperature at sea level in[K], T is local temperature in [K], $\rho(h)$ is local density in $[kg/m^3]$, ρ_0 is density at sea level in $[kg/m^3]$.

Table 4.5 : Model Constants

Constant		**Value**
Lapse Rate $[K/m]$	a	9.80665
Gravity at sea level $[m/s^2]$	g_0	9.80665
Molecular mass of air [kg/mole]	M	$28.97\ 10^{-3}$
Temperature at sea level [K]	T_0	288
Gravitational constant $[m^3/kg\ s^2]$	G	$3.9893\ 10^{14}$
Perfect gas constant [J/mole K]	R	8.31432
Earth Radius [m]	R_E	6371
Density at sea level $[kg/m^3]$	ρ_0	1.29

Dynamic pressure “q” can be formulated as below equation:

$$q = {}^{1}/_{2}\ \rho\ \upsilon^2 \tag{4.99}$$

Maximum dynamic pressure and g-load checks NS diagrams are showed in Figure 4.14 and 4.15 respectively.

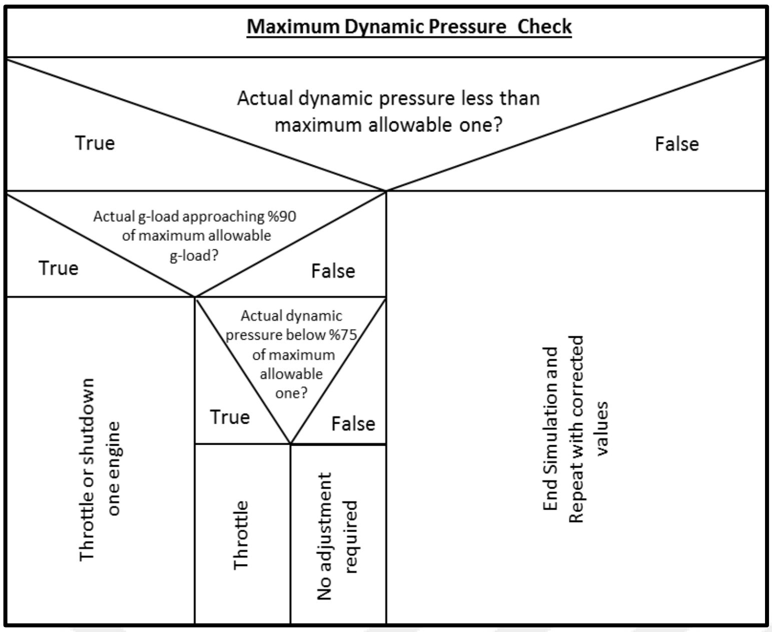

Figure 4.14 : NS Diagram Maximum Dynamic Pressure Check.

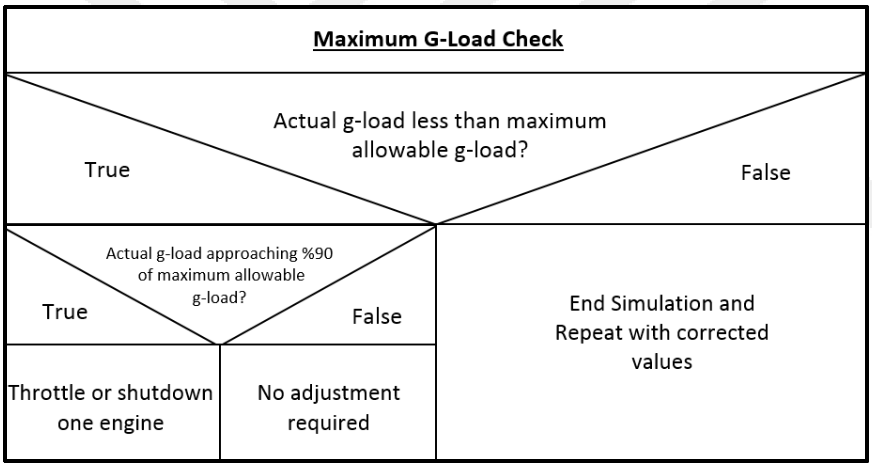

Figure 4.15 : NS Diagram Maximum Gload Check.

Thrust is also function of time because of its dependence on the altitude. The thrust function can be expressed as below:

$$T\,(h) = \dot{m}_e c_a + (p_e - p_a(h))A_e \tag{4.100}$$

Where the $\dot{m}_e c_a$ is the jet thrust and $(p_e - p_a(h))A_e$ is the pressure thrust. As the constant nozzle exit area is constant, the thrust value is not constant and varying the change of ambient pressure due to change of the altitude during the atmospheric flight. Moreover the mass value of the launch vehicle is not constant and it is decreasing with mass flow of propellant throughout the nozzle. This time dependent mass function can be expressed as from equation to;

$$T = I_{sp}\,\dot{m}_e\,g_0 \tag{4.101}$$

Then nozzle exit propellant mass flow rate can be expressed as:

$$\dot{m}_e = \frac{T}{I_{sp}\,g_0} \tag{4.102}$$

Hence the mass function can be expressed as during boost phase of each stage.

$$m(t) = m_i - {}^{dm}\!/_{dt}\,\Delta t \tag{4.103}$$

where m_i is the initial stage/launch vehicle mass in [kg], ${}^{dm}\!/_{dt}$ is the total propellant mass flow rate of current stage stage in [kg/s] and Δt is time difference between initial and current moments in [s].

5. VALIDATION & APPLICATION OF TOOL

In this Chapter, firstly each module is validated separately with the comparison of different programs and Launch Vehicle's User Manual's data. Firstly, propulsion module is validated with NASA Chemical Equilibrium Application program. Thermochemical performance analysis is performed for current selected propellant combination of hybrid rocket motor with both the developed tool and NASA CEA.

Secondly the mass and volume module is validated via comparison of the results which are obtained by the tool and with provided user' manuals. Two different launch vehicles were compared for mass tool validation: HLV and Minotaur 1. Third, a trajectory comparison is performed to validate the trajectory tool with comparison of user manual data of selected launch vehicles. VEGA LV is used for trajectory tool validation.

At the final of this chapter, a nanosatellite launch vehicle is designed with whole design tool regarding the initially defined design constraints. The properties and illustrations regarding to this designed nanosatellite launch vehicle are showed in this chapter regarding to design launch vehicle.

5.1 Validation

Validation process is important prior to use the tool for designing the launch vehicle. This validation process was performed in three separated phases, starting with the validation of the propulsion, mass module and ending with the validation of the trajectory tool. For the mass model and trajectory tool simulations with launcher are performed. HLV launcher has a capacity to launch 20 kilograms of payload into a circular orbit, at an altitude of 300 kilometers, and the Minotaur - 1 has a capacity to launch 200 kilograms of payload in a circular orbit at an altitude of 700 kilometers.

5.1.1 Propulsion

The propulsion module is consisted of two parts. One of them is thermochemical performance code which is explained in detailed in Chapter 3 and the second part is about its system sizing which is explained in detail in Chapter 4. For this section, the validation the thermochemical performance code is showed.

5.1.1.1 Validation with CEA

Thermochemical performance code results are compared with the results of the NASA CEA with the same propellant combination. The propellant combination is nitrous oxide as an oxidizer and the paraffin ($C_{28}H_{58}$) as a fuel. The main objective behind the validation of the code is, comparison of the fuel mixture ratio vs. specific impulse graphics. This graphic is important when a propellant combination is chosen for the launch vehicle system. According to this graphic, most efficient mixture ratio can be selected easily for the highest specific impulse value. The comparison between the code and NASA CEA is shown in Figure 5.1.

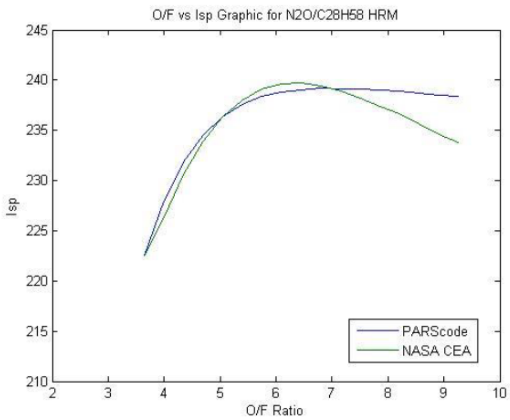

Figure 5.1 : O/F vs I_{sp} Selection Curve.

According to Figure 5.1 the difference between above two curves in high O/F ratios can be seen easily. This difference is because of the dissociation reactions which is led by high combustion temperature. However, the code which is presented in this paper uses simplified reaction mechanism as mentioned above whereas NASA CEA code solves hundreds of elementary reactions. As a result of this situation, there is a small difference between these curves in high O/F ratios.

5.1.1.2 Tests

The hybrid rocket motor test stand and the feed system have been designed and established by PARS Rocketry Group members. The oxidizer feed system consists of thermocouples, pressure transducers, manometers, valves and associated fittings. Oxidizer's first valve before the main valve is controlled manually to check the flow. Oxidizer main valve is a ball valve which is actuated via high torque DC motor and an additional gearbox system. This valve opening system is showed in Figure 5.2.

Figure 5.2 : Valve Opening System.

The main objective behind this valve system is controlling the opening/closing time accurately since many of the high torque DC motors have low speed in rpm unit; however, with this design the opening time is reduced to 0.75 seconds. Purging of the feed system is controlled manually.

Relief, bleed and remote and automatic operation of the overall ignition system is achieved through the PARS Rocketry Group's own designed and produced data acquisition and control system. Actuation of the oxidizer flow and ignition of pyros are controlled via this main computer.

The first step is cold-flow tests to determine the discharge coefficient of the injector. Different type of the injector designs are tested with constant tank pressure and oxidizer mass. The discharge coefficient was found according to these test results. For this reason, these tests were helpful to characterize the initial conditions of oxidizer.

In addition, different igniter combinations were tested as an intermediate tests to ensure the successful and sustained combustion initiation. A photograph of the motor plume during the one of the hot-fire test is shown in Figure 5.3.

Figure 5.3 : First Fire Test.

The tests of lab-scale motor have been performed; however, some of the results are not desirable because of the feed system pressure losses. The next step is a high reliable test feed system establishment to get more accurate results.

Because of the pressure losses, the oxidizer pressure decreased to 30 bar and combustion pressure decreased to 16 bar. The burn time increased due to slow regression rate. Therefore, the average oxidizer mass flow rate was implemented to verify the analytical model to have the thrust curve shown in the Figure 6.x. The modelled thrust profile is reasonably close to experimental results. Also the total impulse of designed motor and the test results are very close to each other.

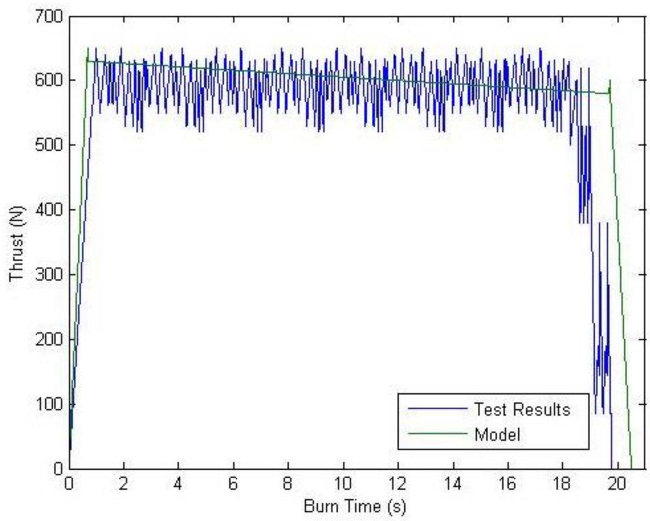

Figure 5.4 : The test results comparison.

The control ball valve is opened and closed at 0 second and 18 seconds during the tests. A peak thrust of 620 N reached at the burnout of igniter. The full combustion achieved at the burn time 18 seconds.

5.1.2 Mass & geometry

The parameters which are introduced in Chapter 4, are listed in Table 5.1 for the following 2 launch vehicle simulations.

Table 5.1 : Mass & Geometry Simulation Parameters

Characteristics	Units
Number of Stages	-
Diameter of Stages	m
Length of Stages	m
Mass of Stages	kg
Propellant Selection	-
Thrust	kN
ΔV Division	-

As mentioned in Chapter 4 before, because of the it's iterative nature of design process when the mass model converges with staging optimization results itself, the trajectory tool is used to check the vehicle flight performance for improvements regarding the ascent phase etc. via reducing or increasing the propellant mass of the stages with the change of O/F Ratio or expansion ratio of the nozzle. As a result of these actions this change in the propellant can be transformed into change on velocities "ΔV" value and iterate the new values of ΔV losses.

Firstly, propellant and structural masses have been compared with the values which are presented in HLV Paper [77]. Simulation results comparison is presented in the table number from 5.4 to 5.6. Mass and Geometry Tools validations are realized with a Hybrid Rocket Launch Vehicle (HLV) and Minotaur Launch Vehicle. The details of HLV are listed in table 5.2.

Table 5.2 : HLV Launch Vehicle Specifications

	1. Stage	2. Stage	3. Stage
Propellant Mass	5530	695	116,35
Structural Mass	2283	353	63
Propellant Mass	H_2O_2/Paraffin	H_2O_2/Paraffin	H_2O_2/Paraffin
Isp	257	290	297
Thrust	192	26	4,4
Burn Time	73	77	78
Diameter	1,2	1	0,6

The objective of this work is to make a preliminary analysis of mass distribution of hybrid propulsion systems and to compare the performance of air launched and ground launched hybrid rockets. The propellants are an aqueous solution of 98% H2O2, in mass, burning with solid paraffin mixed with 10% aluminum, in mass. The effects of mixture ratios, thrust/weight ratios and chamber pressures are analyzed. Three stage rockets are considered for placing a 20 kg nanosat into a low Earth circular equatorial orbit at 300 km.

The details of Minotaur Launch Vehicle are listed in table 5.3.

Table 5.3 : Minotaur Launch Vehicle Specifications [77]

-	Stage 1	Stage 2	Stage 3	Stage 4
Length	7.49	4.12	3.07	1.34
Diameter	1.67	1.33	1.28	0.97
Propellant Mass (kg)	20785	6237	2645	770.2
Structural Mass	2292	795	1391	102.3
Gross Mass	23077	7032	4036	872.3
Propellant	Solid TP - H1011	Solid ANB - 3066	HTPB	HTPB
Isp(s) (Vacuum)	262	288	289	287
Thrust	792	267.7	194.4	36.9
Burn Time	61.3	66	71	66.8

The Minotaur Launch Vehicle is a small launch vehicle which is developed in USA. Minotaur is a rocket family which includes from Minotaur I to VI and also Minotaur-C. Minotaur Launch Vehicle family is developed by derivation of land – based Intercontinental Ballistic Missile which is LGM-118 Peacekeeper. The manufacturer of this rocket family is Orbital ATK. In this study Minotaur 1 is used for simulation. Validation. This launch vehicle has 4 solid propelled stages. First two stage are coming from the Minuteman missile, respectively SR19 and M55A1.Moreover, the third and fourth stages are coming from Pegasus Rocket, respectively Orion 50XL and Orion 38.

The comparison of simulation and HLV Paper data is showed in Table 5.4. It can be seen that differences on second stage and first stage structural masses are coming from the design idea differences between two studies.

Table 5.4 : HLV Mass Tool Simulation Results Comparison

	Stage 1			Stage 2			Stage 3		
	m_p	m_s	m_0	m_p	m_s	m_0	m_p	m_s	m_0
	[kg]	[kg]	[kg]	[kg]	[kg]	[kg]	[kg]	[kg]	[kg]
HLV	5530	2283	9039	695	353	1230	116,35	63	179,35
Simulation	5142,9	1826,4	8632,25	666,51	254,16	1131,6	102,389	57,33	168,41
Deviation %	7	20	4,5	4,1	28	8	12	9	5,8

Because of the design tool's base optimization criteria is propulsion systems which are hybrid rocket motors, the most significant differences were obtained in structural masses, especially in the second stage where the difference is almost 28%. This difference is especially coming from the idea behind the design processes of studies. The current validated study assumes a constant structural mass ratio and there is no iterative process to minimize the GLOW. As a result of this situation, these differences are occurred. Moreover, especially the last stage has usually "more structure" for instance more wirings, more complicated attitude and propulsion control units and avionics for the re-ignitions of the motor, hence the structural mass ratio must be greater for the last stage . These results show that the necessity of the "self-learning iteration" process for the structural mass ratio estimations during the staging optimization. This iteration process is integrated to the tool and its results are showed in Chapter 5.2. In general, the mass model is resulting with over predicted values on structural mass of the stages but on the other hand the model predicts the propellant masses proximate to theoretical.

The minor differences on the lower stages of propellant masses can be explained with the nonexistence of the propellant mass margin. Except the last stage, the major difference on propellants masses is observed on the third stage which is %18.3. When the deviation of the GLOW of the launcher is analyzed, it looks about 3.8% and which is under 8%. This value is relatively small for a preliminary design tool. The payload mass is included in the last stage. After the mass model validation, also the geometry model is validated. The validation of the geometry model is achieved via taking the stage diameter as a constant during the analysis. The results for the HLV are presented in the table 5.5.

Table 5.5 : Geometry Tool Simulation Results Comparison for HLV

	Stage 1			Stage 2			Stage 3		
	d	*l*	*V*	*d*	*l*	*V*	*d*	*l*	*V*
	[m]	[m]	[m3]	[m]	[m]	[m3]	[m]	[m]	[m3]
HLV	1.20	10.40	11.76	0.99	4.40	3.39	0.57	3.20	0.82
Simulation	1.20	9.85	11.14	0.99	4.20	3.23	0.57	2.88	0.74
Deviation %	-	5.3	5.6	-	4.55	4.76	-	10	11.1

All results are proximate to the HLV's data. For many of launch vehicles, the total volume of the vehicles is accompanied by the propellants. The mass model of the tool has a good accuracy on the propellant masses. This accuracy on the propellant masses is affecting also the results for the geometry model in a good way. This situation explains the why the geometry model is also accurate as mass model. The validation with HLV is finalized for the mass and geometry models, the next validations are with Minotaur -1 Launch Vehicle [77]. The results are showed in table 5.6.

Table 5.6 : Mass Tool Simulation Results Comparison for Minotaur

	Stage 1			Stage 2			Stage 3			Stage 4		
	m_p	m_s	m_0	m_p	m_s	m_0	m_p	m_s	m_0	m_p	m_s	m_0
	[kg]	[kg]	[kg]	[kg]	[kg]	[kg]	[kg]	[kg]	[kg]	[kg]	[kg]	[kg]
MLV	20785	2292	34114	6237	795	11940	2645	1391	4908,3	770,2	102,3	872,3
Sim.	19330,03	2085,72	32578,87	5981,283	735,375	11223,6	2380,5	1265,81	4608,8937	697,031	93,6045	793,793
Dev. %	7	9	4,5	4,1	7,5	6	10	9	6,1	9,5	8,5	9

Structural, propellant and total mass values are compared between model results and user manual data. It can be seen that the propellant and structural mass deviations are again proximate to user manual data. Moreover, contrary to HLV Launch Vehicle analysis results, the last stage deviations for Minotaur 1 Launch Vehicle are most proximate results compare to lower stages.

This difference is coming from the mission requirement differences between two launch vehicles. Minotaur – 1 last stage is a solid propelled rocket, on the other hand HLV Launch Vehicle last stage has multi-ignition capable liquid rocket engine. Also the Minotaur Vehicle target orbit requirements are different from HLV Launch Vehicle. This creates the difference between the required systems in the last stage and also creating the difference between structural mass ratios between last stages of launch vehicles.

The minor differences on the lower stages for the propellant masses can be explained with the nonexistence of the propellant margin once again. When the deviation of the GLOW of the launcher is analyzed, it looks about 8.7 % and which is again under 10%.

5.1.3 Trajectory

The validation of the trajectory module is processed via using the motor specifications which are thrust, burn time, propellant combination and the mass properties of the each stages of the launch vehicle VEGA. The main objective behind this validation is confirming whether if the launch vehicle will follow the proposed trajectory or not to achieve the mission requirement which is transporting the required payload mass into target orbit. The validation of the trajectory tool is realized with the simulation of VEGA Launch Vehicle and this launch vehicle's specifications are presented in the table 5.7.

Table 5.7 : VEGA Launch Vehicle Specifications

-	Stage 1	Stage 2	Stage 3	Stage 4
Length	7.49	4.12	3.07	1.34
Diameter	1.67	1.33	1.28	0.97
Propellant Mass (kg)	20785	6237	2645	770.2
Structural Mass	2292	795	1391	102.3
Gross Mass	23077	7032	4036	872.3
Propellant	Solid TP - H1011	Solid ANB - 3066	HTPB	HTPB
Isp(s) (Vacuum)	262	288	289	287
Thrust	792	267.7	194.4	36.9
Burn Time	61.3	66	71	66.8

The trajectory tool simulation results are compared with the user manual data of the VEGA LV. There are some considerable differences between the user manual data and simulation results because of difference on the flight control methods between the simulation model and the actual launch vehicle operations. The modern launch vehicles have powerful and sufficient control and guidance models for their ascent flight even though the tool is using gravity turn as a guidance model.

Moreover, in the tool thrust is taken as a constant and with its maximum value even though the real launch vehicles are not using the maximum thrust during the all flight phases, sometimes they are using less power or reverse thrust to provide an accurate flight profile to achieve the target orbit requirements.

Sometimes this is also required for manned missions and for sensitive payloads. In the below figures, different variables of the trajectory simulation are shoed. All flight phases are represented just in these two figures. Second and the third stage flights are showed detail in the rest of the figures.

The gravity turn ends at the 95. Seconds of the flight according to simulation results. After this time, launch vehicle is reaching to higher velocities to reach target orbit. All coasting phases are assumed as 4 seconds and the total resulted flight duration is 350.4 seconds. In the figure 5.5 (a) it's showed that the change of the altitude with respect to time. In the figure 5.5 (b) it's showed that the change of the downrange of the trajectory with respect to time.

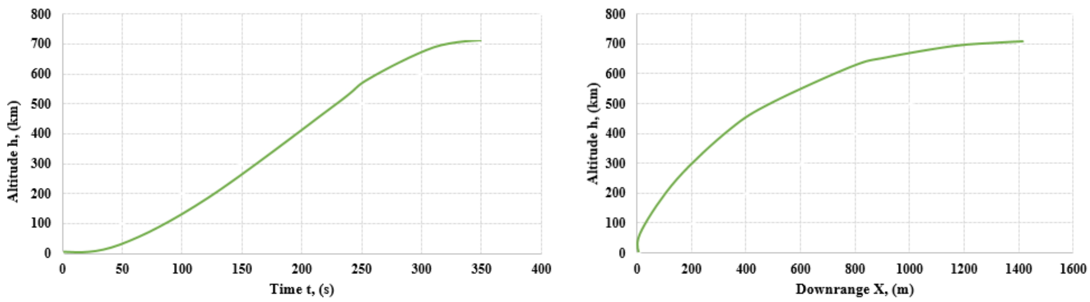

Figure 5.5 : (a) Altitude vs. Time **(b)** Altitude vs. Downrange of VEGA LV.

In fig 5.6 (a), it can be easily seen that the flight path angle is changing during the three flight phases of the stages. First one is the ascent phase in which the flight path angle has no change, the second one is gravity turn and then the third one is free-flight phase. In the figure 5.6 (b), it can be easily seen that the change in the velocity with respect to time and it changes when the gravity turn ends.

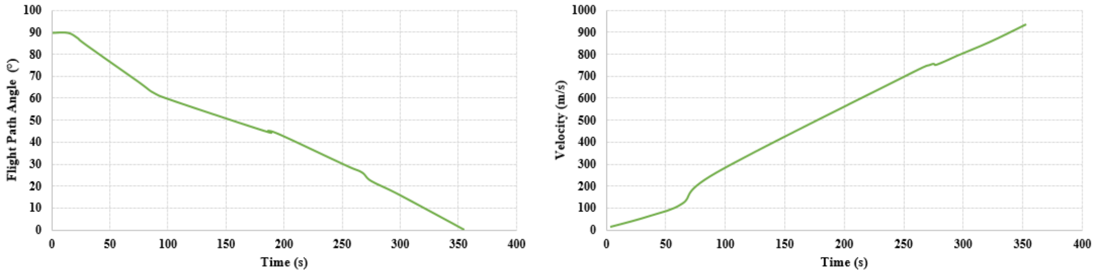

Figure 5.6 : (a) Flight path Angle vs. Time **(b)** Velocity vs. Time of VEGA LV.

To show the end time of the gravity turn and the start of the free flight phase just after that event more clearly, altitude is graphed as a function of velocity in the figure 5.7 (a). The Dynamic Pressure change during the flight is showed in the figure 5.7 (b). As mentioned in Chapter 4, this specification has importance for structural design phase from strength of the materials point of view and the reliability of the fairings. The maximum dynamic pressure is observed around 10 km of altitude according to simulation results. This result shows the accuracy of the model also because according to real launch data and user manual data of the VEGA LV show that the maximum dynamic pressure usually occurs around the altitude of 11 km.

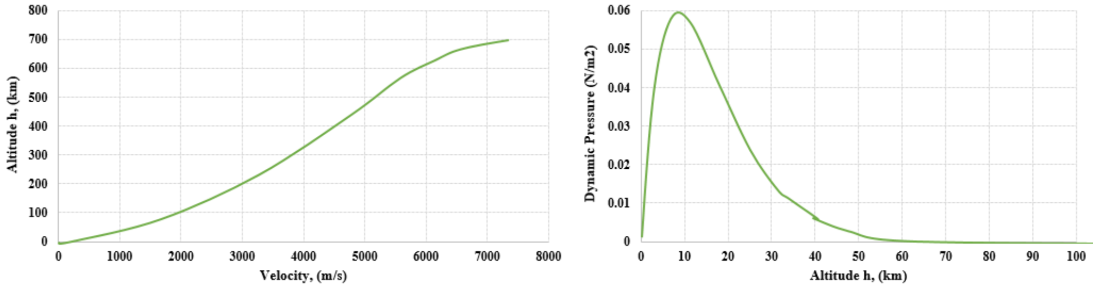

Figure 5.7 : (a) Altitude vs. Velocity **(b)** Dynamic Pressure vs. Altitude.

On the other hand, the simulations are resulted with smaller drag losses unexpectedly. These results may occur because of two reasons. One of them is launch vehicle may have lower velocity compare to real launch vehicle trajectories and the other one is the drag model of the tool. Drag model may underestimate the drag coefficient. These results will be improved for future studies via improving the models.

Finally, at the end of simulations the total flight times are lower than the real trajectory values. As because the coasting phases are shortened during the simulations. This situation is resulted with unburned propellant for each launch vehicle last stages, % 30 and %35 respectively unburned propellant is left VEGA LV. All of these results show that the trajectory model is compatible to use for a preliminary design tool.

5.2 Application of Code

5.2.1 PANUFA mission requirements & constraints

It's mentioned in previous chapters, Nano and microsatellite market and their mission capabilities are increasing extremely thanks to improving technology. PANUFA Launch Vehicle main mission targets are launching 60 kg payload to 350 km polar circular orbit. This launch vehicle will have "green hybrid rocket engines".

According to these main mission parameters and user defined vehicle and engine constraints which are listed for PANUFA in Table 5.8, a three stage launch vehicle is designed, optimized and simulated. The main objective behind the stage number selection is coming from the nature of hybrid d rocket engines, as hybrid rocket engines have long burning time and as a result of this situation their solid fuel diameter grows steadily.

To maintain the burning times as short as possible, a three stage launch vehicle is considered also to optimize the GLOW. Table 5.9 shows the trajectory phases PANUFA.

The first stage burns during the first four phases, after which the stage separation is conducted. During the code validation process coast phases for the HLV and Minotaur Rockets are limited with 3 seconds, unless to these validation procedure longer coast phase is conducted to this nanosatellite launch vehicle's trajectory to follow.

According to first simulation results, it has been seen that the target apogee is already achieved after this long coast phase of the ascent phase which is just the burning.

Table 5.8 : User Defined Constraints & Main Mission Parameters

Constraints	Value
1. Max. Allowable Instant Thrust	20 kN
2. Targeted Altitude	300 km
3. Maximum Diameter	2 m
4. Maximum Length	4 m
5. Payload	60 kg

Table 5.9 : Trajectory Phases of PANUFA

Stage	Component	Final
1	**Lift-Off**	0
	Gravity Turn	5
	Pitch Constant	55
	Coast	58
2	**Second Stage Ignition**	59
	Second Stage Burn Out	144
3	**Third Stage Ignition**	145
	Orbit Insertion	272

The first stage burns during the first four phases, after which the stage separation is conducted. During the code validation process coast phases for the HLV and Minotaur Rockets are limited with 3 seconds, unless to these validation procedure longer coast phase is conducted to this nanosatellite launch vehicle's trajectory to follow. According to first simulation results, it has been seen that the target apogee is already achieved after this long coast phase of the ascent phase which is just the burning

The change from the initial mass estimations to optimized one in Table 5.10. As mentioned before, the structural masses were heuristic estimations and were not changed during the optimization progress dramatically as propellant masses.

Table 5.10 : Change of the mass values from the initial estimations to final

Stage	Component	Initial	Final
1	**Fuel**	645	261
	Oxidizer	3867	1569
	Engine Structure	650	270
	Fuel Case	100	25
	Tank Structure	1200	415
	Total Stage Mass	6462	2540
	Structural Mass Ratio	0.32	0.28
2	**Fuel**	214	144
	Oxidizer	1286	867
	Engine Structure	130	30
	Fuel Case	70	12
	Tank Structure	300	260
	Total Stage Mass	2000	1313
	Structural Mass Ratio	0.27	0.23
3	**Fuel**	44	50
	Oxidizer	264	300
	Engine Structure	10	14
	Fuel Case	4	6
	Tank Structure	35	42
	Total Stage Mass	357	412
	Structural Mass Ratio	0.14	0.15
	Payload	**60**	**60**
	Fairing	**25**	**25**
	GLM	**8942**	**4350**
	Total Propellant Mass	**6320**	**3191**

As this is a preliminary design tool, the main objective is not to optimize a real micro launcher in the level of critical design phase. The claim of this study is creating a concept study for a project Nano Launch Vehicle at the beginning. On the other hand, this study can be the fundamental for further studies in hybrid rocket powered launch vehicle design.

5.2.2 Propulsion system

According to user's maximum value of instant thrust and the minimum required thrust value from the T/W and GLOW, the engine number and their instant thrust values are defined during the simulations. For first two stages, 17 kN engine is designed with different burn times. Their specific values are different because of the difference on the expansion ratios of the nozzle regarding to atmospheric conditions. The propellant combination is chosen for fuel as $C_{28}H_{58}$ paraffin and for oxidizer liquid nitrous oxide. The main specifications of engines are listed in Table 5.11.

Table 5.11 : Engine Specifications

Specifications	Stage 1	Stage 2	Stage 3
Fuel	$C_{28}H_{58}$	$C_{28}H_{58}$	$C_{28}H_{58}$
Oxidizer	LN_2O	LN_2O	LN_2O
Operation Altitude	Atmospheric	80 km	300 km
Payload of Stage	2542 kg	542 kg	60 kg
Chamber Pressure	40 bar	35 bar	30 bar
Max. Thrust Requirement per Engine	17 kN	17 kN	6 kN

In Table 5.12 the changes from the initial estimations to final optimized engine specifications are listed. The nominal thrust, nominal mean mixture ratio and the burn time per engine are listed in the table. Table 5.12 shows the optimizable parameters that define the hybrid rocket engines of the three stages.

Table 5.12 : Optimizable Parameters of Hybrid Rockets

Stage	Engine Thrust	Final	Engine Number	Final	O/F	Specific Impulse	Burn Time	Final
1	30	17	5	5	6	260	77	55
2	15	17	3	2	6	285	93	83
3	7	8	1	1	6	300	118	127

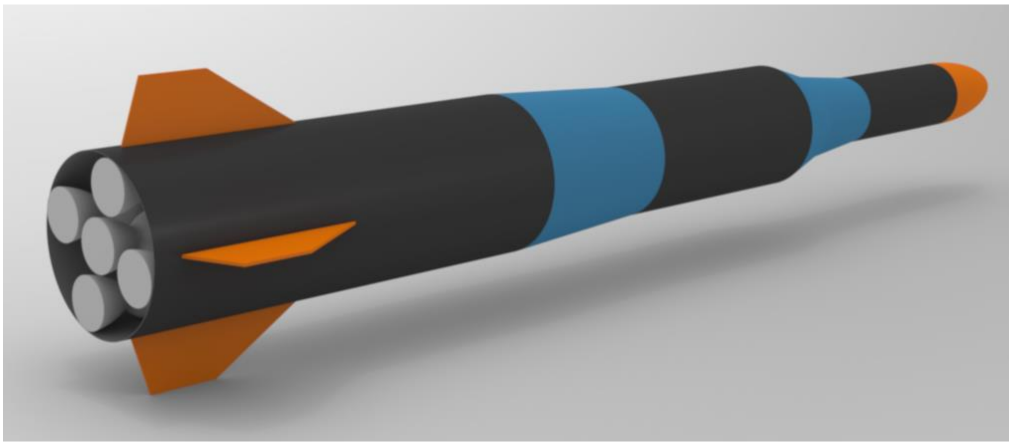

Figure 5.8 : 3 –Stage Nanosat Launch Vehicle PANUFA.

The first stage is consisted of five parallel rocket engines which fed from one unique oxidizer tank, while the second stage uses two parallel engines. First Stage and stages are showed in Figure 5.11, 5.12 and 5.13. The upper stage have a single small engine compare to lower stages because of its requirements. Table 5.13 shows the overall specifications about geometry of the engines for each stages.

Table 5.13 : Overall Geometric Specifications of Engines

Stage	Component	Final Value
1	Fuel Length	66 cm
	Fuel Diameter	35 cm
	Throat Diameter	70 mm
	Expansion Ratio	5
	Tank Diameter	115 cm
	Tank Length	226 cm
2	Fuel Length	62 cm
	Fuel Diameter	42 cm
	Throat Diameter	50 mm
	Expansion Ratio	7.5
	Tank Diameter	100 cm
	Tank Length	192 cm
3	Fuel Length	50 cm
	Fuel Diameter	38 cm
	Throat Diameter	35 mm
	Expansion Ratio	20
	Tank Diameter	57 cm
	Tank Length	146 cm

The illustration of the launch vehicle with its dimensional details is showed in Figure 5.10.

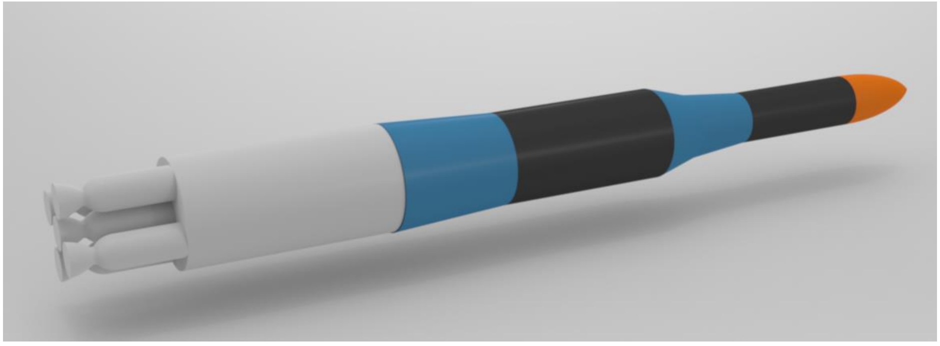

Figure 5.9 : First Stage 5- Clustered Engine Details.

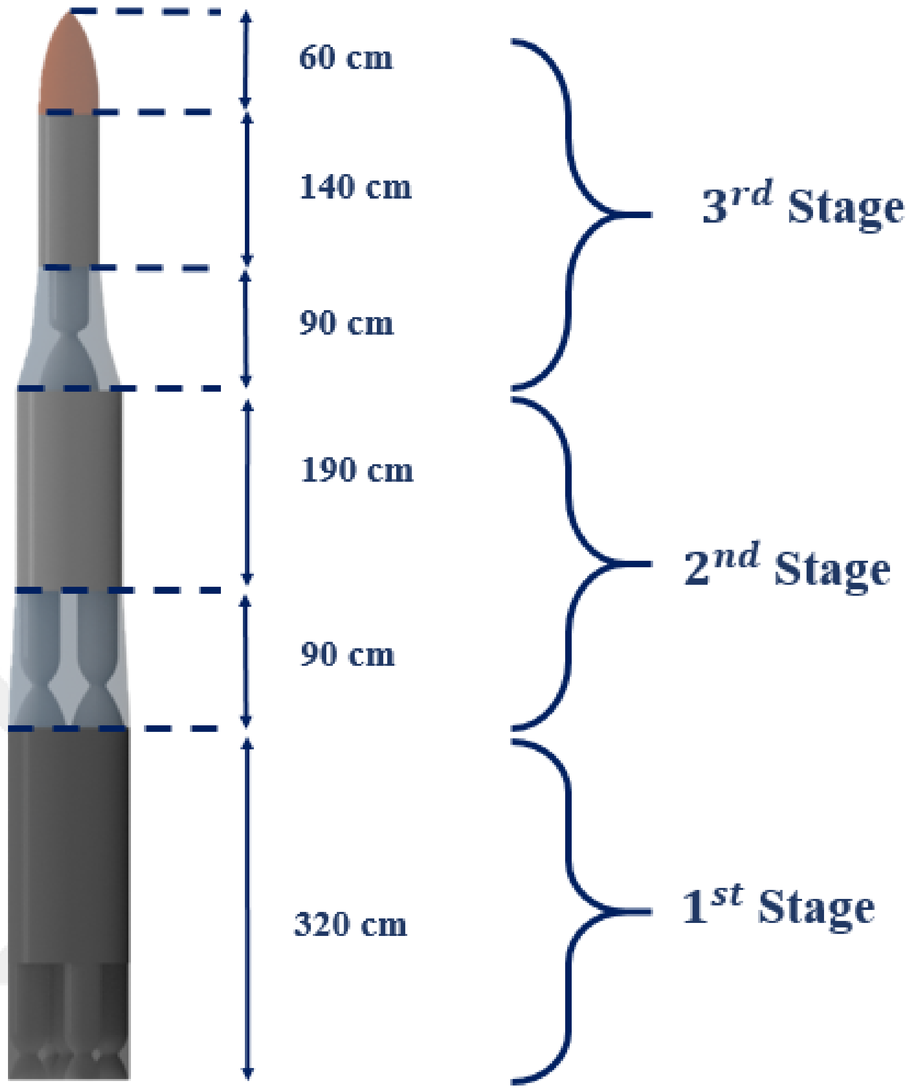

Figure 5.10 : Dimensional Description Illustration of PANUFA.

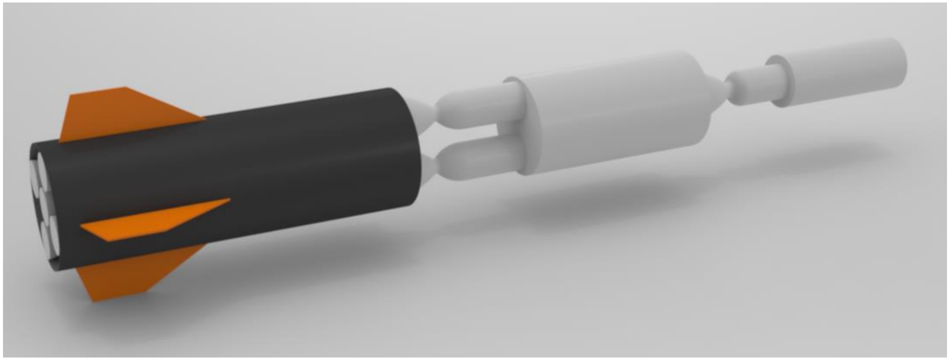

Figure 5.11: Second Stage Engine and Third Stage Engine Details.

The trajectory simulation results of PANUFA is showed in Figures 5.12 through 5.14.

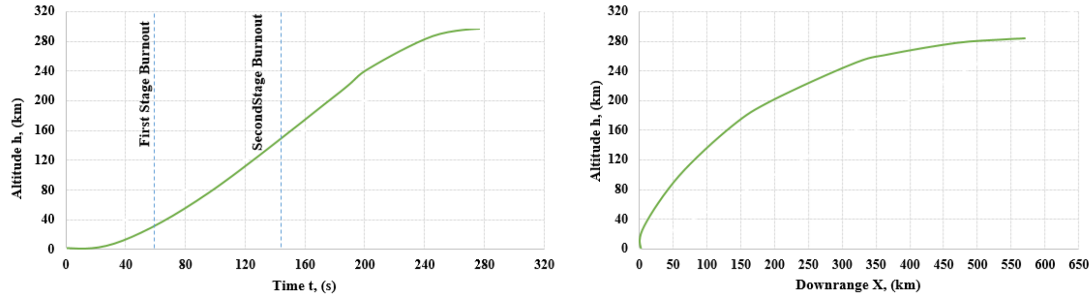

Figure 5.12 : (a) Altitude vs. Time **(b)** Altitude vs. Downrange of PANUFA.

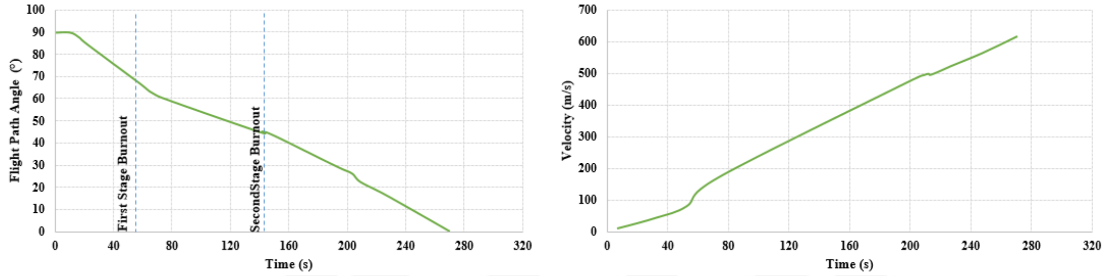

Figure 5.13 : (a) Flight path Angle vs. Time **(b)** Velocity vs. Time of PANUFA.

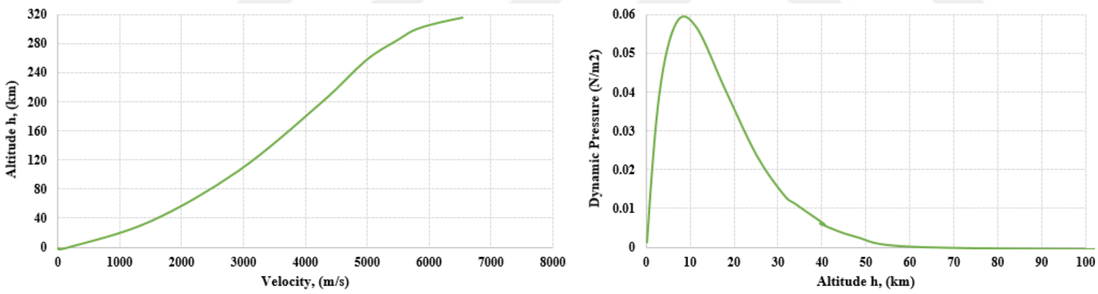

Figure 5.14 : (a) Altitude vs. Velocity **(b)** Dynamic Pressure vs. Altitude PANUFA.

5.2.3 Simulation results for PANUFA

The initial guess of the structural mass ratios of each stages were not approach to mass estimation relation results. There were an iterative process to approaches to staging optimization results with the mass model. The results about this optimization process are showed in table 5.9. On the other hand the initial guess of trajectory did not achieve the desired orbit requirements which is 350 km circular orbit. First simulation of the trajectory model is resulted with a suborbital trajectory with apogee of 370 km and the perigee of 400 km. The iteration process is initiated also for trajectory model to achieve the desired orbit requirements via reducing total mass of the launch vehicle. According to these optimization process, the results for the optimized vehicle is showed in the Table 5.10,5.11,5.12 and 5.13.To reach the final orbit, the burn phases of the second and third stages were prolonged, while the first stage's burn duration was reduced by 15 seconds. The maximal thrust level of the first and second stage was reduced, due to the lowered total mass.

The GLOW of the Launch Vehicle is reduced by %25 via optimizing the propulsion system parameters such as O/F Ratios, expansion ratio of the nozzle and the chamber pressures according to outputs of the trajectory model. Most of the reduced mass is consisting of propellant mass. The total reduced mass is 5700 kg and the 5500 kg of them is propellant. One of the constraint is the stage diameter for the tool, this constraint limits the maximum diameter of the nozzle and as a result of this maximum achievable expansion ratio is limited.

To keep the exit diameter of the nozzle diameter increment as small as possible, the throat diameter should be decreased via increasing the chamber pressure which is limited with the oxidizer tank pressure. Tank pressure should be minimum 1.5 times of the chamber pressure to keep the oxidizer mass flow in a regular region with correct flow velocity. On the other hand, nitrous oxide density is decreasing with the increment of the tank pressure. This is also limiting the maximum tank pressure. 60 bar of the nitrous oxide tank pressure is maximum allowable for practical applications to keep the oxidizer tank mass & volume values in an optimum range. According to all these limitations, optimization problem is solved and vacuum thrust values are increased and the total engine structure mass is decreased with smaller nozzles.

All these constraints and optimization processes are important to improve the models. One of the main difference of this tool is its own propulsion design module. This situation makes more changes on the system design available. When it's analyzed, the first results are still very promising for this nanosatellite launch vehicle design. While the total propellant mass of the 2^{nd} and 3^{rd} stages are increased, first stage size is really decreased with respect to other stages. This was an expected results because of the mission phases in which first stage has the atmospheric flight mostly and larger first stage means more drag losses and gravity losses.

6. HYBRID ROCKET MOTOR DESIGN & DEVOLOPMENT STUDIES

6.1 Specifications and Design Goals

The mission requirement for the ITU PARS Team experimental rocket was to reach an apogee of 2 km with the capability of 4.5 kg payload. The propulsion system should be designed to propel the rocket for 2 km of apogee. The mission requirements are conducted to motor analysis in the previous study to find the required thrust and burn time value. The total impulse obtained from the regarding mathematical model and the SONUS motor is designed accordingly.

SONUS hybrid rocket motor design and manufacturing process will be discussed in the following chapter. This chapter also includes the optimization of the motor for the limited diameter of the rocket body according to these mission requirements. Detailed description of the final design is also included within this chapter.

6.2 SONUS Propulsion System Design

6.2.1 Nitrous oxide/Paraffin wax performance analysis

Before starting the design of the rocket motor, as mentioned in the chapter 3, a performance analysis of the propellant combination must be realized. For this project, nitrous oxide was chosen as an oxidizer and paraffin wax was chosen as a fuel. This thermochemical performance analysis characterizes the optimum oxidizer-fuel mixture ratio for the user defined chamber pressure.

The thermochemical performance analysis can generate graphics and tables of performance outputs for a range of chamber pressures and oxidizer-fuel mixture ratios. Two of these graphs are shown Figures 6.1 (a) and (b) which contains the information about change of the specific impulse and characteristic velocity with respect to oxidizer to fuel ratio and for different chamber pressures of 30, 40 and 50 bars. In these graphics, it is assumed that the ambient pressure is 0.9 bar approximately and there is no losses on combustion efficiency. [24]

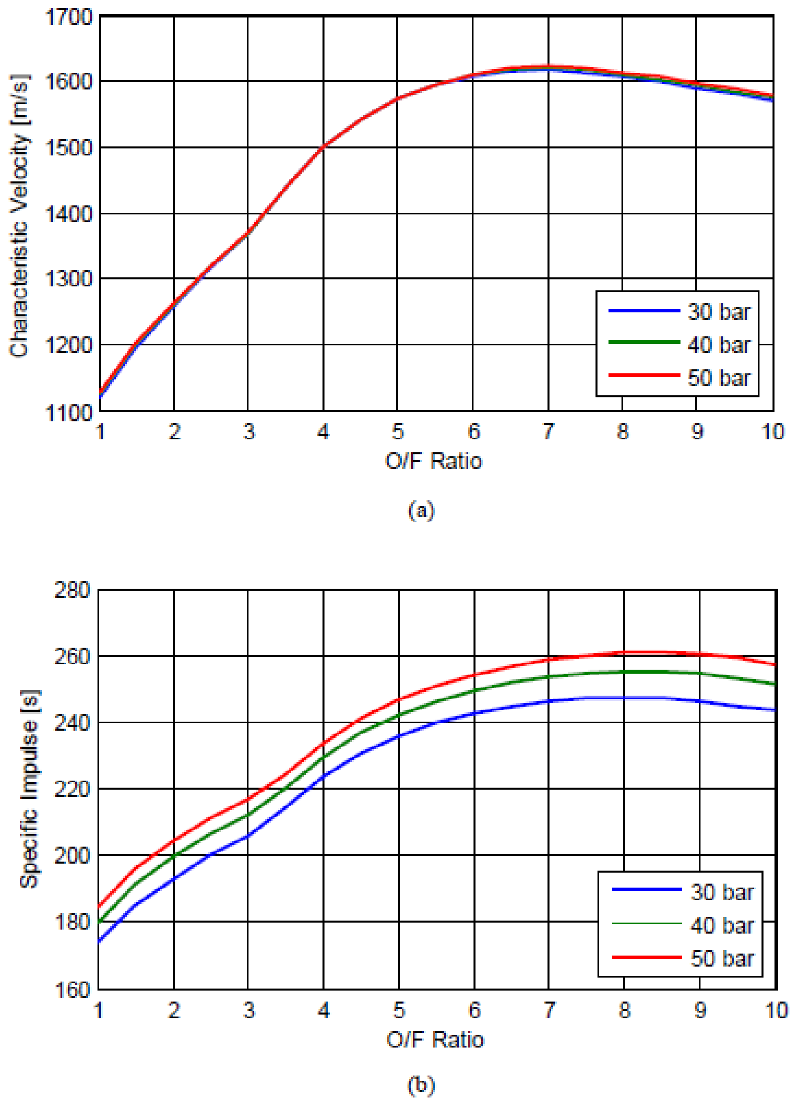

Figure 6.1 : Specific Impulse and Characteristic Velocity vs. O/F Ratio.

Figure 6.1 (a) shows that the increasing of the chamber pressure is resulting with the higher specific impulse which is one of the most important motor performance parameter to design an efficient system. However, for the characteristic velocity it can be seen that the increment on the combustion pressure is relatively insignificant shown in Figure 6.1 (b).

Generally, chamber pressure of the hybrid rocket motors is limited with by the oxidizer tank pressure. To maintain the oxidizer flow as stable from tank to combustion chamber, the pressure from tank to combustion chamber needs to be at least %20 approximately. This will also guarantee the stable combustion. According to the many of test results, average tank pressure of 51 bars was used for a self-pressurized blowdown process. In actual, tank pressure is starting with 56 bars and ending with 46 bars at the end of the blowdown process. Also the feed system losses are approximately 5 bar. As a result of all these assumptions, the expected operating chamber pressure is 32 bars for a tank pressure of 51 bars in average. According to graph 6.1 (a) higher chamber pressure is more efficient compare to lower values, however the higher chamber pressures can produce more likely unstable combustion. On the other hand, if the chamber pressure is lowered under 30 bars, the motor performance decreases considerably. Therefore, an oxidizer-to-fuel ratio and chamber pressure of 6 and 32 bars were selected for the SONUS experimental motor**.**

6.2.2 SONUS motor design

Hybrid rocket engine SONUS was designed by PARS Rocketry via using this study tool. The final performance parameters (Specific impulse, characteristic velocity, combustion chamber pressure, etc.) were obtained after analyzing the design requirements. Firstly, rocket dry mass was determined. After that, the first value of engine total mass was determined according to statistical data. The code ran in order to find the required thrust and burn time values for the rocket. The flow diagram for initial thrust requirements determination is showed in Figure 6.2 and 6.3.

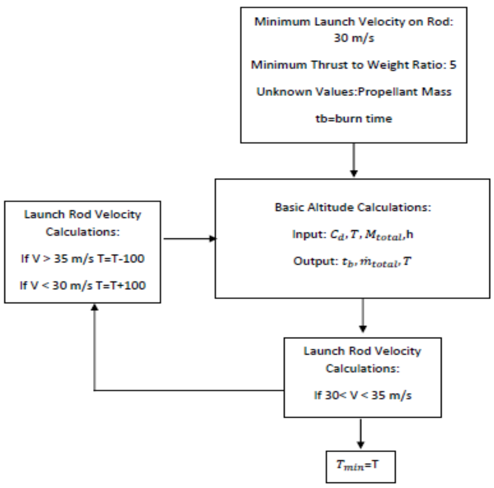

Figure 6.2: Thrust –Burn Time Determination Flow Diagram.

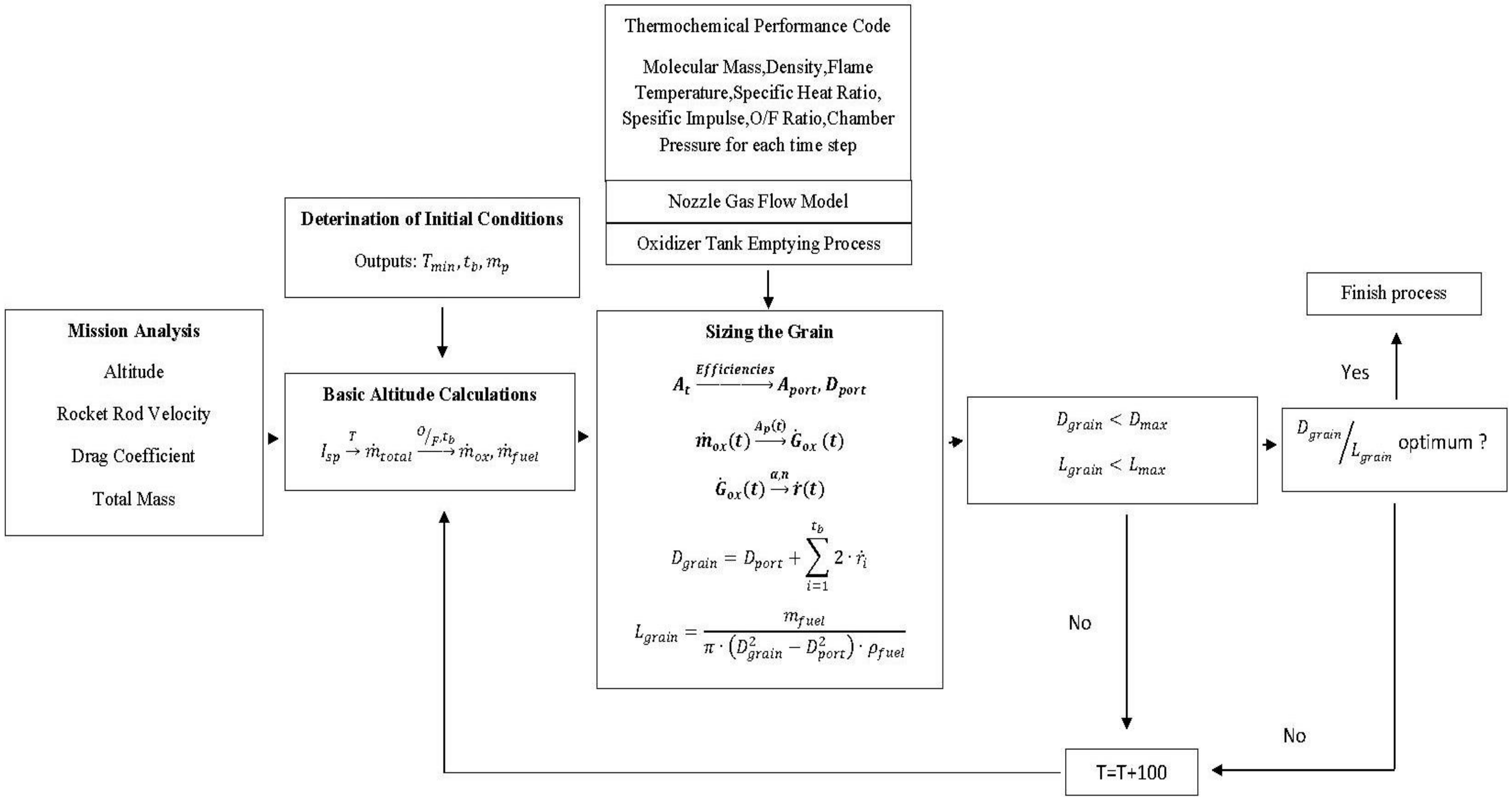

Figure 6.3 : Previous Study General Flow Diagram.

After determination of the thrust and burn time values, the thermochemical performance and motor sizing tools were ran to find the optimum motor design parameters such as specific impulse, oxidizer to fuel ratio, mass flow rates and total propellants masses. In this previous work, the sizing process was related with the external dimension of the solid fuel. User can input maximum allowable solid fuel diameter according to their manufacturing capabilities. Therefore, changing the burn time and thrust values (keeping total impulse as constant) possible external diameters can be obtained from the sizing tool. The sample result of the sizing process shown in Table 6.1. The 3D Section of the SONUS is showed in below Figure 6.4.

Table 6.1: Sizing Process Sample Results

Thrust(N)	Burn Time(s)	Grain Diameter(mm)
1600	7.5	80.27
1800	6.7	78.67
2000	5.94	78.28
2200	5.32	76.4

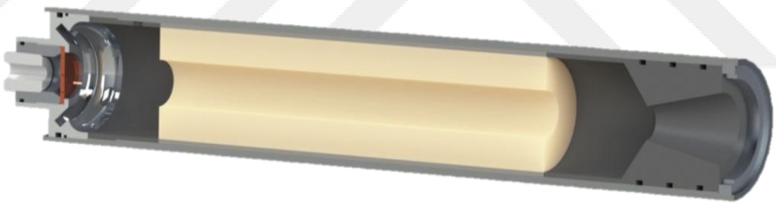

Figure 6.4 : 3D Section of SONUS.

According to the tool simulations, the resulted motor design SONUS is expected to give about 9625 N.s of total impulse and will have 3.85 seconds of burn time. Specific impulse is 241 N with an oxidizer to fuel ratio of 6. Paraffin was used as solid fuel and it has 600 gr of total mass; as the oxidizer, nitrous oxide was found to be proper and has a mass of 4 kg. Oxidizer mass flow rate is 0.9976 kg per second. According to this value, head losses and maximum values for the piping were calculated. According to these assumptions, ¾ “pipeline and valves were used.

Fuel grain has an outside diameter of 76.4 mm, a port diameter of 32 mm and a length of 190 mm. In order to reduce weight and the complexity of the system, a single tank was used. The tank will be wrapped directly with the body. The cylinder is made of composite material. Other than this, the cylinder has the same thread profile at its cap.

The resulted motor design geometrical information is tabulated in Table 6.2

Table6.2 : SONUS Propulsion System Final Design.

SONUS				
SONUS MOTOR	**Fuel Grain**	**Propellant**		$C_{28}H_{58}$ Paraffin Wax
		Composition		%90 Wax % 5 PE %2 C %3 Acid
		Grain Configuration		Cylindrical
		Number of Ports		1
		Initial Port Diameter	**m**	0.025
		Grain Diameter	**m**	0.078
		Grain Length	**m**	0.25
		Oxidizer to Fuel Ratio		6
	Nozzle	**Material**		Graphite
		Shape		De-Laval
		Expansion Ratio		4.85
		Throat Diameter	**m**	0.0023
		Exit Diameter	**m**	0.0056
Oxidizer Tank	**Oxidizer**			LN_2O
	Loaded Oxidizer Mass		**kg**	6
	Tank Volume		**m3**	0.008
	Ullage		**%**	6
	Initial Tank Pressure		**bar**	62

SONUS is expected to give about 9625 N.s of total impulse and will have 3.85 seconds of burn time. Specific impulse is 241 N with an oxidizer to fuel ratio of 6. Paraffin was used as solid fuel and it has 600 gr of total mass; as the oxidizer, nitrous oxide was found to be proper and has a mass of 4 kg. Oxidizer mass flow rate is 0.9976 kg per second. According to this value, head losses and maximum values for the piping were calculated. According to these assumptions, ¾ “pipeline and valves were used. The full section view of SONUS is shown in Figure 6.5.

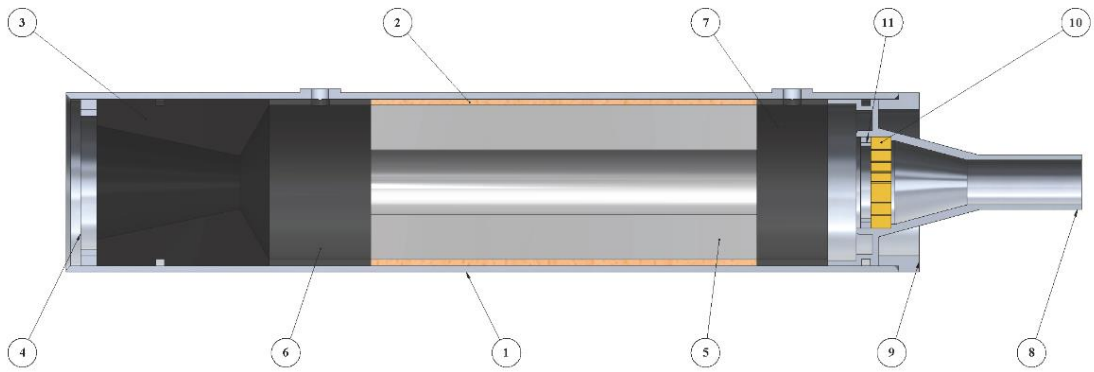

Figure 6.5 : Cross Section of the SONUS Hybrid Rocket Motor.

Table 6.3 : Sub-Components of SONUS

Item No.	Item Name
1	Motor Case
2	Propellant Liner (Craft)
3	Nozzle
4	Nozzle Retainer Ring
5	Solid Propellant
6	Post-Combustion Chamber
7	Pre-Combustion Chamber
8	Bulkhead
9	Bulkhead Retainer Ring
10	Injector
11	Injector Retainer Ring

The motor has pre and post-combustion chambers which are 35 mm and 50 mm in length, respectively. Other than this, it has a graphite casing. The nozzle is a converging-diverging nozzle which is made of graphite. It is held in its position with a nozzle retainer ring which is made of aluminum. The nozzle and the bulkhead will be assembled with Viton O-rings in order to ensure the sealing at high temperatures. The feeding system is sealed with Loctite, and it is made of AISI 316L stainless steel. The engine is made of Al 7075-T6. Chamber was designed to operate at 32 bars of pressure. The injector discharge coefficient is determined via cold flow tests. Discharge coefficient is 0.65 with 80 holes diameter of each is 0.8 mm to maintain 23 bar pressure drop across the injector plate. Injector plate has a showerhead geometry.

6.3 Fuel Grain Manufacturing

The fuel grain section of the motor consists of the paraffin wax fuel, pre- and post-combustion chambers which are 35 mm and 50 mm in length, respectively and machined from graphite. The paraffin fuel is coated by a craft liner to reduce the heat transfer to wall of the motor case. In the previous studies, it was observed that producing the paraffin fuel just with paraffin wax and stearic acid is not enough to provide required strength to fuel. The fuel was not durable to such a high pressure of 32 bars. Moreover, the production process was not easy for rotational casting process. Therefore, the new fuel criteria are determined, listed below:

- Low cost easy manufacturing,
- Providing good mechanical properties with no slosh possibility,
- Providing fine thermal stability,
- Moderate viscosity for liquid layer to get maximum possible regression rate,
- Allows the possible maximum heat of formation.

Karabeyoglu and his team developed an original mixture of paraffin-based hybrid rocket fuel with the name of SP-1 at Stanford University and its content is secret. PARS Team has researched the possible paraffin wax production processes to increase their thermal stability, strength and the other properties. This research was on site industrial research with the paraffin producer companies. The result of this research is fuel SONUS-14, which contains following additives:

Table 6.4 : SONUS- 14 Fuel Content

Compound Name	Percentage (%)
PE AC@6A	4.5
EVA	1.5
Stearic Acid	7
Aluminum	8
DCPD	0.8
Carbon Black	1.7
Dispersant	1.7
Carbon Master batch	0.8
Microcrystalline wax	6
Paraffin Wax	68

Polyethylene Wax (PE wax) is used to increase the mechanical properties, density and thermal stability. However, PE Wax has high viscosity which means that the regression rate will tend to decrease. Therefore, PE Wax addition percentage is chosen under 5 according to studies in the literature. EVA is copolymer of ethylene and vinyl acetate. It is very important to add vinyl acetate content for wax reinforcement because of EVA's good adhesion and cohesive strength features. However EVA is also viscous material and it also has an effect on regression rate. According to same study, EVA is more viscous then PE Wax and its content is lower than PE Wax. DCPD is required to get better adhesion of EVA in wax reinforcement.

It is often to use stearic acid in candle industry to get better mechanical properties of paraffin waxes. On the other hand, stearic acid is decreasing the viscosity of the waxes which means that the regression rate will tend to increase. Using stearic acid will compensate the losses from PE and EVA waxes. Moreover stearic acid provides better dipping properties. Carbon black is used to improve the radiation absorption of the fuel. The role of Carbon Black Master Batch is dispersing the carbon black powder homogenous along the fuel. Dispersant also has the same role with master batch.

The Microcrystalline wax is a mix of saturated hydrocarbons. When it compared with paraffin waxes, it has more poorly defined crystal structure. This feature of microcrystalline waxes provides higher melting point and strength properties itself. However, its viscosity is much higher than paraffin waxes. This will block the required unstable liquid layer on the combustion surface if it used high level in the fuel content. Because of its branched molecular structure, the slosh possibility is decreasing. As a result of this it's decided to use this wax 6 percentage in the fuel composition. The density of final fuel mixture is approximately $900 kg/m^3$, the heat of formation $\Delta H_f =$ $-976 kJ/kg$. The molecular formula of 1kg of mixed wax fuel is;

$$C_{70}H_{140}O_{0.6}$$

The mixture process is explained in the following section. The content is divided into two mixtures. The first mixture contains microcrystalline wax, paraffin, stearic acid, master batch and carbon black and aluminum.

The first mixture was heated up to 90 °C without aluminum and mixed approximately 30 minutes. After then the aluminum is added to the mixture and they mixed again for 10 mins. The second mixture contains EVA, DCPD, PE Wax AC@6A and small portion of first mixture. This mixture is mixed at temperature of 130 °C 30 minutes. At the final stage, these two mixtures were mixed together at temperature of 175 °C for 25 mins and then directly casted into mold. A special centrifugal casting machine is designed for wax grain manufacturing. The general view of casting machine is presented on the Figure 6.6.

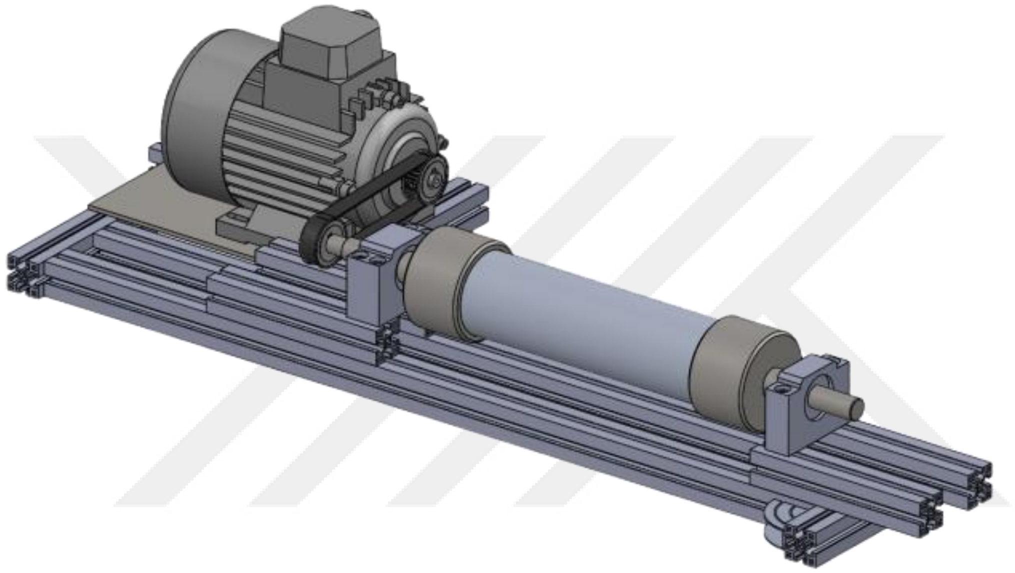

Figure 6.6 : Centrifugal Casting Machine.

A washing machine motor is used to provide and control the rotational speed. The wax grain production capability of machine is maximum of 100 mm in diameter and 600 mm in length. The production process follows there steps. First the mixture is casting into steel mold in a vertical position then the mold is closed horizontally. At the final stage, the motor is started to spin around from 1200 to 2900 rpm. This changeable rate is important to create homogenous distribution of the every compound of the content of the mixture. This centrifugal casting process also provides the forming of the port with a good finish surface. The port diameter has a tolerance of ±1 mm. The casted grain is showed on Figure 6.7.

Figure 6.7 : Casted Grain.

6.4 Propulsion System Test

6.4.1 Test stand design

SONUS Experimental motor is a laboratory scale motor which is designed, manufactured, and tested to study the combustion characteristics and motor performance of a paraffin wax/nitrous oxide propellant combination. The assembled test rig, shown in Figure 6.8, incorporates the lab-scale motor, load cell, oxidizer delivery system and control sub-systems on a movable test stand.

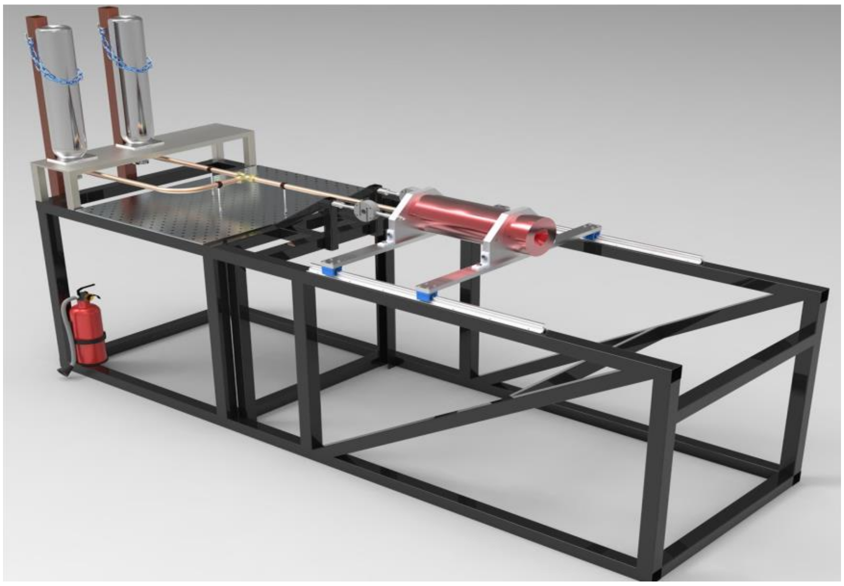

Figure 6.8 : Assembled Test Rig.

Main feeding system has a ¾” of tubing. The beginning of the feeding system has 3/8” tubes, because of the cylinder having the same profile. To avoid any expansion of nitrous oxide through the pipeline, %20 area ratio rule was used to design pipeline. A conical connector was designed and used to increase the pipe diameter from 3/8 “to 3/4 “. Staubli quick coupling was used for the filling line. These couplings are easy to use with no external tools needed. There is a check valve inside it to make the system leak proof. There are a female and a male parts of it, one will be inside the rocket and the other will be connected to the filling tank. With a single push and turn movement, the tank will be filled. The oxidizer flow will be controlled by a solenoid valve, actuated by the controller. The ignition is performed by solid fuel charges in the bulkhead, which will be fired after the oxidizer flow starts.

6.4.2 Cold flow test

The main aim of the tests is to measure the pressure throughout the feeding system at certain locations such as valve inlet, valve outlet, and injector inlet. Tests were performed sixteen times with different cylinders, valves and, connectors. Due to the difficulty of using ball valve with a reduction system, it was decided to use a solenoid valve even though it has more head loss in comparison to a ball valve. The obtained data at early tests showed that the pressure drop was caused by orifice effect, mainly. The test setup and one of the results are shown in Figure 6.9 and Figure 6.10, respectively.

Figure 6.9 : The Cold Flow Test Setup.

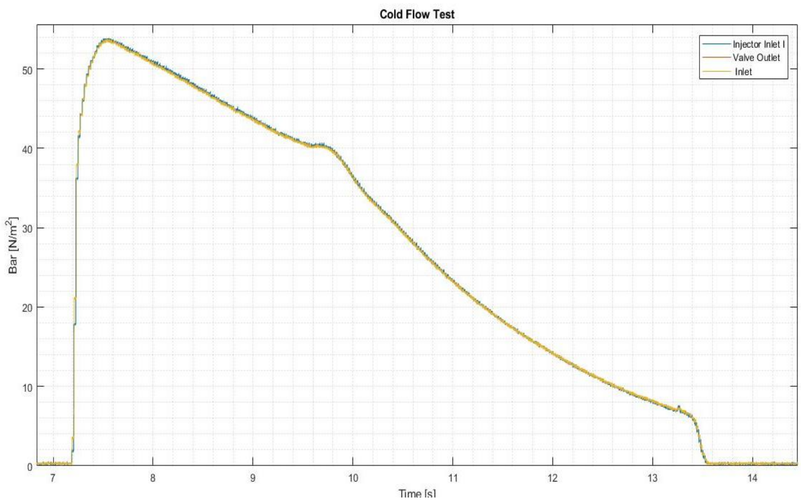

Figure 6.10 : Cold Flow Test Results.

6.4.3 Hot fire test

The main aim of the tests is measuring the thrust force generated by the motor by using two S-type load cells. Tests were performed eight times. At the early tests, maximum instantaneous thrust force was measured about 600 N due to orifice effect, detected after one of the cold flow tests. Peak thrust force was increased to 1600 N after the problem, because of orifice effect, had been solved. Eventually, in the latest test, the approximate value of 2700 N peak thrust was measured by optimizing the chemical ingredients of the solid fuel and the feeding system. Fluid circuit diagrams are depicted below in Figure 6.11, Figure 6.12, Table 6.5 and Table 6.6, respectively.

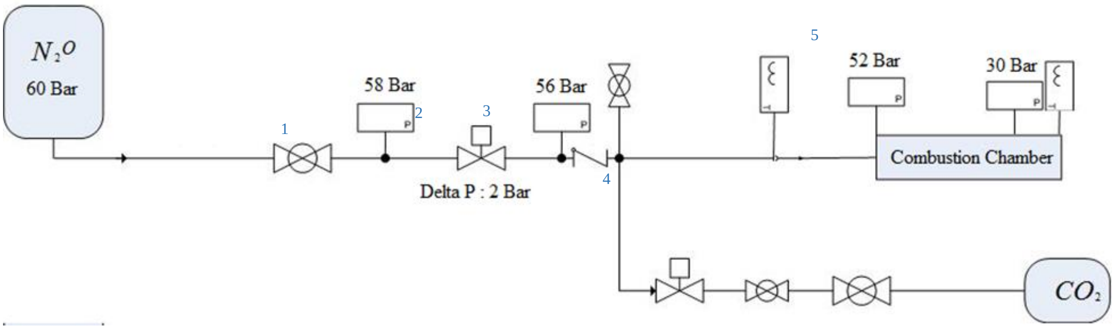

Figure 6.11 : Test Stand Fluid Circuit Diagram.

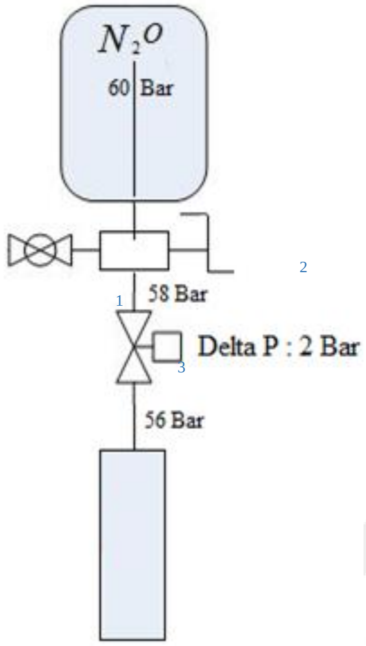

Figure 6.12 : Fluid Circuit Diagram for Flight.

Table 6.5 : (a) Static Test Part List **(b)** Flight Configuration Component List

Item No.	(a) Description	(b) Description
1	Ball Valve	Ball Valve
2	Pressure Transducer	Solenoid Valve
3	Solenoid Valve	Quick Connector
4	Check Valve	-
5	Thermocouple	-

7. CONCLUSION

The main objective of this study is development of a preliminary design tool for hybrid rocket powered nanosatellite launch vehicles. To code the tool, MATLAB is used in which many of sub tools are developed to finalize the design. A system of parameters is created to understand the variables behavior when they are dependent to each other in a design process. These variables are diameter, length, burning time, thrust, specific impulse, geometry, masses and many of others. As mentioned before, one of the main difference of this design tool is its propulsion system optimization tool which is directly integrated to tool nonetheless differ from other studies which are generally based on trajectory optimization. As a result of this situation, firstly a propulsion analysis tool is developed.

The main idea behind this tool is creating the optimum design of the propulsion system for the selected fuel and oxidizer combination. To find the optimum oxidizer to fuel ratio, O/F Ratio vs. specific impulse graphic is generated as a result of this tool. According to this graph, for the maximum specific impulse value the oxidizer to fuel ratio is selected. To achieve this, firstly thermochemical performance analysis are initiated in the tool. In this analysis, a set of chemical reactions are solved to find the combustion temperature to find the performance parameters of the oxidizer fuel combination. This set of chemical equations are solved simultaneously with the Gibbs energy minimization method and ordering the chemical reactions. When all performance parameters of the motor are settled, the motor design can be performed according to results of the further tools such as mass and thrust tool.

A tool is created to estimate the mass of every main component of the launch vehicle. Mass estimation relations are established and linked to this tool to perform better estimations. Moreover, detailed calculations for hybrid rocket motor component masses are integrated to this tool. On the other hand, there is still lack of information about hybrid rocket motor powered launch vehicles because of the immaturity of this technology. This situation still makes the mass estimation process harder compare to estimation of liquid or solid motor powered launch vehicles. In addition to this shortcoming during the analysis, there is no operational hybrid launch vehicle according to current technology level. This situation makes the validation process limited for the mass estimation tool. However, for the rest of the vehicle, such as avionics or fairing the general mass estimation relations are working properly. The results show that the combined working of staging optimization and mass estimation tool, provides realistic results for the structural masses of the launch vehicles. In the tool, the structural mass ratio iterates with the staging optimization tool until it converges to the mass estimation tool results. The tool also calculates the volume and dimensions of the main components with the goal of getting more realistic results for the mass estimations. Hence a material selection database is also created to support this tool.

To define the required thrust and engine numbers, a small tool is created. Using the T/W relations, the minimum required thrust is determined within the program. Using the user input of maximum allowable thrust which can be generated from their engine instantly. the number of engine and the external & internal geometry of the vehicle can be settled. Using the outputs of the above three tools, the motor design can be finalized. According to motor design, the final launch vehicle mass & geometry model can be initiated to transfer that data to trajectory tool.

For the target orbit and payload mass, a hybrid launch vehicles is designed to analyze its trajectory to check whether it follows required mission profile. As a result of this situation, a basic trajectory tool is integrated to this design tool just for trajectory analysis not for optimization. In this tool, the trajectory was analyzed for three main phases. The first phase is lift-off phase which is simulated till 500 m altitude in this program. But this value can be optimized for the further studies. After lift – off, the gravity turn starts. Gravity turn is used as a natural maneuverer in this code hence it ends when atmospheric affects are negligible. The final phase is free-flight phase which starts with the exo-atmospheric conditions occurrence.

A simplified drag model was used, where the drag coefficient only varies with Mach number. For the atmospheric model, a combination of the US standard of 1962 and 1976 standards is used and this is valid up to an altitude of 2000 kilometers. Moreover, a simplified gravity model is used where the gravity only varies with altitude.

Validation the design tool is important to show its accuracy with these validation results. In this study, the model validation was realized with Minotaur and Hybrid Launch Vehicle Design.

Before starting to validation, all the parameters were selected & fixed for two different vehicles. For HLV Launch Vehicle all values are gathered from its user manual. On the other hand, all values for the designed hybrid launch vehicles are gathered from it's study. The results showed that all the structural masses were almost proper, when they compared with the original data of the launch vehicles. For the HLV Rocket, the mass model overestimates the structural mass; on the other hand for the designed hybrid rocket launch vehicle, the results were almost same to study data. This difference is coming from the mainly their propulsion systems. Because hybrid rocket motors occupies more volume compare to solid rocket motors. This creates the difference in the model. Moreover, the VEGA Rocket is built with the latest level of the technology and that rocket is one of the lightest launch vehicle in the world. Nonetheless all these information, all the propellant masses were inferior both for the VEGA and designed hybrid rocket, this can be explained by the fact that the mass model and staging optimization working together also with correct structural mass ratio. hence the propellant masses can be calculated very properly for all type of the vehicles.

After the validation of the mass estimation tool, it was possible to validate the trajectory tool. The main idea behind the validation of trajectory tool is checking whether the launch vehicle achieve the desired orbit targets. Both for the VEGA and designed hybrid launch vehicle simulations were successful, they achieved the desired orbit. Definitely there are some differences between results and their original data, can be explained by maximum constant thrust assumption for every stage of the vehicles.

Moreover, all propellant masses are assumed to be consumed during the flight in the tool, which was not reflect the real launch vehicle flight performance and operation.

When the trajectory tool simulations were ended, if the desired mission parameters are not achieved, the tool can change some parameters on the propulsion system. These parameters are thrust, burn time, O/F Ratios. For an example, increment on the thrust values (within the limits & with constant total thrust) will be resulted with faster atmospheric phase flight. Moreover, increment on the thrust means that the burn time decrement. This will be resulted with decreased outer diameter of the launch vehicles. Hence launch vehicle will have less drag and less atmospheric phase duration. Moreover, with the change of O/F Value also changing the total propellant mass and volume and it can improve the performance of the vehicle. If the vehicle is not converging to its desired mission requirements nonetheless the program can check also the maximum allowable altitude for the targeted payload and maximum allowable payload for the targeted altitude.

After all validation processes, a nanosatellite launch vehicle is designed. All the masses were calculated. During the iteration process all masses are changed and the final and initial masses were showed in the related chapter.

According to all these information to make a conclusion it can be said that this tool can assist the design process of a nanosat launch vehicle and can improve the configuration. All sub tools validations were realized and compared with designed and real launch vehicles. All results show that this design tool can be used as a starting point to design a nanosat launch vehicle. It is also showed that by varying some parameters it is possible to obtain a whole new configurations, for the different mission requirements which are defined by the user earlier.

7.1 Future Work

For the future developments of the design tool, below ideas are listed to link them to further studies on this area.

- Graphical User Interface (GUI) implementation which will allow the usage of the code without the knowledge of the programming language.
- Improving the mass model for the motor and its feed system.
- Implementing an improved drag model. An external aerodynamic tool can be integrated to the tool such as RASEARO or DATCOM etc. For different nosecone shapes, different drag models can be developed to get more realistic results on the trajectory analysis.
- Multi-Disciplinary Design Optimization algorithm development and implementation to tool for finding the most optimistic launch vehicle design with respect to prioritize disciplines which are defined by users.
- Creating more flexibility for the users via adding more options for different staging strategies, different grain geometries and special nose cones into the content of the code.
- Cost model implementation to the tool. As a result of this implementation, one more discipline will be considered to optimize the system.
- Different orbital scenario selection will be adapted via developing an orbital mechanics module to implement it into the current tool. As a result of this, GEO and interplanetary trajectories can be modelled within the program.
- Ascent Trajectory Module will be improved (Implement constrains in the Trajectory model, such as Max. Dynamic Pressure, Heat Flux, Bending Load and Axial Acceleration. Thrust vector control have to be created and a commercial tool will be implemented to improve results.
- For the velocity change losses, including the thrust vectoring losses and effect of earth’s non-spherical gravitational field. Moreover, adapting the effect of the gravity of the other celestial bodies.
- Re-program the code with object oriented language.
- CD is a function of both geometry and the current Mach number. While there are tools such as DATCOM which can calculate all aerodynamic coefficients, it is the goal of this new software to size a large number of launch vehicles in a short period of time. Integrating in high fidelity tools such as DATCOM would increase run time significantly and introduces potential

REFERENCES

[1] **L.B.J.S.C.E.W.** (1999). *Rocket: a teacher's guide with activities in science, mathematics, and technology.* SAE Division – National Aeronautics and Space Administration, Office of Human Resources.

[2] **Winter**, F. (1992). Who First Flew in a Rocket? *Journal of the British Interplanetary Society*, *45*, 275 - 280.

[3] **Kennedy, G.** (2006). Germany's V-2 Rocket. *Schiffer Military History*.

[4] **http://www.citizensinspace.org/wp-content/uploads/2012/06/size_comparison.jpg.** <*http://www.citizensinspace.org*> , date retrieved 05.05.2019

[5] **http://s7space.ru/en/launch-sea/** <*http://s7space.ru*> , date retrieved 05.05.2019

[6] **http://www.northropgrumman.com/Capabilities/Pegasus/Pages/default.aspx.** <*http://www.northropgrumman.com*> , date retrieved 05.05.2019

[7] **http://fortune.com/2016/04/29/ula-rocket-grounded/.** <*http://fortune.com*> , date retrieved 05.05.2019

[8] **https://www.grc.nasa.gov/www/k-12/rocket/rktstage.html**. <*https://www.grc.nasa.gov*> , date retrieved 05.05.2019

[9] **Wiesel, W.** (2010). *Spaceflight Dynamics, Third Edition.* Create Space Independent Publishing Platform.

[10] **Depasquale, J., Charania, A., Kanamaya, H., & Matsuda, S.** (2010). Analysis. *AIAA SPACE 2010 Conference & Exposition* (p. 8602). AIAA.

[11] **Vance, A.** (2015). *Elon Musk: Tesla, SpaceX, and the Quest for a Fantastic Future.* Ecco.

[12] **Stanley, D., Engelund, W., Lepsch, R., McMillin, M., Wurster, K., Powell, R., Unal, R.** (1994). Rocket-powered single-stage vehicle configuration selection and design. *Journal of spacecraft and rockets, 31(5)*, 792 - 798.

[13] **Griffin, M.** (2004). *Space Vehicle Design, Second Edition (AIAA Education).* AIAA.

[14] **Fortescue, P., Swinerd, G., & Stark, J.** (2011). *Spacecraft systems engineering.* John Wiley and Sons.

[15] **Larson, W., & Wertz, J.** (1992). *Space mission analysis and design.* Torrance,CA(UnitedStates): Microcosm,Inc.

[16] **Peters, J.** (2004). *Spacecraft Systems Design and Operations: Essential Subsystems for Manned and Unmanned Spacecraft.* Kendall/Hunt.

[17] **Hammond, W.** (1999). *Space transportation: A two systems approach to analysis and design.* AIAA.

[18] **Hammond, W.** (2001). *Design methodologies for space transportation systems.* AIAA.

[19] **Coskunpinar, N., Ozen, K., Grate, S., & Aslan, A.** (2016). Devolopment of Hybrid Rocket Design and Performance Code. *Asian Joint Conference on Propulsion and Power* (pp. 480-485). AJCPP.

[20] **Braun, R., Moore, A., & Kroo, I.** (1997). Collaborative Approach to launch vehicle design. *Journal of spacecraft and rockets, 34(4)* (pp. 478 - 486). Journal of spacecraft and rockets.

[21] **VanKesteren, M**. (2013). *Air Launch versus Ground Launch: A Multidisciplinary Design Optimization Study of Expendable Launch Vehicles on Cost and Performance.* Master Thesis.

[22] **Jamilnia, R., & Naghash, A.** (2012). Simultaneous optimization of staging and trajectory of launch vehicles using two different approaches. *Aerospace Science and Technology, 23(1)* (pp. 85 - 92). Aerospace Science and Technology.

[23] **Zotes, F., & Peñas, M.** (2010). Multi-criteria genetic optimization of the maneuvers of a two-stage launcher. *Information Sciences, 180(6)* (pp. 896 - 910). Information Sciences.

[24] **Genevieve, B., Brooks, M., Pitot de la Beaujardiere, J., & Roberts, L.** (2011). Performance modeling of a paraffin wax/nitrous oxide hybrid rocket motor. *49th AIAA Aerospace Sciences Meeting including the New Horizons Forum and Aerospace Exposition* (p. 420). AIAA.

[25] **Lestrade, J., Messineo, J., Hijlkema, J., Prévot, P., Casalis, G., & Anthoine, J.** (2016). Hybrid Chemical Engines: Recent advances from sounding rocket propulsion and vision for spacecraft propulsion. *Journal of Aerospace Lab.* , 14.

[26] **Altman, D.** (1991). Hybrid Rocket Development History. *27th AIAA Joint Propulsion Conference* (p. 2515). AIAA.

[27] **Korting, P., Schöyer , H., & Timnat, Y.** (1987). Advanced hybrid rocket motor experiments. *Acta Astronautica, 15(2)* (pp. 97-104). Acta Astronautica.

[28] **Kuo, K., & Chiaverini, M.** (2007). *Fundamentals of hybrid rocket combustion and propulsion.* AIAA.

[29] **George, P., Krishnan, S., Varkey, P., Ravindran, M., & Ramachandran, L**. (2001). Fuel regression rate in hydroxyl-terminated-polybutadiene/gaseous-oxygen hybrid rocket motors. *Journal of Propulsion and Power, 17(1)*, 35 - 42.

[30] **Karabeyoglu, A., Altman, D., & Cantwell, B.** (2002). Combustion of liquefying hybrid propellants: Part 1, general theory. *Journal of Propulsion and Power, 18(3)*, 610 - 620.

[31] **Karabeyoglu, A., Stevens, J., Cantwell, B., & Micheletti, D.** (2011). High Performance hybrid upper stage motor. *47th AIAA/ASME/SAE/ASEE Joint Propulsion Conference and Exhibit,* 6025.

[32] https://www.lcsun-news.com/story/news/local/spaceport/2018/12/13/virgin-galactic-space-ship-unity-reached-space-lands/2300194002 <*https://www.lcsun-news.com*> date retrieved 05.05.2019

[33] **Larson, W., Henry, G., & Humble, R.** (1995). *Space Propulsion Analysis and Design.* McGraw-Hill.

[34] **Wilson, I.** (2012). Powered flight: The engineering of aerospace propulsion. *The Astronautically Journal,* 1224 - 1225.

[35] **Delpozzo, S., Williams, C., & Doncaster, B.** (2019). *NANO/MICROSATELLITE MARKET FORECAST, 9.* SpaceWork Enterprise.

[36] **Niederstrasser, C.** (2018). Small Launch Vehicles – A 2018 State of the Industry Survey. *32nd Annual AIAA/USU Conference on Small Satellites.* 32nd Annual AIAA/USU Conference on Small Satellites.

[37] **Inc., R.** (2019). *Electron Payload's User Guide June 2019 Version 6.4.* RocketLab Inc.

[38] **Inc., V. L.** (2019). *Vector-H Payload User's Guide.* Vector Launch Inc.

[39] **PwC.** (2017). *Micro-launchers: what is the market?* PwC.

[40] **https://www.grc.nasa.gov/WWW/CEAWeb/ Retrieved from** <*https://www.grc.nasa.gov/*>, date retrieved 05.05.2019

[41] **Larson, W., Henry, G., & Humble, R.** (1995). *Space Propulsion Analysis and Design.* McGraw-Hill.

[42] **Leung, J.** (1986). A generalized correlation for one-component homogeneous equilibrium flashing choked flow. *AIChE Journal, 32(10)*, 1743 - 1746.

[43] **Dyer, J., Zilliac, G., Sadhwani, A., Karabeyoglu, A., & Cantwell, B.** (2007). Modeling feed system flow physics for self-pressurizing propellants. *43rd AIAA/ASME/SAE/ASEE Joint Propulsion and Conference* (p. 5702). AIAA/ASME/SAE/ASEE.

[44] **Darby, R., Meiller, P., & Stockton, J.** (2001). Select the best model for two - phase relief sizing. *Chemical engineering progress, 97(5),* 56 - 65.

[45] **Henry, R., & Fauske, H.** (1971). The two-phase critical flow of one-component mixtures in nozzles, orifices and short tubes. *Journal of Heat Transfer, 93(2)*, 179 - 187.

[46] **Yuan, W., & Schnerr, G.** (2003). Numerical Simulation of Two-Phase Flow in Injection Nozzles: Interaction of Cavitation and External Jet Formation. *Journal of Fluids Engineering, 125(6)*, 963 - 969.

[47] **Whitmore, S., & Chandler, S.** (2010). Engineering model for self-pressurizing saturated-N2O-propellant feed systems. *Journal of Propulsion and Power, 26(4)*, 706 - 714.

[48] **John, D., & Anderson, D.** (2003). *Modern Compressible Flow*. McGraw-Hill Education.

[49] **Sutton, G., & Biblarz, O.** (2016). *Rocket Propulsion Elements.* John Wiley & Sons.

[50] **Fiorina, B., Veynante, D., & Candel, S.** (2013). *Modeling combustion chemistry in large eddy simulation of turbulent flames.* TSFP DIGITALLIBRARY ONLINE, BegelHouseInc.

[51] **Anetor, L., Osakue, E., & Odetunde, C.** (2012). Reduced mechanism approach of modeling premixed propane-air mixture using ANSYS Fluent. *Engineering Journal, 16(1),* 67 - 86.

[52] **McBride, B., Gordon, S., & Reno, M.** (1993). Coefficients for calculating thermodynamic and transport properties of individual species.

[53] **Chang, S. L.** (2005). The Enhancement of Regression Rate of Hybrid Rocket Fuel by Various Methods. *43. Aerospace Sciences Meeting and Exhibit.* Reno, Nevada: AIAA.

[54] **Sutton, G. P., & Biblarz, O.** (2001). *Rocket Propulsion Elements*. New York: John & Wiley.

[55] **Yoder, C. M., & Schrag, M.** (1978). Nassi-Shneiderman Charts an Alternative to Flowcharts for Design. *SIGSOFT/BIGMETRICS Software and Assurance Workshop* (pp. 386 - 393). New York: ACM.

[56] **Tewari, A.** (2007). *Atmospheric and space flight dynamics: Modeling and simulation with Matlab and Simulink.* Boston: Birkhaeuser.

[57] **Curtis, H. D.** (2014). *Orbital mechanics for engineering students*. Burlington, MA: Elsevier Butterworth-Heinemann.

[58] **Turner, M. J.** (2009). *Rocket and spacecraft propulsion: Principles, practice and new developments.* Germany: Springer-Praxis.

[59] **Curtis, H. D.** (2014). *Orbital mechanics for engineering students*. Burlington, MA: Elsevier Butterworth-Heinemann.

[60] **Walter, U.** (2008). *Astronautics.* VCH: Wiley.

[61] **Marti and Sarigul-Klijn, N. S.-K.** (2001). A Study of Air Launch Methods for RLVs. *American Institute of Aeronautics and Astronautics*.

[62] **Anetor, L., Osakue, E., & Odetunde, C.** (2012). Reduced mechanism approach of modeling premixed propane-air mixture using ANSYS Fluent. *Engineering Journal, 16(1)*, 67 - 86.

[63] **Tewari, A.** (2007). *Atmospheric and space flight dynamics: Modeling and simulation with Matlab and Simulink.* Boston: Birkhaeuser.

[64] **Loftus, J. P., & Teixeira, C.** (1999). Chapter 18: Launch systems. In W. J. Larson, & J. Wertz, *Space mission analysis and design* (pp. 719-744). El Segundo, CA & New York, NY: Microcosm Press & Springer.

[65] **Ley, W., Wittmann, K., & Hallmann, W.** (2009). Chapter 3: Space transportation systems. In *Handbook of space technology* (pp. 115 - 200). Sussex, UK: Wiley & Sons.

[66] **Fischer, H. M.** (2005). *Trajectories and orbital mechanics: Ascent of launchers, orbits and orbital transfers.* Retrieved May 5, 2019 from: http://www.scribd.com

[67] **Costa, F., & Vieira, R.** (2010). Preliminary Analysis of Hybrid Rockets for Launching Nanosats into LEO. *J. of the Braz. Soc. of Mech. Sci. & Eng.*, 502 - 509

[68] **Miranda, F.** (2015). *Development of an Optimization Tool for Multi-Technology Rocket Launch Vehicle Design.* Master Thesis.

[69] **Rohrschneider, R. R.** (2002). *Development of a Mass Estimating Relationship Database for Launch Vehicle Conceptual Design.* Georgia Institute of Technology AE8900 Lesson Document.

[70] **AIGA, A. I.** (2013). *Safe Practices for Storage and Handling of Nitrous Oxide.* AIGA 081/16.

[71] **Woodward, D.** (2017). *2017Conceptual design of rocket powered, vertical takeoff, fully expendable and first stage boost back space launch vehicles.* Master Thesis.

[72] **Barret, C.** (1997). *Review of Our National Heritage of Launch Vehicles Using Aerodynamic Surfaces and Current Use of These by Other Nations (Center Director's Discretionary Fund Project Number 93-05Part II).* Technical Report NASA-TP-3704: NASA.

[73] ***MatWeb.*** (2019,5). **Retrieved from www.matweb.com**

[74] **Ballard, C.** (2012). *Conceptual Lay-out of a Small Launcher.* Master’s Thesis.

[75] **Krevor, Z. C.** (2007). *A Methodology to Link Cost and Reliability for Launch Vehicle Design.* PhD Thesis.

[76] **Ritter, P. A.** (2012). *Optimization and Design for Heavy Lift Launch Vehicles.* Master’s Thesis

[77] ***Minotaur IV, V, VI User's Guide.*** (2015). Orbital ATK.

[78] **Burghes, D. N.** (1974). Optimum staging of multistage rockets. *International Journal of Mathematical Education in Science and Technology, 5(1),* 3- 10.

APPENDICES

APPENDIX A: Orbit Velocity Calculations

APPENDIX B: Nitrous Oxide Filling Properties

APPENDIX C: MATLAB Propulsion Code Scripts

APPENDIX A: Orbit Velocity Calculations

There are six parameters required to uniquely identify a specific orbit and they are called classical orbital elements, also known as Keplerian parameters. The two main elements, which are the semimajor axis (a) and the eccentricity (e), respectively define the size and the shape of the ellipse.

1. *Semimajor axis* (a) defines the size of the orbit and it is the half length of the major axis of the ellipse.

$$a = \frac{r_a + r_p}{2}$$

2. *Eccentricity* (e) defines the shape of the orbit and it is the ratio of the distance between the two foci to the length of the major axis.

$$e = \frac{c}{a} = \frac{r_a - r_p}{r_a + r_p}$$

For a circular orbit $e = 0$ ($a = r$); whereas for an elliptical orbit $0 < e < 1$ ($a > 0$). Trajectory is parabolic when $e = 1$ ($a = \infty$) and hyperbolic when $e > 1$ ($a < 0$).

Two elements, namely the inclination (i) and the right ascension of the ascending node (Ω) define the orientation of the orbital plane in space (Figure A.2).

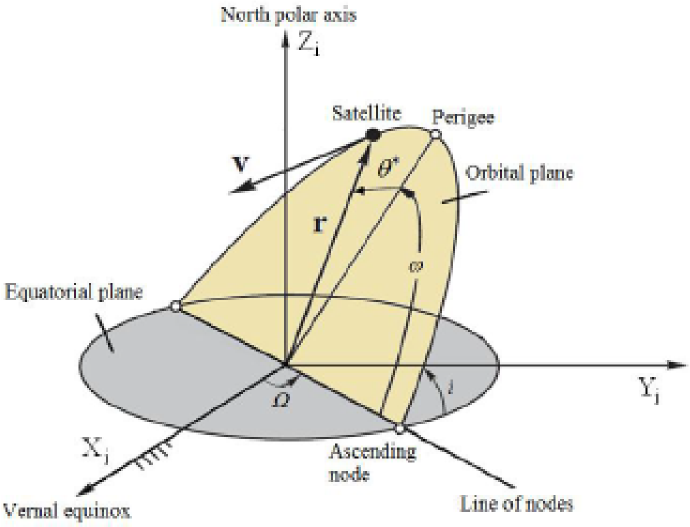

Velocity of the satellite at any point in an orbit can be calculated using the following *vis viva equation* derived from the orbital energy conservation equation.

$$V_{orbit} = \sqrt{\mu\left(\frac{2}{r} - \frac{1}{a}\right)}$$

In Eq. (A.10),

V_{orbit} is the orbital velocity at radial distance r,

μ is the Earth's gravitational parameter, i.e. $\mu = 398600.4\ km^3/s^2$,

r is the radial distance from the Earth's center to the satellite,

a is the semimajor axis.

Satellite reaches its maximum speed at perigee ($r = r_{min}$) and minimum speed at apogee ($r = r_{max}$) as Eq. (A.10) implies. For circular orbits r is constant and equals to a, thus Eq. (A.10) reduces to a constant speed of circular orbit.

$$V_{circ} = \sqrt{\frac{\mu}{r}}$$

Time taken for a satellite to make one complete revolution along an elliptical orbit is called *orbital period* (τ) and can be calculated by

$$\tau = \frac{2\pi a^{3/2}}{\sqrt{\mu}}$$

The time elapsed from perigee point along an elliptical orbit can be calculated as a fraction of orbital period using Kepler's second law. Or, more generally, it can be expressed for an arbitrary θ^* as derived by Addison (2009).

$$t(\theta^*) = \begin{cases} \sqrt{\frac{a^3}{\mu}}\left\{2\arctan\left(\sqrt{\frac{1-e}{1+e}}\tan\left(\frac{\theta^*}{2}\right)\right) - \sqrt{1-e^2}\,\frac{e\sin\theta^*}{1+e\cos\theta^*}\right\}, & 0 \le \theta^* < \pi \\ \sqrt{\frac{a^3}{\mu}}\left\{2\pi + 2\arctan\left(\sqrt{\frac{1-e}{1+e}}\tan\left(\frac{\theta^*}{2}\right)\right) - \sqrt{1-e^2}\,\frac{e\sin\theta^*}{1+e\cos\theta^*}\right\}, & \pi \le \theta^* < 2\pi \end{cases}$$

APPENDIX B: Nitrous Oxide Filling Properties

AIGA 081/13

4.2 Physical properties and hazards

Table 2 Properties of nitrous oxide

Chemical formula N_2O		
Colour, odour, taste None, Sweet odour, no taste		
Characteristics Non-flammable Supports combustion Oxidizing gas Anaesthetic Nitrous Oxide is non-corrosive and does not form an acid in water		
	Metric Units	**Customary Units**
Molecular weight	44.01	44.01
Density of gas at reference conditions: 21.1 °C (70 °F), 101.325 kPa,abs (14.696 psia) 15 °C (59 °F), 14.696 psia (101.325 kPa, abs)	1.947 kg/m^3 1.88 kg/m^3	0.1146 lb/ft^3 0.1172 lb/ft^3
Density of gas, at 0 °C(32F) and 14.696 psia, (101.325 kPa, abs)	1.977 kg/m^3	0. 123 lb/ft^3
Specific gravity of gas compared to air	1.53	1.53
Density of liquid, at 1 atmosphere pressure (101.325 kPa)	1227 kg/m^3	76.6 lbs/ft^3
Critical temperature	36.5 °C	97.7 °F
Critical pressure	71.45 bar	1039 psig
Boiling point at 1 atmosphere pressure (1.013 bar)	–88.3°C	–127°F
Melting point of solid at 1 atmosphere (1.013 bar)	–90.8°C	–131.5°F
Heat of fusion at melting point	148.9 kJ/kg	64 Btu/lb
Heat of vaporization at normal boiling point	376.3 kJ/kg	161.8 Btu/lb
Triple point pressure	8.78 bar	12.7 psia
Triple point temperature	–90.8°C	–131.5°F
Heat capacity, C_p, of gas at 59 °F (15°C) and 1 atmosphere (101.325 kPa)	0.866 kJ/kg°C	0.207 Btu/lb°F
Heat capacity, Cv, of gas at 59 °F (15°C) and 1 atmosphere (101.325 kPa)	0.665 kJ/kg°C	0.159 Btu/lb°F
Solubility in water at 25°C(77 °F) at atmospheric pressure	0.59 v/v	0.59 v/v

Properties of saturated liquid nitrous oxide

Temperature °F	Temperature °C	Vapour pressure psia	Vapour pressure bar abs	Liquid density lb/gal	Liquid density kg/litre
–131.5	–90,82	12.73	0,878		
–127.2	–88,47	14.69	1,013	10.20	1,2228
–110	–78,89	26	1,793	10.36	1,241
–90	–67,78	46	3,172	10.02	1,201
–70	–56,67	73.98	5,102	9.69	1,161
–50	–45,56	111.97	7,722	9.26	1,110
–30	–34,44	166.95	11,514	8.95	1,073
–10	–23,33	239.93	16,547	8.65	1,036
10	–12,22	334.9	23,097	8.18	0,980
32	0	453.7	31,290	7.54	0,904
50	10,00	589.85	40,679	6.99	0,838
59	15,00	654.24	45,120	6.83	0,818
70	21,11	759.8	52,400	6.22	0,745
97.5	36,41	1050.5	72,450	3.86	0,452

The following additional requirements shall be met:

- The installation shall be designed and operated in accordance with local regulations for oxidizing and medical gases;
- Written operating procedures, which describe all steps of the filling process (prefill check and reconditioning of the cylinders, tare weight check, control of filling weight). For details of a recommended gravimetric filling procedure see for example, EN 1919, *Transportable Gas Cylinders. Cylinders for gases (excluding acetylene or LPG. Inspection at time of filling* [58] and check CGA copy. Filling of non-empty cylinders ("top filling") and filling by pressure without scale shall not be applied; and
- The admissible filling ratio is dependent on the test pressure of the cylinder, see Table 7 or by local regulations In North America the admissible filling ratio is 68%.

Table 7 Extract from Packing instruction P200 [2]

Minimum cylinder test pressure, bar	Maximum filling ratio
180	0,68
225	0,74
250	0,75*)

*) This means for example, that a cylinder with 10 litre capacity and test pressure 250 bar (3625 psi) may be filled with 7,5 kg nitrous oxide.

All parts of a filling installation shall be bonded and earthed to ensure electrical continuity. The electrical potentials between the cylinder / bundle and the ground should be equalised during filling. If necessary the cylinder / bundle should be bonded directly to ground.

APPENDIX C: MATLAB Propulsion Code Scripts

```
clear all;
clc;
close all;
l=input('Select the fuel\n1-Paraffin\n2-PMMA\n3-HTPB\n4-HDPE\nEnter the
number of selection between 1-4:');
m=input('Select the oxidizer\n1-N2O\n2-LOX\n3-H2O2\nEnter the number of
selection between 1-3:');
N=input('Enter the oxidiser to fuel ratio:starting and final point with
the\nrequired increment between square paranthesis. For example
[5:0,5:12]:');
disp(N);
Pc=input('Enter the combustion pressure in bar unit:');
k=length(N);
[M,L]=xlsread('Properties_Fuel.xls');
[X,Y]=xlsread('Properties_Oxidiser.xls');
[S,A]=xlsread('Cp_Gibbs_Products.xls');
[G,H]=xlsread('Products.xls');
Spesific_impulse=zeros(1,k);

ge=9.81;
ij=1;
for OF=N(1:k)
    if M(l,4)>X(m,5)
        MoleNuOxi=(M(l,4)*OF)/X(m,5);
        MoleNuFuel=1;
        Mole_React =[MoleNuOxi MoleNuFuel];
        disp(Mole_React)
    elseif X(m,5)/M(l,4)==1
        Mole_React=[1 1];
        disp(Mole_React)
    else
        MoleNuOxi=(M(l,4)*OF)/X(m,5);
        MoleNuFuel=1;
        Mole_React =[MoleNuOxi MoleNuFuel];
        disp(Mole_React)
    end
    Total_C=M(l,1);
    Total_H=M(l,2)+MoleNuOxi*X(m,2);
    Total_O=M(l,3)+MoleNuOxi*X(m,1);
    Totals=[Total_C Total_H Total_O];
    disp(Totals)
    Ru=8.31446218;
    T_lower=1000;
    T_upper=5000;
    increment=7;
    T_matrice=linspace(T_lower,T_upper,increment);
    e=length(T_matrice);
    i=1;
    Enthalpy_difference=zeros(1,e);
    while i<e+1
        t=T_matrice(i);
```

```
z=S(1:50,1);
s=S(1:50,4);
er=ismember(t,z);
if er>0
    Gibbs_H2O=S(t/100,10);
    Gibbs_CO=S(t/100,2);
    Gibbs_CO2=S(t/100,4);
    Gibbs_OH=S(t/100,14);


                Gibbs_H=S(t/100,16);
                Gibbs_NO=S(t/100,12);
                Gibbs_O=S(t/100,18);
                DeltaGibbs=Gibbs_CO2-Gibbs_CO-Gibbs_H2O;
                DeltaGibbs1=Gibbs_OH-Gibbs_H2O;
                DeltaGibbs2=Gibbs_CO-Gibbs_CO2;
                DeltaGibbs3=2*Gibbs_H;
                DeltaGibbs4=2*Gibbs_O;
                DeltaGibbs5=2*Gibbs_NO;
                K=exp(-DeltaGibbs/(t*Ru));
                K1=exp(-DeltaGibbs1/(t*Ru));
                K2=exp(-DeltaGibbs2/(t*Ru));
                K3=exp(-DeltaGibbs3/(t*Ru));
                K4=exp(-DeltaGibbs4/(t*Ru));
                K5=exp(-DeltaGibbs5/(t*Ru));
            else
            a=t/100;
            c=floor(a);
            d=ceil(a);
            o1=(t-S(c,1))*(S(c,2)-S(d,2))/(S(d,1)-S(c,1));
             o2=(t-S(c,1))*(S(c,4)-S(d,4))/(S(d,1)-S(c,1));
              o3=(t-S(c,1))*(S(c,10)-S(d,10))/(S(d,1)-S(c,1));
              o4=(t-S(c,1))*(S(c,14)-S(d,14))/(S(d,1)-S(c,1));
              o5=(t-S(c,1))*(S(c,16)-S(d,16))/(S(d,1)-S(c,1));
              o6=(t-S(c,1))*(S(c,12)-S(d,12))/(S(d,1)-S(c,1));
              o7=(t-S(c,1))*(S(c,18)-S(d,18))/(S(d,1)-S(c,1));
            Gibbs_H=-o5+S(c,16);
            Gibbs_NO=-o6+S(c,12);
            Gibbs_O=-o7+S(c,18);
            Gibbs_OH=-o4+S(c,14);
            Gibbs_CO=-o1+S(c,2);
            Gibbs_CO2=-o2+S(c,4);
            Gibbs_H2O=-o3+S(c,10);
            DeltaGibbs=Gibbs_CO2-Gibbs_CO-Gibbs_H2O;
            DeltaGibbs1=Gibbs_OH-Gibbs_H2O;
            DeltaGibbs2=Gibbs_CO-Gibbs_CO2;
            DeltaGibbs3=2*Gibbs_H;
            DeltaGibbs4=2*Gibbs_O;
            DeltaGibbs5=2*Gibbs_NO;
            K=exp(-DeltaGibbs/(t*Ru));
            K1=exp(-DeltaGibbs1/(t*Ru));
            K2=exp(-DeltaGibbs2/(t*Ru));
            K3=exp(-DeltaGibbs3/(t*Ru));
            K4=exp(-DeltaGibbs4/(t*Ru));
            K5=exp(-DeltaGibbs5/(t*Ru));
            end
            u=1-K;
            v=(K-1)*Total_O+(Total_H)/2+Total_C;

            q=Total_C*Total_C*K-K*Total_O*Total_C;
            %q=-Total_C*Total_C-
    (K*Total_C*Total_O)+(K*Total_C*Total_C)+(0.5*Total_C*Total_H*K);
            coefficients=[u v q];
            MoleNu1CO2=roots(coefficients);
            yj=find(MoleNu1CO2>0 & MoleNu1CO2<29);
            MoleNuCO21=MoleNu1CO2(yj);
            u12=((2*Pc*Pc)/((K4^(3/2))*K2));
    u22=((3*Pc)/K4)+Pc/(sqrt(K4)*K2);
    u32=2;
    u42=-1;
```

```
coefficientsXO=[u12 u22 u32 u42];
XO11=roots(coefficientsXO);
XOj=(XO11<1 & XO11>0);
XO12=XO11(XOj);
XO2=XO12*XO12*Pc/K4;
XCO=2*XO2+XO12;
XCO2=sqrt(XO2)*sqrt(Pc)*XCO/K2;
z7=((2*XO12*XO2*MoleNuCO21/(2*XO2+2))-(4*XO2*MoleNuCO21/(2*XO2+2))-
MoleNuCO21*XO12)/((XO12/2)+(XO12/(2*XO2+2))-(XO12*XO2/(2*XO2+2))-
(2/(2*XO2+2))+(2*XO2/(2*XO2+2)));
z2=(((1-XO2)*z7/2)-MoleNuCO21*XO2)/(XO2+1);
MoleNuO=2*z2;
MoleNuO21=z7/2-z2;
MoleNuCO1=z7;
MoleNuCO2=MoleNuCO21-z7;
        u1=Pc;
        v1=K4;
        q1=-K4;
        coefficients1=[u1 v1 q1];
        XO1=roots(coefficients1);
        XO1j=find(XO1>0 & XO1<1);
        XO=XO1(XO1j);
        z4=(XO*MoleNuO21)/(2-XO);
        MoleNuO=2*z4;
        MoleNuO211=MoleNuO21-z4;
        MoleNuCO=(Total_C-MoleNuCO21)+MoleNuCO1;
        u11=((2*Pc*Pc)/((K3^(3/2))*K1));
u21=((3*Pc)/K3)+Pc/(sqrt(K3)*K1);
u31=2;
u41=-1;
coefficientsXH=[u11 u21 u31 u41];
XH11=roots(coefficientsXH);
XHj=(XH11<1 & XH11>0);
XH12=XH11(XHj);
XH2=XH12*XH12*Pc/K3;
XOH=2*XH2+XH12;
XH2O=sqrt(XH2)*sqrt(Pc)*XOH/K1;
z3=((2*XH12*XH2*MoleNuH2O1/(2*XH2+2))-(4*XH2*MoleNuH2O1/(2*XH2+2))-
MoleNuH2O1*XH12)/((XH12/2)+(XH12/(2*XH2+2))-(XH12*XH2/(2*XH2+2))-
(2/(2*XH2+2))+(2*XH2/(2*XH2+2)));
z6=(((1-XH2)*z3/2)-MoleNuH2O1*XH2)/(XH2+1);
MoleNuH1=2*z6;
MoleNuH21=z3/2-z6;
MoleNuOH=z3;
MoleNuH2O=MoleNuH2O1-z3;
        %MoleNuOH=z3;
        %MoleNuH21=z3/2;
        %MoleNuH211=(Total_H-2*MoleNuH2O1)/2;
        u2=Pc;
        v2=K3;
        q2=-K3;
        coefficients2=[u2 v2 q2];
        XH1=roots(coefficients2);
        XH1j=find(XH1>0 & XH1<1);
        XH=XH1(XH1j);
        z1=(XH*MoleNuH211)/(2-XH);
        %disp(z1)
        %disp(z2)
        %disp(z3)
        %disp(z4)
        MoleNuH=2*z1+MoleNuH1;
        MoleNuH2=(MoleNuH211-z1)+MoleNuH21;
        if m==1
        XO2=1/(2+sqrt(K5));
        z5=MoleNuO211-2*MoleNuO211*XO2;
        MoleNuO2=MoleNuO211-z5;
```

```
        MoleNuN2=MoleNuOxi-z5;
        MoleNuNO=2*z5;
        MoleNuProducts=[MoleNuCO2 MoleNuH2O MoleNuCO MoleNuH2 MoleNuO
MoleNuH  MoleNuO2 MoleNuOH MoleNuNO MoleNuN2];
        disp(MoleNuProducts);
        MoleTotal=sum(MoleNuProducts);
        %MoleFraction=MoleNuProducts/MoleTotal
        MolarWeight=[G(1,8) G(2,8) G(3,8) G(4,8) G(5,8) G(6,8) G(7,8)
G(8,8) G(9,8) G(10,8)];
        else
        MoleNuProducts=[MoleNuCO2 MoleNuH2O MoleNuCO MoleNuH2 MoleNuO
MoleNuH  MoleNuO211 MoleNuOH];
         disp(MoleNuProducts);
        MoleTotal=sum(MoleNuProducts);
        MolarWeight=[G(1,8) G(2,8) G(3,8) G(4,8) G(5,8) G(6,8) G(7,8)
G(8,8)];
        end

hTCO2=(((Ru)*((G(1,1)*t)+(G(1,2)*(t*t)/2)+(G(1,3)*(t^3)/3)+(G(1,4)*(t^4)/4)
+(G(1,5)*(t^5)/5)+G(1,6)))+393520);

hTH2O=(((Ru)*((G(2,1)*t)+(G(2,2)*(t*t)/2)+(G(2,3)*(t^3)/3)+(G(2,4)*(t^4)/4)
+(G(2,5)*(t^5)/5)+G(2,6)))+241820);

hTCO=(((Ru)*((G(3,1)*t)+(G(3,2)*(t*t)/2)+(G(3,3)*(t^3)/3)+(G(3,4)*(t^4)/4)+
(G(3,5)*(t^5)/5)+G(3,6)))+110541);

hTH2=(((Ru)*((G(4,1)*t)+(G(4,2)*(t*t)/2)+(G(4,3)*(t^3)/3)+(G(4,4)*(t^4)/4)+
(G(4,5)*(t^5)/5)+G(4,6)))+0);

hTO=(((Ru)*((G(5,1)*t)+(G(5,2)*(t*t)/2)+(G(5,3)*(t^3)/3)+(G(5,4)*(t^4)/4)+(
G(5,5)*(t^5)/5)+G(5,6)))-249197);

hTH=(((Ru)*((G(6,1)*t)+(G(6,2)*(t*t)/2)+(G(6,3)*(t^3)/3)+(G(6,4)*(t^4)/4)+(
G(6,5)*(t^5)/5)+G(6,6)))-217977);

hTO2=(((Ru)*((G(7,1)*t)+(G(7,2)*(t*t)/2)+(G(7,3)*(t^3)/3)+(G(7,4)*(t^4)/4)+
(G(7,5)*(t^5)/5)+G(7,6)))+0);

hTOH=(((Ru)*((G(8,1)*t)+(G(8,2)*(t*t)/2)+(G(8,3)*(t^3)/3)+(G(8,4)*(t^4)/4)+
(G(8,5)*(t^5)/5)+G(8,6)))-38985);
        if m==1

hTNO=(((Ru)*((G(9,1)*t)+(G(9,2)*(t*t)/2)+(G(9,3)*(t^3)/3)+(G(9,4)*(t^4)/4)+
(G(9,5)*(t^5)/5)+G(9,6)))-90297);

hTN2=(((Ru)*((G(10,1)*t)+(G(10,2)*(t*t)/2)+(G(10,3)*(t^3)/3)+(G(10,4)*(t^4)
/4)+(G(10,5)*(t^5)/5)+G(10,6)))+0);
        hTProducts=[hTCO2 hTH2O hTCO  hTH2 hTO hTH hTO2 hTOH hTNO hTN2];
        else
        hTProducts=[hTCO2 hTH2O hTCO  hTH2 hTO hTH hTO2 hTOH];
        end
        if m==1
        HfTotalProducts=G(1,7)*MoleNuCO2 + G(2,7)*MoleNuH2O
+G(3,7)*MoleNuCO+G(5,7)*MoleNuO+G(6,7)*MoleNuH+G(8,7)*MoleNuOH+G(9,7)*MoleN
uNO;
        disp(HfTotalProducts);
        else
        HfTotalProducts=G(1,7)*MoleNuCO2 + G(2,7)*MoleNuH2O
+G(3,7)*MoleNuCO+G(5,7)*MoleNuO+G(6,7)*MoleNuH+G(8,7)*MoleNuOH;
        %disp(HfTotalProducts);

        end
```

```
    HtTotalProducts=MoleNuProducts*(hTProducts)';
    %disp(HtTotalProducts);
    %disp(HfTotalProducts);
    TotalEnthalpy_Products=HfTotalProducts+HtTotalProducts;
    %disp(TotalEnthalpy_Products);
    TotalEnthalpy_Reactants=M(1,5)*MoleNuFuel+X(m,4)*MoleNuOxi;
    ed=abs(TotalEnthalpy_Products-TotalEnthalpy_Reactants);
   %disp(ed);
    Enthalpy_difference(1,i)=ed;
    %disp(Enthalpy_difference(1,i));
    i=i+1;

    w=min(Enthalpy_difference);

    if w>800
        h=find(Enthalpy_difference==w);
        T_lower=T_matrice(h-1);
        T_upper=T_matrice(h+1);
        increment=10;
        T_matrice=linspace(T_lower,T_upper,increment);
        e=length(T_matrice);
        i=1;
        Enthalpy_difference=zeros(1,e);

    elseif w>0 & w<800
                j=find(Enthalpy_difference==w);
                Temperature=T_matrice(j)+7.5*T_matrice(j)/100;
                %disp(Temperature);
                fprintf(1, 'Temperature = %8.4f\n\n', Temperature);


end
end

    ab=(Temperature-298)/2;
    abc=ab/100;
    cb=floor(abc);
    db=ceil(abc);
    o1b=(ab-S(cb,1))*(S(db,5)-S(cb,5))/(S(db,1)-S(cb,1));
    Cp_CO21=o1b+S(cb,5);
    Cp_CO2=hTCO2/(Temperature-298);
    o3b=(ab-S(cb,1))*(S(db,11)-S(cb,11))/(S(db,1)-S(cb,1));
    Cp_H2O1=o3b+S(cb,11);
    Cp_H2O=hTH2O/(Temperature-298);
    o2b=(ab-S(cb,1))*(S(db,3)-S(cb,3))/(S(db,1)-S(cb,1));
    Cp_CO1=o2b+S(cb,3);
    Cp_CO=hTCO/(Temperature-298);
    o4b=(ab-S(cb,1))*(S(db,9)-S(cb,9))/(S(db,1)-S(cb,1));
    Cp_H21=o4b+S(cb,9);
    Cp_H2=hTH2/(Temperature-298);
    o5b=(ab-S(cb,1))*(S(db,19)-S(cb,19))/(S(db,1)-S(cb,1));
    Cp_O1=-o5b+S(cb,19);
    Cp_O=hTO/(Temperature-298);

    Cp_H1=20.786;
    Cp_H=hTH/(Temperature-298);

    o7b=(ab-S(cb,1))*(S(db,21)-S(cb,21))/(S(db,1)-S(cb,1));
    Cp_O21=o7b+S(cb,21);
    Cp_O2=hTO2/(Temperature-298);
    o8b=(ab-S(cb,1))*(S(db,15)-S(cb,15))/(S(db,1)-S(cb,1));
    Cp_OH1=o8b+S(cb,15);
```

```
        Cp_OH=hTOH/(Temperature-298);
        if m==1
        o9b=(ab-S(cb,1))*(S(db,13)-S(cb,13))/(S(db,1)-S(cb,1));
        Cp_NO1=o9b+S(cb,13);
        Cp_NO=hTNO/(Temperature-298);
        o10b=(ab-S(cb,1))*(S(db,7)-S(cb,7))/(S(db,1)-S(cb,1));
        Cp_N21=o10b+S(cb,7);
        Cp_N2=hTN2/(Temperature-298);
        Cp=[Cp_CO2 Cp_H2O Cp_CO  Cp_H2 Cp_O Cp_H Cp_O2 Cp_OH Cp_NO Cp_N2];
        Cp1=[Cp_CO21 Cp_H2O1 Cp_CO1  Cp_H21 Cp_O1 Cp_H1 Cp_O21 Cp_OH1
Cp_NO1 Cp_N21];
        else

          Cp=[Cp_CO2 Cp_H2O Cp_CO  Cp_H2 Cp_O Cp_H Cp_O2 Cp_OH];
          Cp1=[Cp_CO21 Cp_H2O1 Cp_CO1  Cp_H21 Cp_O1 Cp_H1 Cp_O21 Cp_OH1];
        end


        Cp_Total=MoleNuProducts*Cp';
        Cp_Total1=MoleNuProducts*Cp1';
        AvrgCpProd=Cp_Total/MoleTotal;
        AvrgCpProd1=Cp_Total1/MoleTotal;
        MoleFractions=MoleNuProducts/MoleTotal
        TotalWeight=MoleNuProducts*MolarWeight';
        AvrgM=TotalWeight/MoleTotal
        Rmix=8314/AvrgM;
        gama=AvrgCpProd/(AvrgCpProd-Ru);
        gama1=AvrgCpProd1/(AvrgCpProd1-Ru);

C_star=sqrt(gama*Rmix*Temperature)/(gama*((2/(gama+1))^((gama+1)/(2*(gama-
1)))))
        Cf=sqrt(((2*gama^2)/(gama-1))*((2/(gama+1))^((gama+1)/(gama-
1)))*(1-(1/Pc)^((gama-1)/gama)))
        Isp=Cf*C_star/ge


        disp(gama)
        disp(gama1)
        %disp(Gibbs_H)
        %disp(Gibbs_NO)
        %disp(Gibbs_OH)
        %disp(Gibbs_O)
        %disp(o5)
        %disp(o6)
        %disp(o7)
        %disp(o4)
        %disp(K2)
        %disp(MoleNu1CO2)
        %disp(MoleNuCO2)
        %disp(XCO)
        %disp(MoleNuProducts)
        %disp( hTProducts)
        Spesific_impulse(1,ij)=Isp;
        ij=ij+1;

end


 axis([2 10 0 250])
 plot(N,Spesific_impulse)
```

CURRICULUM VITAE

Name Surname : Nazmi Erdi Coşkunpınar

Place and Date of Birth : Fatih 22/11/1992

E-Mail : n.erdicoskunpinar@gmail.com

EDUCATION :

- **B.Sc.** : 2015, Istanbul Technical University, Faculty of Aeronautics and Astronautics, Astronautical Engineering
- **M.Sc.** : 2020, Istanbul Technical University, Faculty of Aeronautics and Astronautics, Aeronautical and Astronautical Engineering

PROFESSIONAL EXPERIENCE AND REWARDS:

- 2016 – FORD OTOSAN R&D Engineer
- 2015 – 2019 PARS Rocketry Group Technical Advisor
- 3rd Place Chamber of Mechanical Engineers Istanbul 6th Necdet Eraslan Innovation Ideas for Aeronautics and Astronautics Design Competition

PUBLICATIONS, PRESENTATIONS AND PATENTS ON THE THESIS:

- **Coşkunpınar, N. E., Özen K., Grate S., Aslan, A. R.** 2016: Development of Hybrid Rocket Motor Design and Performance Code, 8th Asian Joint Conference on Propulsion and Power - March 16-19, 2016 Takamatsu,Jaa